Model and parameter identification for nonlinear ice-structure interaction

Master of Science Thesis

H.Zeng

TU Delft

M.Sc. Offshore & Dredging Engineering

Model and Parameter Identification for Nonlinear Ice-structure Interaction

by

H. Zeng

to obtain the degree of Master of Science
at the Delft University of Technology,
to be defended publicly on Wednesday November 25, 2015 at 10:00 AM.

Student number:	4313666	
Project duration:	April 1, 2015 – November 25, 2015	
Thesis committee: Chairman:	Prof. dr. A. Metrikine,	TU Delft
	Dr. E. Lourens,	TU Delft
	Dr. Ir. K. N. van Dalen,	TU Delft
	Ir. H. Hendrikse ,	TU Delft

This thesis is confidential and cannot be made public until December 31, 2015.

TU Delft

List of Figures

List of Tables

Abstract

Structures deployed in arctic and subarctic regions are inevitably subjected to loading tue to floating ice. The failure of the ice at the interaction point can result in complex dynamic behavior of the structure. The ice-induced vibration of structures can be generally categorized into: (1) intermittent crushing, (2) frequency lock-in, and (3) continuous crushing. The aim of this thesis is to estimate the unknown parameters as well as identify the shape of ice crushing strength and stress rate curve in a numerical model proposed by M. Maattanen under low, high and medium ice velocity. Based on measured vibration data, the least squares method and the extended Kalman filter has been used.

Using the least squares method for the case of low ice velocity, all of the five unknown model parameters reach their target value when no noise is assumed to be present on the measurements. However, the result obtained under 5% noise level is poor. The reason is the discontinuity in the ice crushing stress rate curve used in the model at $\dot{\sigma} = 0MPa/s$. Under high ice velocity, the least squares method fails due to the lack of information. While for medium ice velocity, the estimated ice curshing strength curve differs from the original one.

On the other hand, the extended Kalman filter, which can estimate both the model parameters and the structural states, works better. For the case of low ice velocity, the estimated parameters converge to the target value for three parameter estimation also in the presence of noise. When estimating more model parameters, the result doesn't converge to the target value due to nonuniqueness issues. However, the ice crushing strength curve obtained from fitting the ice crushing strength points at each time step is successful. Under high ice velocity, the estimated ice crushing strength curve is constant, reaching the target constant value. Moreover, the estimated curve is close to the original one within $0.4MPa/s < \dot{\sigma} < 1.8MPa/s$ under medium ice velocity.

Contents

1 Introduction

1.1. Background

After the innovation of steam engine, an unprecedented age of industry opened the Pandora's box of large amount of energy consumption, with incredible growth every year. Various ways of acquiring energy from the nature has been continuously discovered, including fossil energy, wind energy, solar energy, etc. Even though the demand of energy decreased along with the economic recession every seven or eight years, the demand has and will keep growing in general.

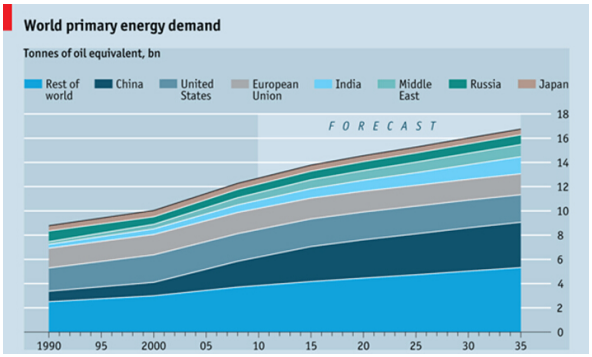

Figure 1.1: World primary energy demand (courtesy of The Economist)

Among all the form of energy, hydrocarbon and wind energy are perhaps the mostly mentioned, due to their large reserves. Enormous onshore drilling rigs and wind farms have been erected from last century. Moreover, human being's imagination has once again been pushed one step forward by high commercial profit from onshore to offshore. Offshore platforms with various functions have been fabricated and deployed in the ocean.

Figure 1.2: Statoil's Troll A Platform and Sheringham Shoal Offshore Wind Farm (courtesy of Wikipedia)

Exploring new frontier of energy has been executed for a long time by large oil companies, Shell and Exxonmobil for instance. In 1991, the Madrid Protocol, an addition to the Antarctic treaty, came into force, prohibiting exploration and extraction of hydrocarbons on Antarctica until at least 2048. Gradually, oil companies' interest turned to arctic and subarctic regions, for large reserves believed hidden beneath the soil there. By using a probabilistic geology based methodology, the United States Geological Survey has assessed the area north of the Arctic Circle and concluded that about 30% of the world's undiscovered gas and 13% of the world's undiscovered oil may be found there, mostly offshore under less than 500 m of water.

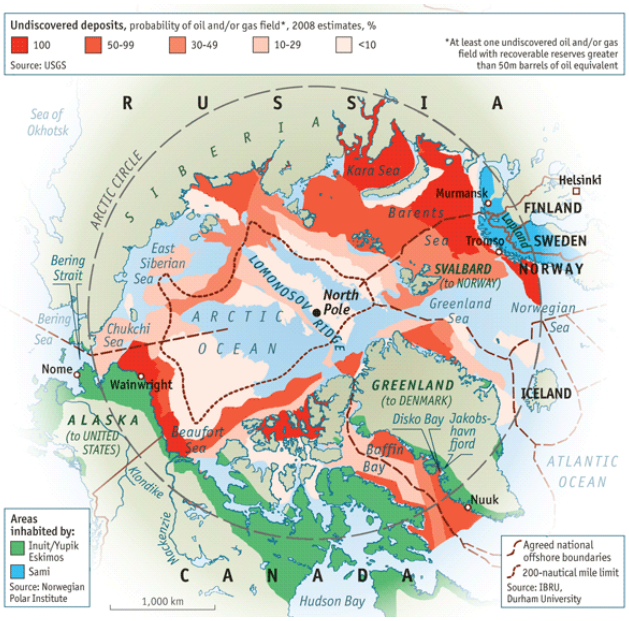

Figure 1.3: Arctic and subarctic oil and gas resource(courtesy of The Economist)

Since then, the exploitation of hydrocarbon in arctic and subarctic regions was ignited, along with the query of the public. Nevertheless, the activities in arctic and subarctic areas has never been stopped, including offshore platforms, lighthouses, piers etc. Some examples of structures has been installed in arctic and subarctic region are Prirazlomnaya platform and Berkut platform.

Figure 1.4: Prirazlomnaya platform and Berkut platform(courtesy of Wikipedia)

The most challenging issue for structures in arctic and subarctic regions is the impact of floating ice. Ice can float on the surface of ocean due to its relative low density compared with salt water. Meanwhile, the ocean current can carry the floating ice into moving state. And the moving floating ice will inevitably crush on the surface of artificial structures. Then severe vibrations, with devastating impact on the operational reliability and safety of offshore structures, may be caused by the failing ice along

the contact surface.

1.2. Previous research on ice induced vibration

From the first ice induced vibration (abbreviated as IIV) measurement on Cook Inlet [2] in 1960s, the intrinsic mechanism of IIV has been studied by numerous scientists and researchers.
It has been shown that the ice forces exerted on the structure are dependent on the ice velocity, the compliance of the structure, and the state of the ice. In the design code for arctic offshore structures, a distinction is made between three dynamic interaction scenarios: intermittent crushing, frequency lock-in and continuous brittle crushing.
At very low ice velocities ice behavior is ductile. Ice load is pseudo-stationary. Ice load and stresses, as well as structural deflection build up until ice compressive strength level is reached. As ice fails the load level drops suddenly, and the deflection of the structure springs back. Thereafter the advancing ice edge makes contact to the structure and a new load cycle starts. This produces a saw tooth like ice force or displacement history
At higher velocities, the response history will gradually change to frequency lock-in. Displacement history approaches a sinusoidal one. A resonant state occurs.
At still higher ice velocities conditions for the resonance are lost. Ice failure turns into totally brittle and ice load fluctuations randomly.

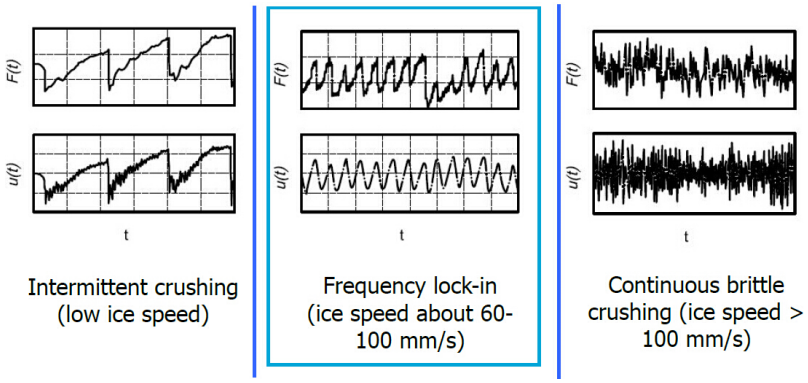

Figure 1.5: ISO classification of Ice-Induced Vibrations (Courtesy of ISO 19906)

The frequency lock-in is of paramount importance. Within the frequency lock-in range, the structure will experience the excitation near its natural frequency, which can arouse severe vibration of the structure. In this case, the working condition of staffs on the structure, as well as the health condition of the structure will be deteriorated. In order to design structures that can avoid this frequency lock-in phenomenon, first the phenomenon of frequency lock-in has to be understood.
In the past several decades, an enormous amount of theories has been proposed, even though none of them has accepted worldwide comprehensive consensus.
In 1988, Sodhi introduced a concept of crushing length and characteristic failure frequency [27]. Models employing this approach assume that a moving ice sheet acting on a structure tends to break into fragments of certain size. This phenomenon determines a characteristic failure frequency. Resonant vibrations may arise when the characteristic frequency is close to the natural frequency of the structure. The main problem associated with this type of models is that they deny the feedback of the motion of the structure on the ice loading[25].
In the year of 1989, a new model was proposed by Tuomo Karna [17]. The dynamic equations of equilibrium for the structure and the undamaged ice field are coupled by a nonlinear element describing the crushing and clearing processes at the ice-structure interface. The ice in that model was assumed to fail with a more or less constant nominal crushing depth. Good correspondence with field measurements was achieved with this model for slender vertically-sided offshore structures.
In addition, several scientists claim that IIV should be described by self-excited models with negative damping. Among them, Prof. Maattanen [20] presented a numerical model related to negative damping in 1978. In this model, the excitation force is coupled with the relatively velocity of the structure. A specific relationship between ice crushing strength and relative velocity was introduced to describe

this excitation force.

1.3. Previous research on ice force identification

Even though the intrinsic mechanism within IIV has not yet been fully understood, force exerting on the structure is the direct actuator that result in dynamic motion. Hence, it is one step forward if one can determine the ice force, or ice action directly.

Ice action has been measured since 1964 on the Cook Inlet, Alasks.[2]. Since then, direct measurement has been widely used by means of deploying load panels on different location of the structure. For instance, A total of 31 Medof panels in arrays were distributed on three faces of the Molikpaq platform, in order to measure first-year sea ice interacting with the Molikpaq [10, 35].

However, the force are likely to be underestimated if the location of the panels are far from the ice interaction point. Due to the fluctuation of sea level, finding perfect location of load panels is very difficult [13]. Moreover, the measurement accuracy may be deteriorated due to the structural properties, internal damping and natural frequency for instance, of the load panels. The operation accuracy and reliability of load panel has been looked into detail by Frederking et al [10],Jefferies et al[15] and Spencer [28]

In this case, using load panel to directly measure the ice force sometime is not accurate. Except direct measurement method, force can also be identified using indirect method – frequency domain deconvolution [33]. The disadvantage of frequency domain deconvolution is that it utilizes the frequency response function, which is often difficult to accurately determine, of the structure.

A new indirect method of ice force identification is proposed [32] using a joint input-state estimation algorithm. By augmenting the Kalman Filter, the displacement and ice force are identified, compared with the experimental measured displacement and force derived from the frequency domain deconvolution.

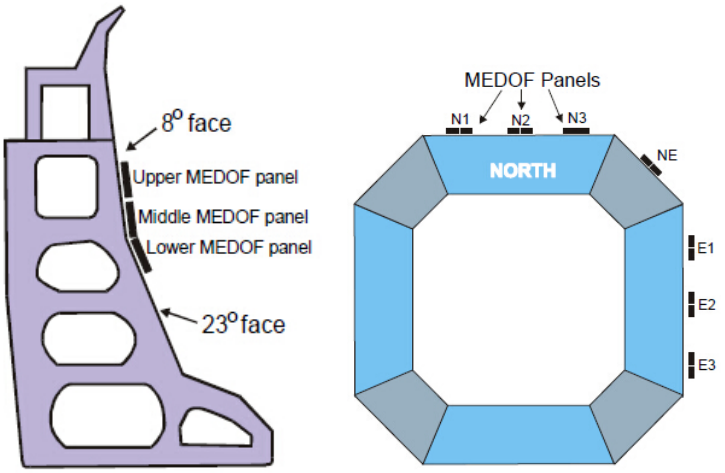

Figure 1.6: Location of the MEDOF panels on the Molikpaq showing side view (left) and plan view (right) locations (courtesy of [31])

1.4. Previous research on system and parameter estimation

The estimation problem can be categorized into state estimation (subcategory of filtering, prediction and smoothing problem[30]) which estimate the time varying state of the dynamic system, and system identification which deals with the problem of estimating time-invariant unknown parameters of dynamic systems using measurements of the outputs and(or) inputs from the system. Estimating the model parameters given a set of data is often referred to as the inverse problem.

Among the enormous estimators, the maximum likelihood method, which is quite well-known for solving the system identification problem, was introduced by Ronald Fisher between 1912 [8] and 1922 [9].It is based on the rather natural idea that the parameters should be chosen in such a way that the observed measurements are as likely as possible. The interesting thing is that under certain criterion [4], the maximum likelihood method is equivalent to least squares method, proposed by Carl Friedrich Gauss

over one hundred years earlier, which minimizes the sum of the squares of the errors. Expectation maximization algorithm is an iterative method for finding maximum likelihood. Some detailed introduction can be found in [6] and[24]. On the basis of recursive least squares method [5], Kalman filter, which has received comprehensive application, was primary developed by Rudolf Emil Kalman in 1960 [16]. The Kalman filter uses system update and measurement update [1] to recursively estimate the state and parameters. Some derivatives of Kalman filter, extended Kalman filter and unscented Kalman filter [3, 5, 26] for instance, have been proposed to solve problems of nonlinear dynamic system. Moreover, Applying the expectation maximization algorithm together with the Kalman filter constitutes a robust iterative procedure to estimate model parameters in the state space model as well as an approach to denoise the signal [22].

1.5. Research aim

Although actual dynamic model of IIV has not been discovered yet, if a proper identification approach can be used to estimate the unknown parameters in a proposed model based on measurement, then applying this identification technique to full scale or experimental measurement may lead to the real dynamic model of IIV.

The purpose of this research is to investigate into the numerical model proposed by Prof. Maattanen in the year of 1978. The curve describing the relationship between ice crushing strength and relative velocity is the key segment of his model. Two state-of-art parameter identification technique, least squares method and extended Kalman filter, are used to estimate the unknown parameters as well as the shape of the curve in the dynamic model, based on measurement. The feasibility of parameter identification algorithm and quality of the result will be assessed under different ice velocities.

2

Models of ice-induced vibration

2.1. Mathematical model

As introduced in chapter 1, many researchers address that the frequency lock-in can be described as a self-excitation phenomenon. Many self-excitation models have been proposed by mathematicians and engineers, for instance Lord Rayleigh [29], Van der Pol [7] and John E. Gibson [11]:

- Rayleigh differential equation: $\ddot{x} - \mu(1 - \frac{1}{3}\dot{x})\dot{x} + x = 0$
- Van der Pol equation: $\ddot{x} - \mu(1 - x^2)\dot{x} + x = 0$

An example phase portrait of the Rayleigh equation is shown below. The state of the system will grow at first due to the so-called negative damping in structural dynamics. After certain development time, the state will reach a limit circle, when the damping becomes positive.

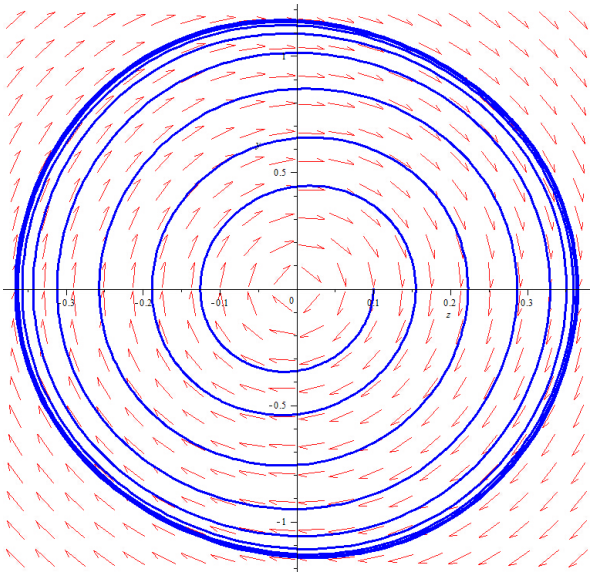

Figure 2.1: Example phase portrait of Rayleigh differential equation

Due to the fact that these equations only describe the self-excitation regardless of relating the physical properties of ice and structure, estimating the parameter in pure mathematical equations is impractical.

2.2. Mechanical model

In order to predict ice-structure interaction, H. Matlock used a mechanical model for simulation [23]. It simply consists of a mass-spring-dashpot system, representing a linear model of the elastic structure,

which is excited by elastic brittle bars moving on a kind of conveyor belt, representing the moving ice. At a certain deflection the bar, which is in contact with the mass, fails and the mass swings back until the next bar has moved forward and reaches contact with the mass. Recently, G. Huang et al [14] and H. Hendrikse et al [12] made some expansion of the Matlock model by taking the ice properties and randomness etc. into account.

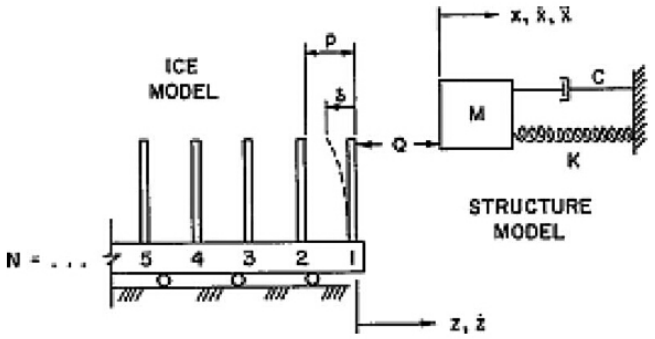

Figure 2.2: Dynamic ice-structure interaction model (courtesy of Matlock et al, 1969, 1971)

Similar to the Matlock model, T.S.J. van Dijk [34] used a stick-slip model as well as different friction models to simulate the ice-structure interaction. Good results have been obtained for the intermittent crushing and continuous brittle crushing range. Figure 2.3 presents the different friction model, with Y-axis stands for the friction and X-axis represents the relative velocity.

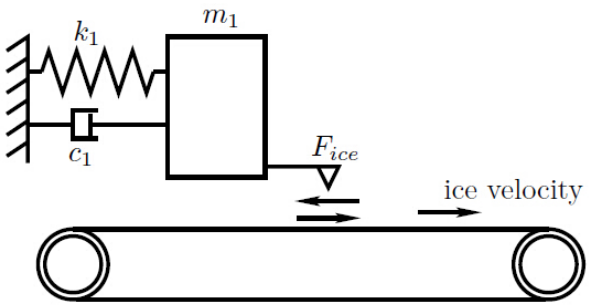

Figure 2.3: Stick-slip model (courtesy of T.S.J. van Dijk, 2015)

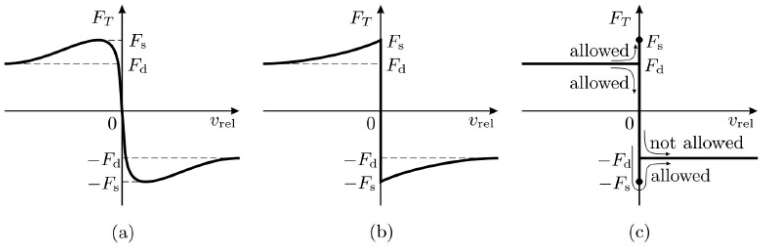

Figure 2.4: Friction models (courtesy of Leine and Nijmeijer [18], 2013)

2.3. Karna's numerical model

As briefly introduced in Chapter 1, Karna [17] proposed a numerical model by coupling the structure and undamaged ice field with a nonlinear element describing the crushing and cleaning process. The

numerical model can be summarized as follows:

$$M\ddot{u}_c(t) + C\dot{u}_c(t) + Ku_c(t) = F_c(t) \tag{2.1}$$

$$C_{ice}[\dot{w}_c(t) - v] + K_{ice}[w_c(t) - s_{ice}(t)] = -F_c(t) \tag{2.2}$$

$$F_c(t) = F_c[u(t) - w_c(t)] \tag{2.3}$$

$$s_{ice}(t) = vt - \sum_k \Phi(t - t_k) \tag{2.4}$$

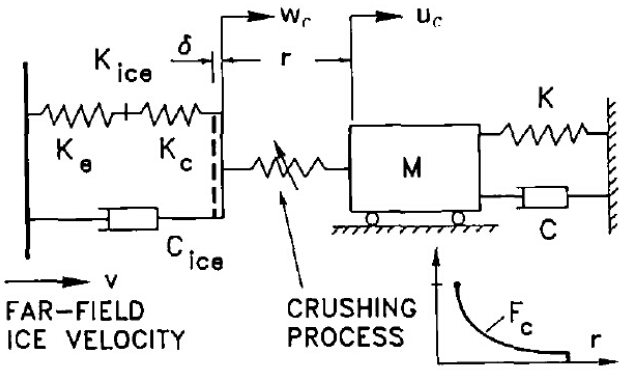

Figure 2.5: Karna's model for IIV of a single degree of freedom system (courtesy of [17],1989)

Equation (2.1) describes the dynamic properties of the structure. Equation (2.2) and (2.3) present the rushed ice between the structure and the ice sheet. While the last equation is used to represent the ice sheet undergoing damage at the ice edge.

2.4. Maattanen's numerical Model

In 1978, Prof. Maattanen proposed a self-excited numerical model [21] to describe the synchronized resonant type frequency lock-in of IIV which has been widely observed in full scale measurement [2]. Ice failure by crushing against a vertical offshore structure induces non-stationary loads. Even in the case of a narrow single pile structure there are always random variations in the total ice load.
The principle idea in his model is based on the ice crushing strength dependence on loading rate. In another word, the excitation force acting on the structure depend not only on the properties of ice, but also on the motion of structure. The existing of a special range in the ice crushing strength and stress rate curve ,Figure 2.6 [21], induces a so called **negative damping**.

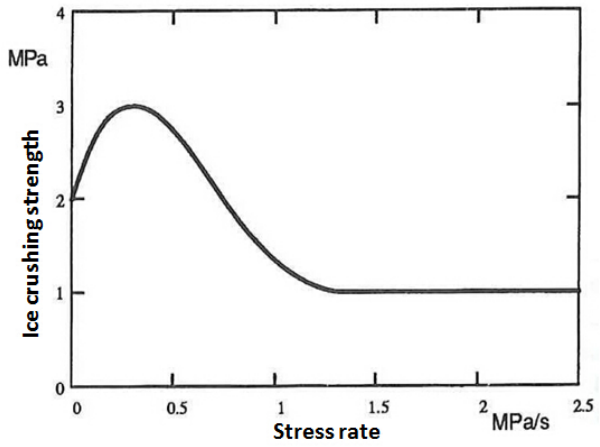

Figure 2.6: Ice Crushing Strength vs. Stress Rate

The numerical model can be summarized as follow[21].

$$\dot{\sigma} = (V_{ice} - \dot{u})\frac{8\sigma_0}{\pi D} \tag{2.5}$$

$$\sigma_c = \begin{cases} 0 & \dot{\sigma} < 0MPa/s \\ (7.8\dot{\sigma} - 18.57\dot{\sigma}^2 + 13\dot{\sigma}^3 - 2.91\dot{\sigma}^4 + 2) & 0MPa/s < \dot{\sigma} < 1.3MPa/s \\ 1 & 1.3MPa/s < \dot{\sigma} \end{cases} \tag{2.6}$$

$$F = A\sigma_c\sqrt{\frac{A_0}{A}} \tag{2.7}$$

$$F = m\ddot{u} + c\dot{u} + ku \tag{2.8}$$

The physical meaning of the above parameters are:

- σ_0:Reference ice strength
- D:Diameter of the cylindrical structure
- u:displacement of structure
- V_{ice}:Velocity of ice
- $\dot{\sigma}$:Stress rate
- σ_c:Ice crushing strength
- A_0:Reference area
- A:Projected crushing area
- m:Mass of structure
- c:Damping coefficient
- k:Stiffness of structure

Equation (2.6) uses a fourth order polynomial to describe the ice crushing strength between $0MPa/s$ stress rate to $1.3MPa/s$ stress rate, refer to figure 2.6. For $\dot{\sigma} < 0$, $\sigma_c$is zero (structure velocity larger than ice velocity). For $\dot{\sigma} > 1.3$, σ_c is constant $1MPa$.

2.5. Application of Maattanen's Numerical Model

In Prof. Maattanen's research, two different structures have been used to apply the numerical model described above – a three legged jacket platform and a caisson retained island [21]. By discretizing the big structure into finite element model, the system is regarded as multi-degree of freedom system.

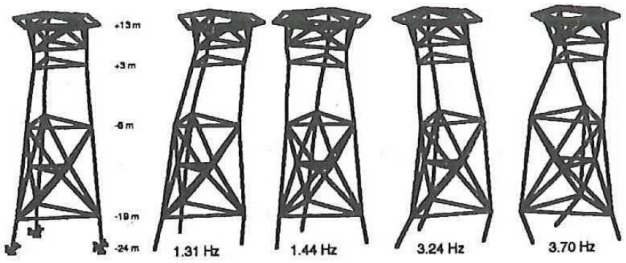

Figure 2.7: Three legged jacket platform [21]

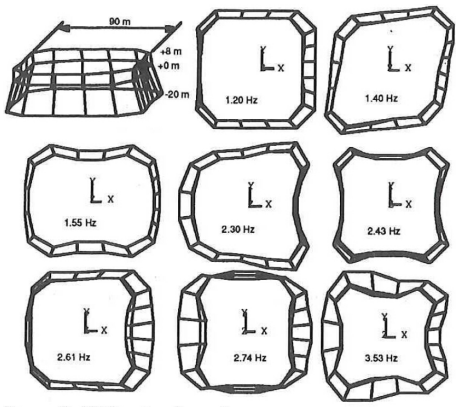

Figure 2.8: Caisson retained island [21]

2.6. Implementation of Numerical Model

In order to effectively estimate the parameters as well as verify the applicability of the identification techniques, only a single degree of freedom system will be used for simplicity.
Due to the constraint that no full scale measurement is available at the moment, artificial measurement data has been generated through applying the numerical model to a single degree of freedom system. All the parameters used in this thesis can be found in the table below.
By simulating the response using the parameters in table 2.1, displacement and velocity signals (with noise) can be obtained given a certain initial state using 4th order Runge-Kutta numerical method (”ODE45” in MATLAB). The detailed elaboration of numerical method solving differential equations can be found in Appendix A.

Table 2.1: Parameters for implementation

Parameter	Unit	Value
σ_0	MPa/s	2
D	m	1
A_0	m^2	1
A	m^2	0.5
m	Kg	50000
c	Ns/m	1000
k	kN/m	250
$V_{ice}(low)$	m/s	0.1
$V_{ice}(medium)$	m/s	0.18
$V_{ice}(high)$	m/s	0.3

Under different ice velocity, different part of the ice crushing strength and stress rate curve will be evoked. In the case of low ice velocity $0.1m/s$, σ_c only stays in the range of $\sigma_c < 1.3MPa/s$, which is called **polynomial range**. For high ice velocity of $0.3m/s$, the ice crushing strength is constant ($1MPa$),

constant range of $\sigma_c > 1.3MPa/s$ defines the excitation force. While at $V_{ice} = 0.18m/s$, σ_c crosses two ranges. **Mixed range** is used to denote this transition scenario.

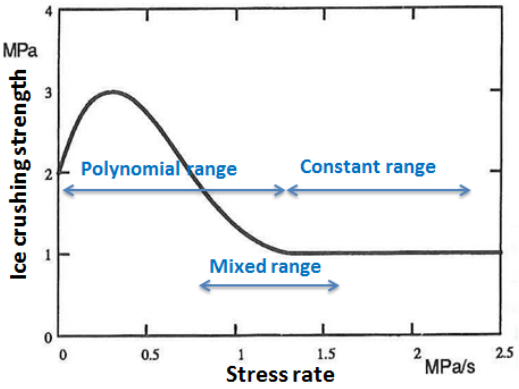

Figure 2.9: Ice Crushing Strength vs. Stress Rate

2.7. Noise Level

In order to simulate the inaccuracy of measurement instrument from electrical noise, white noise has been added to the generated response. In MATLAB, function ”RANDN” can be used to generate white noise with zero mean value and 1 standard deviation.
One can also generate white noise with zero mean and σ variance using ”$\sqrt{\sigma} * randn$”.
The term noise level is used to denote the noise intensity. The noise level is said to be 20% if script ”$20\% * \sqrt{\sigma_u} * randn$” is used in MATLAB, where σ_u is the variance of displacement, $20\% * \sqrt{\sigma_u}$ is the standard deviation of noise.
Below is the noise contaminated displacement signal. [1]

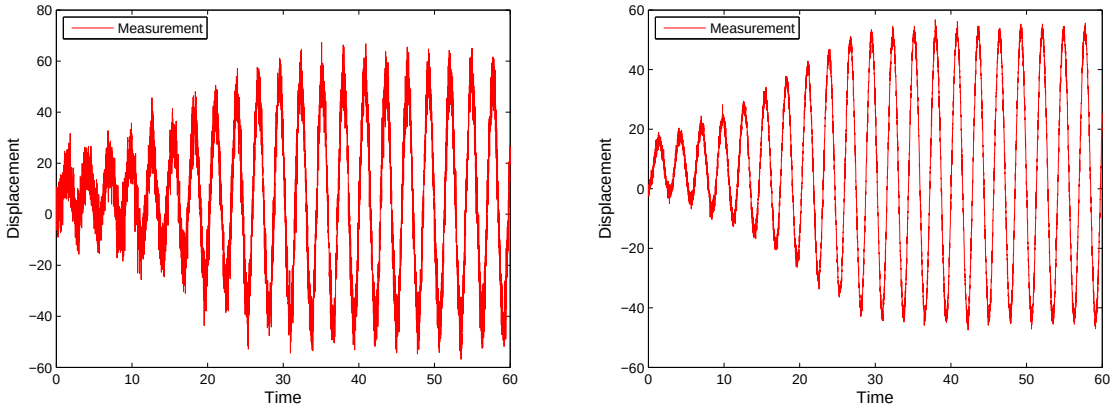

Figure 2.10: Measured displacement under 20%(left) and 5%(right) noise level ($\Delta t = 0.01s$)

2.8. Unknown Parameters

In Prof. Maattanen’s model, a **fourth** order polynomial of $\dot{\sigma}$ has been used to describe the ice crushing strength within range of $0MPa/s < \dot{\sigma} < 1.3MPa/s$.

[1] For simplicity, the unit for displacement is mm, and velocity is mm/s. This applys to the rest of the thesis.

$$\sigma_c = \begin{cases} 0 & \dot{\sigma} < 0MPa/s \\ (7.8\dot{\sigma} - 18.57\dot{\sigma}^2 + 13\dot{\sigma}^3 - 2.91\dot{\sigma}^4 + 2) & 0MPa/s < \dot{\sigma} < 1.3MPa/s \\ 1 & 1.3MPa/s < \dot{\sigma} \end{cases} \tag{2.9}$$

This thesis hold the assumption that all the parameters are known except the shape (including negative damping part) of the ice crushing strength and stress rate curve. So the objective of this thesis is to try to identify the five unknown parameters under $0MPa/s < \dot{\sigma} < 1.3MPa/s$ and the constant $1MPa/s$ under $1.3MPa/s < \dot{\sigma}$ given the "measured" noise contaminated state signal.
For simplicity, the unknown coefficients will be given its name in the following content as follows:

$$a = 7.8$$
$$b = -18.57$$
$$c = 13$$
$$d = -2.91$$
$$e = 2$$

2.9. Quality of measurement in polynomial range

It is obvious that if the measurement only covers small part of the polynomial range, $0MPa/s < \dot{\sigma} < 0.5MP/s$ for instance, in the ice crushing strength and stress rate curve, the estimation will undoubtedly fail due to the lack of information of $0.5MPa/s < \dot{\sigma}$. Thus the quality of the measurement first needs to be assessed under polynomial range.
In order to achieve this, the curve can be divided into different part, where the corresponding order of $\dot{\sigma}$ is dominating.

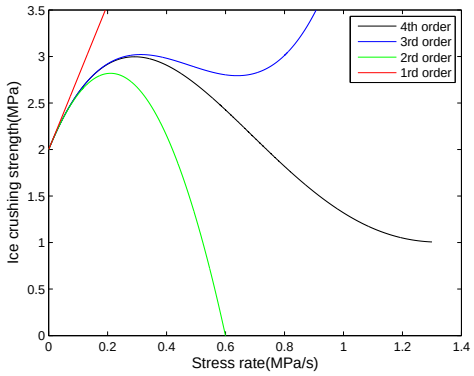

Figure 2.11: Comparison of ice crushing strength and stress rate curve with different order

In figure2.11 above, the 4th order line with black color stands for the full curve expression with 4th order of $\dot{\sigma}$, while the 3rd order line with blue color represents the expression with 3rd order, i.e. $7.8\dot{\sigma} - 18.57\dot{\sigma}^2 + 13\dot{\sigma}^3 + 2$. In this case, the $\dot{\sigma}^4$ term dominating the range of $0.3MPa/s < \dot{\sigma} < 1.3MPa/s$. Similary, the bifurcation point of two lines can approximately determine the range. Then the measurement allocated in each corresponding range can be counted. The result is as below for $\Delta t = 0.01s$ of $60s$ measurement without noise:

Table 2.2: Measurement allocation

$0 < \dot{\sigma} < 0.05$	$0.05 < \dot{\sigma} < 0.15$	$0.15 < \dot{\sigma} < 0.3$	$0.3 < \dot{\sigma} < 1.3$	Total
270	411	637	4330	5648

From the number of measurement allocated in each range, one can conclude that the measurement under $V_{ice} = 0.1m/s$ is qualified for identifying the polynomial range.

3

Least squares method

3.1. Least squares method

Speaking of identification problem, the most basic algorithm may be least squares (abbreviated as LS) method, invented by Carl Friedrich Gauss for calculating the orbits of celestial bodies. The LS method can be regarded as a way to solve an overdetermined problem. Suppose vector x with size of n in the below equation needs to be solved.

$$\mathbf{Ax} = \mathbf{b} \tag{3.1}$$

Where **A** is a $m \times n$ matrix ($m > n$), while **b** is an $m \times 1$ vector. The number of equations (m) is assumed to be larger than the unknowns (n). Theoretically, a perfect **x** that fulfills all m equations cannot be found. But a good solution that minimize the cost function S below can be found by means of LS method.

$$\mathbf{x} = (\mathbf{A}^T\mathbf{A})^{-1}\mathbf{A}^T\mathbf{b} \tag{3.2}$$

$$S = ||\mathbf{Ax\text{-}b}||_2 \tag{3.3}$$

For example, LS method can be used to find the best straight line go through the points in a two dimensional coordinate.

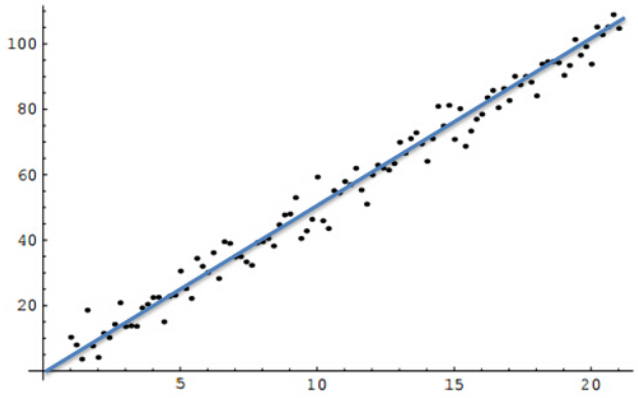

Figure 3.1: LS method for line fitting

3.2. LS method for IIV

Recall the equations from Maattanen's numerical model:

$$\dot{\sigma} = (V_{ice} - \dot{u})\frac{8\sigma_0}{\pi D} \tag{3.4}$$

$$\sigma_c = \begin{cases} 0 & \dot{\sigma} < 0MPa/s \\ (a\dot{\sigma} + b\dot{\sigma}^2 + c\dot{\sigma}^3 + d\dot{\sigma}^4 + e) & 0MPa/s < \dot{\sigma} < 1.3MPa/s \\ 1 & 1.3MPa/s < \dot{\sigma} \end{cases} \tag{3.5}$$

$$F = A\sigma_c\sqrt{\frac{A_0}{A}} \tag{3.6}$$

$$F = m\ddot{u} + c\dot{u} + ku \tag{3.7}$$

If attention is only put on the polynomial range of $0MPa/s < \dot{\sigma} < 1.3MPa/s$, the above set of equations can be simplified as:

$$m\ddot{u} + c\dot{u} + ku = A\sqrt{\frac{A_0}{A}}(a\dot{\sigma} + b\dot{\sigma}^2 + c\dot{\sigma}^3 + d\dot{\sigma}^4 + e)$$

$$\dot{\sigma} = (V_{ice} - \dot{u})\frac{8\sigma_0}{\pi D}$$

The acceleration $\ddot{u}$ can be measured in experiment by means of accelerometer. Moreover, the velocity $\dot{u}$ and displacement u can be obtained by the integration of $\ddot{u}$, or simply measured in lab. In this case, $\dot{\sigma}$ can also be derived given V_{ice}, with only parameters to be identifieda, b, c, d unknown.
Rewrite the equation as:

$$\dot{\sigma}a + \dot{\sigma}^2 b + \dot{\sigma}^3 c + \dot{\sigma}^4 d + e = y \tag{3.8}$$

$$y = \frac{m\ddot{u} + c\dot{u} + ku}{\sqrt{A_0 A}} \tag{3.9}$$

Compared with equation (3.1), then y comprise the entry of **b** vector; unknowns a, b, c, d, e comprise the **x** vector with dimension 5×1; $\dot{\sigma}$ comprise the **A** matrix.
For constant range, the equation is supposed to be:

$$e = y \tag{3.10}$$

$$y = \frac{m\ddot{u} + c\dot{u} + ku}{\sqrt{A_0 A}} \tag{3.11}$$

However, due to the fact that in which range of the ice crushing strength and stress rate the measured signal is, is unknown, equation (3.8) is used for low ice velocity (polynomial range), high ice velocity (constant range) and medium ice velocity (mixture range) without loss of generality.

3.3. Formulation

From the derivation in the previous section, LS method seems to be one of the ways to estimate the parameters.
The measurement time step Δt should be constrained within:

$$\frac{T}{20} < \Delta t < \frac{T}{5} \tag{3.12}$$

Where $T = 3s$ is the period of vibration. The result below is on the base of $\Delta t = 0.4s$
After obtaining the displacement u, velocity $\dot{u}$ and acceleration $\ddot{u}$ at different time steps, enormous

equation in the form of equation(3.8) can be obtained.

$$\begin{aligned}
\dot{\sigma}_1 a + \dot{\sigma}_1^2 b + \dot{\sigma}_1^3 c + \dot{\sigma}_1^4 d + e &= y_1 \\
\dot{\sigma}_2 a + \dot{\sigma}_2^2 b + \dot{\sigma}_2^3 c + \dot{\sigma}_2^4 d + e &= y_2 \\
\dot{\sigma}_3 a + \dot{\sigma}_3^2 b + \dot{\sigma}_3^3 c + \dot{\sigma}_3^4 d + e &= y_3 \\
\dot{\sigma}_4 a + \dot{\sigma}_4^2 b + \dot{\sigma}_4^3 c + \dot{\sigma}_4^4 d + e &= y_4 \\
\dot{\sigma}_5 a + \dot{\sigma}_5^2 b + \dot{\sigma}_5^3 c + \dot{\sigma}_5^4 d + e &= y_5 \\
&\dots
\end{aligned}$$

Rewrite the above set of equations as:

$$\begin{bmatrix}
\dot{\sigma}_1 & \dot{\sigma}_1^2 & \dot{\sigma}_1^3 & \dot{\sigma}_1^4 & 1 \\
\dot{\sigma}_2 & \dot{\sigma}_2^2 & \dot{\sigma}_2^3 & \dot{\sigma}_2^4 & 1 \\
\dot{\sigma}_3 & \dot{\sigma}_3^2 & \dot{\sigma}_3^3 & \dot{\sigma}_3^4 & 1 \\
\dot{\sigma}_4 & \dot{\sigma}_4^2 & \dot{\sigma}_4^3 & \dot{\sigma}_4^4 & 1 \\
\dot{\sigma}_5 & \dot{\sigma}_5^2 & \dot{\sigma}_5^3 & \dot{\sigma}_5^4 & 1 \\
\dots & & & &
\end{bmatrix}
\begin{bmatrix} a \\ b \\ c \\ d \\ e \end{bmatrix}
=
\begin{bmatrix} y_1 \\ y_2 \\ y_3 \\ y_4 \\ y_5 \\ \dots \end{bmatrix} \tag{3.13}$$

The above equation has already been written in the form of :

$$\mathbf{Ax} = \mathbf{b}$$

The vector contains the unknown parameters can be estimated by:

$$\mathbf{x} = (\mathbf{A}^T\mathbf{A})^{-1}\mathbf{A}^T\mathbf{b}$$

3.4. Result

3.4.1. Result for low ice velocity

Under low ice velocity of $0.1m/s$, only the polynomial range will be evoked. The figure below is the ice crushing strength and stress rate curve, with the green part indicating the different points traversed during the simulation.

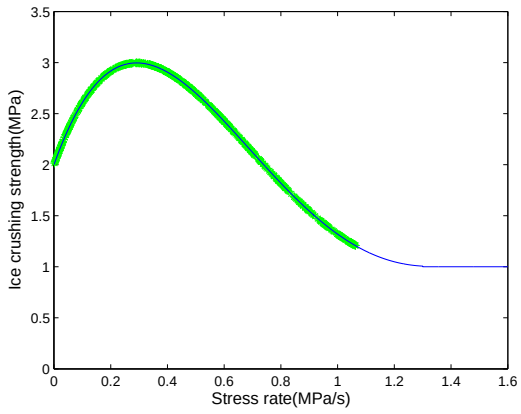

Figure 3.2: Ice crushing strength and stress rate curve for low ice velocity

For simplicity, artificially generated **clean** signals of $\ddot{u}$,$\dot{u}$ and u without noise will first be used to beta test the applicability of LS method. The displacement, velocity can be obtained by numerical method (ODE45 in MATLAB) as follows, with acceleration calculated from displacement and velocity:
In order to use equation (3.2) to implement the LS method, only the $\ddot{u}$,$\dot{u}$ and u data can be used to construct **A** and **b** when the corresponding $\dot{\sigma}$ locates within the range of $0MPa/s < \dot{\sigma} < 1.3MPa/s$. Data points falling outside this range are removed from the set. The result for the LS method under

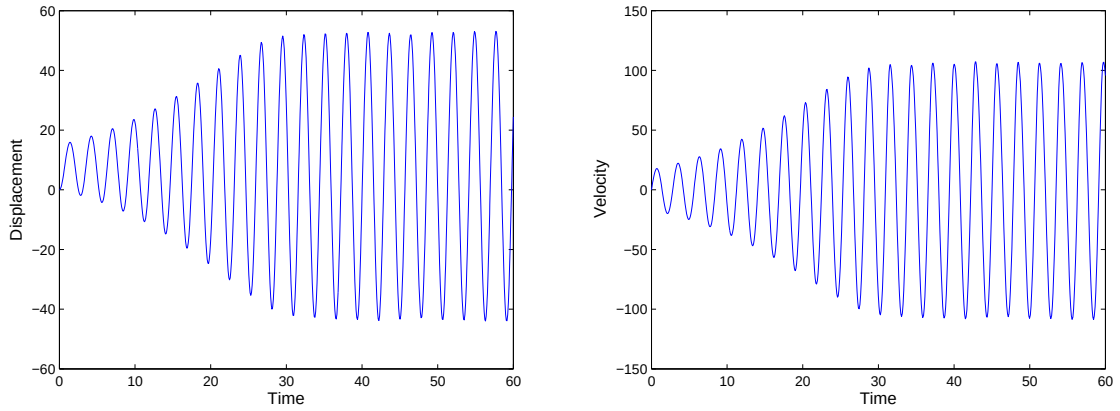

Figure 3.3: Displacement and velocity($\Delta t = 0.4s$, Noise:0%)

$\Delta t = 0.4s$ is:

$$\begin{bmatrix} a \\ b \\ c \\ d \\ e \end{bmatrix} = \begin{bmatrix} 7.8000 \\ -18.5700 \\ 13.0000 \\ -2.9100 \\ 2.0000 \end{bmatrix} \tag{3.14}$$

Which is exactly the same as the target value.
In this case, the LS method works well under zero noise level.
In order to simulate the noise from measurement instrument, noise with level of 5% will be added to the data. The concept of noise level has been introduced in the previous chapter. The displacement and velocity is shown in Figure 3.4.

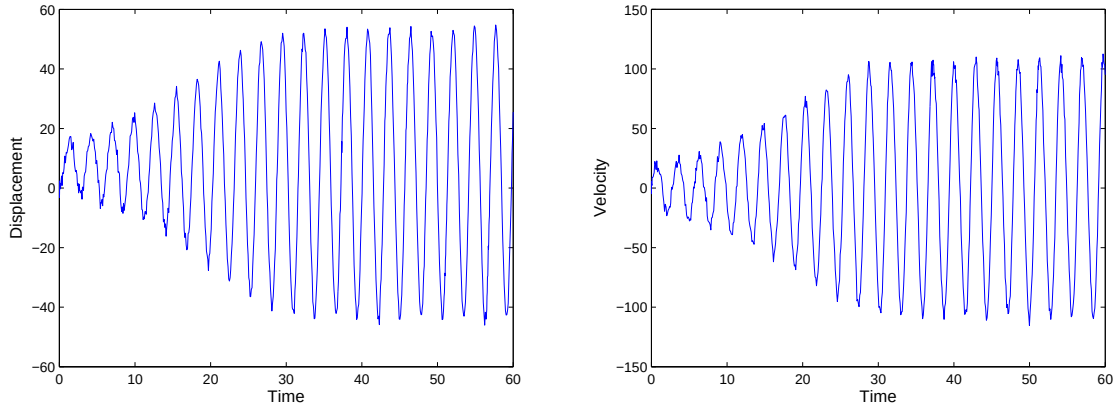

Figure 3.4: Displacement and velocity($\Delta t = 0.4s$,Noise:5%)

Even though noise has been added, again only the $\ddot{u}$,$\dot{u}$ and u data can be used to construct **A** and **b** when the corresponding $\dot{\sigma}$ locates within the range of $0MPa/s < \dot{\sigma} < 1.3MPa/s$. The result is :

$$\begin{bmatrix} a \\ b \\ c \\ d \\ e \end{bmatrix} = \begin{bmatrix} 11.0423 \\ -28.5861 \\ 24.4767 \\ -7.2706 \\ 1.7161 \end{bmatrix} \tag{3.15}$$

It is obvious that the estimated parameters under 5% noise level is not even near the target value.
The ice crushing strength and stress rate curve as well as the response is as follows:

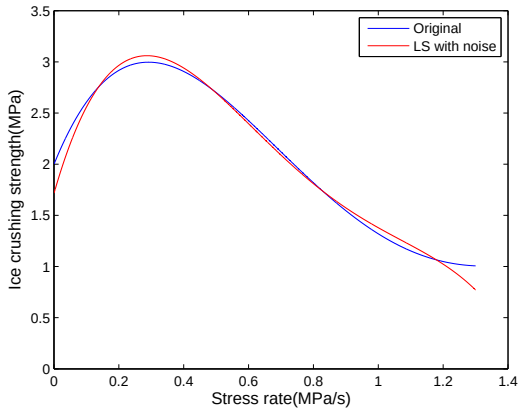

Figure 3.5: Ice strength and stress rate comparison between original and LSM (Noise:5%)

Due to the impact from the noise, it is obvious that there are some difference between the original curve and the result from LS method. Nevertheless, the response of the structure can still be regenerated based on the estimated parameters in comparison with original response.
Figure 3.6 presents the difference between the regenerated response and the original one. From the

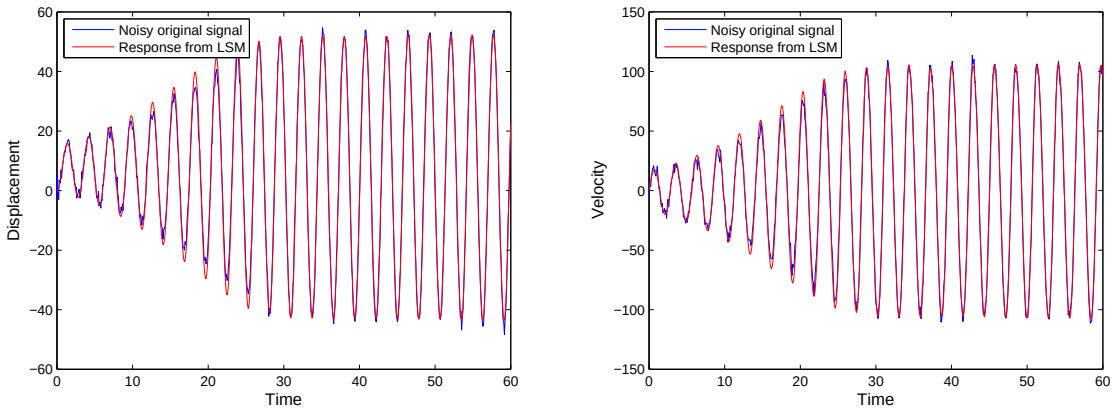

Figure 3.6: Displacement and velocity comparison between original and LS method (Noise:5%)

above figures, there indeed exists some difference between the response on the bases of estimation and original one, especially when the displacement(velocity) is developing.
Meanwhile, the author found that when the noise in the signal is regenerated by means of ”RANDN” with the same noise level again, the estimated parameters will change too.

3.4.2. Result for high ice velocity

Under high ice velocity of $0.3m/s$, the ice crushing strength is constant $1MPa$, which means the ice action is constant. Only the constant range will be evoked. Figure 3.7 below is the ice crushing strength and stress rate curve, with the green part be evoked.
Unfortunately, the result of the LS method is very poor due to the condition number of **A** in equation (3.13) is approximately $2e-18$ whatever Δt is. The singular value of **A** under constant range is shown in Appendix B. This means many rows in equation (3.13) are dependent with each other. Even though large amount of signal can be measured at each time step, they only contains the same information. The lack of information result in the failure of LS method in the case of high ice velocity.

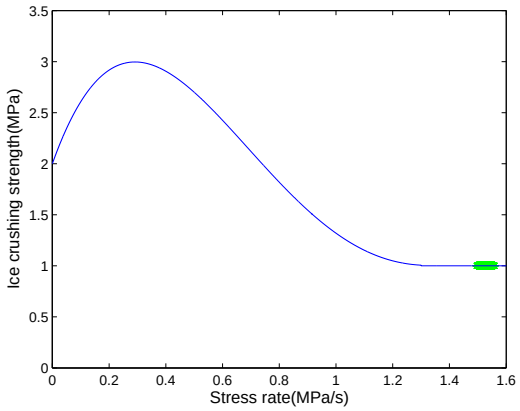

Figure 3.7: Ice crushing strength and stress rate curve for high ice velocity

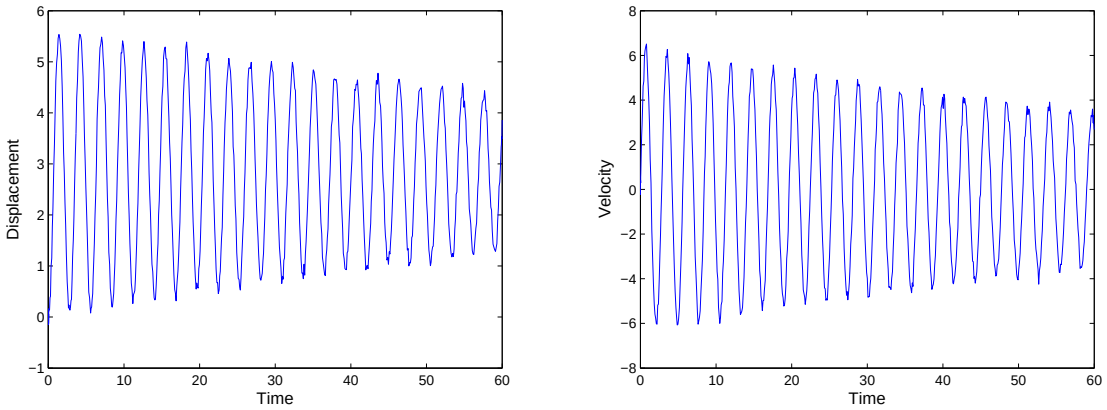

Figure 3.8: Displacement and velocity($\Delta t = 0.4s$,Noise:5%)

3.4.3. Result for medium ice velocity

In the case of $0.18m/s$ ice velocity, both the polynomial range and the constant range will be evoked, as the green part shown in Figure 3.9.

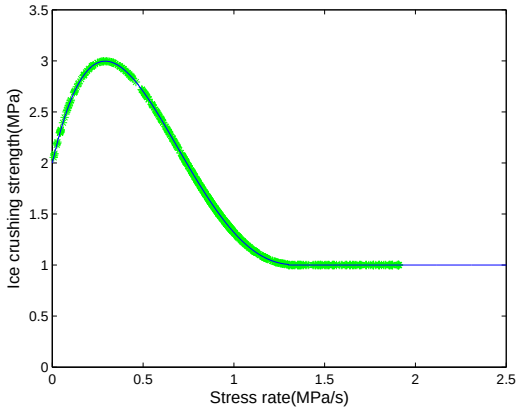

Figure 3.9: Ice crushing strength and stress rate curve for medium ice velocity

The response signal is shown in Figure 3.10

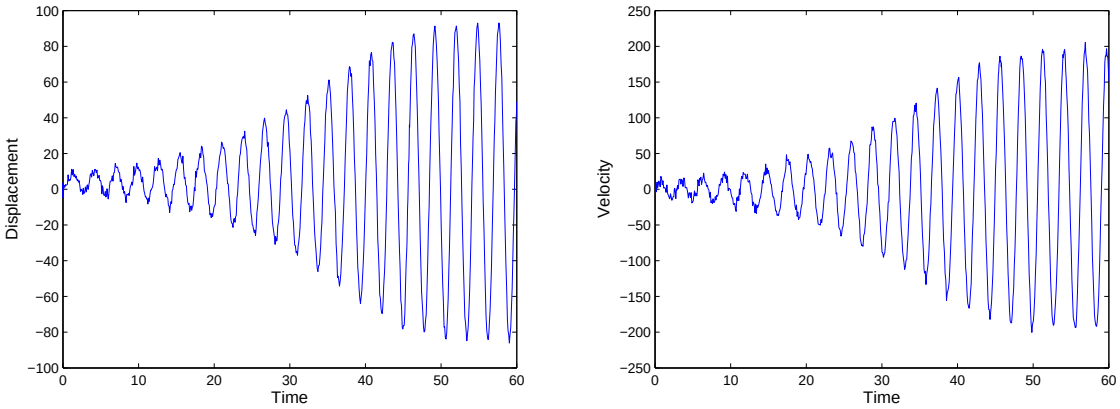

Figure 3.10: Displacement and velocity($\Delta t = 0.1s$,Noise:5%)

The result of the LS method for the mixture range is:

$$\begin{bmatrix} a \\ b \\ c \\ d \\ e \end{bmatrix} = \begin{bmatrix} 13.7851 \\ -28.5670 \\ 19.3033 \\ -4.2333 \\ 0.9747 \end{bmatrix} \tag{3.16}$$

A comparison between the original curve and the estimation one can be made in Figure 3.11.

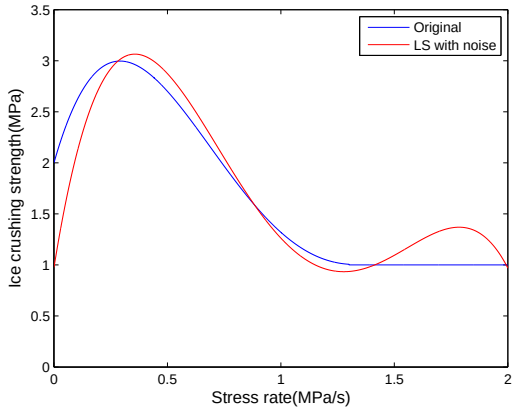

Figure 3.11: Ice strength and stress rate comparison bewteen original and LS method (Noise:5%)

It is obvious that there exist distinct difference between the original ice crushing strength and stress rate curve and the estimated one.

3.5. Conclusion

Under the low ice velocity of $0.1m/s$, the estimated parameters reach the target value under zero noise level by removing the data outside of $0MPa/s < \dot{\sigma} < 1.3MPa/s$. However, in the case of 5% noise level, good result of estimation cannot be obtained. The identified shape of the ice crushing strength and stress rate curve is also different from the original curve. The response, generated from the estimated parameters, has obvious difference from the original response, especially when the state is developing. The reason why LS method fails is that all the matrix and vector in LS method are based on equation below when $0MPa/s < \dot{\sigma} < 1.3MPa/s$:

$$\dot{\sigma}a + \dot{\sigma}^2 b + \dot{\sigma}^3 c + \dot{\sigma}^4 d + e = \frac{m\ddot{u} + c\dot{u} + ku}{\sqrt{A_0 A}}$$

Some data points originally belonging to the range of $\dot{\sigma} < 0MPa/s$, cannot be distinguished as belonging to $\dot{\sigma} < 0MPa/s$ anymore due to the presence of noise, can enter into the set, in the meantime bringing information of $\sigma_c = 0MPa$ into the LS method. Unlike the removal in the case of zero noise level, these bad data cannot be prevented contaminating the estimation. While for data with $\dot{\sigma} > 1.3MPa/s$, the result will not be influenced due to the continuity at $\dot{\sigma} = 1.3MPa/s$. So it is the discontinuity at $\dot{\sigma} = 0MPa/s$ makes the LS method fail under 5% noise level. It has been proved that the LS method can success by removing more data near $\dot{\sigma} = 0MPa/s$, which again verify the reason of discontinuity. In the case of high ice velocity of $0.3m/s$, the result is not reliable any more due to the lack of information.

For medium velocity of $0.18m/s$, the stress rate crosses both the polynomial range and the constant range. The estimated ice crushing strength and stress rate curve differs from the original one. One can imagine that using one polynomial formula to describe both the polynomial range and the constant range is difficult.

4

Kalman filter theory

This chapter will introduce another state of art estimation technique ——the Kalman filter. The ultimate goal of this chapter is to introduce extended Kalman filter, an recursive filter designed for non-linear dynamic system, combining the information from dynamic properties of system and the noisy observation.

4.1. State propogation

The state of the dynamic system cannot be precisely determined due to the noisy measurement. So at each measurement step, one can only more or less ”guess” what the state is. Using modern scientific approach of probability theory, this ”guessed state” can be described as a random variable with mean value and variance. The state also changes with time in a dynamic system.

4.2. Difference equation and differential Equation

Suppose X is a state vector.
The differential equation is as follows

$$\dot{X} = f(X)$$

and can also be represented in the form of a difference equation:

$$X_{k+1} = f_k(X_k)$$

Where f and f_k describe the dynamic properties of system.
It can be easily understood that in order to know how the state propagate in time, the differential equation has to be integrated. However, the difference equation can be directed implemented by using X_k to get X_{k+1}. Due to the fact that the measurement signal can only be obtained at discrete time steps, the advantage of using difference equation is obvious.
If the system is linear, then the difference equation can be written as:

$$X_{k+1} = F_k X_k$$

4.3. Euler method

In order to use the discrete time measurement, the differential equation of numerical model described in Chapter 2 has to be transformed into difference equation.
For linear systems, one can easily transform the differential equation into a difference equation with the help of the matrix exponential.
Unfortunately, for nonlinear dynamic systems, it’s not possible to write the dynamic system in the form of a difference equation without any approximation. In this case, several numerical method, Euler method, Mid Point method, Runge-Kutta method for example, can be helpful in deriving the difference equation. More information on numerical methods can be found in Appendix A. In this thesis, the simplest method – Euler Method is used as a starting point.

The basic idea behind Euler method is that, the state of X_{k+1} can be approximated through the summation of X_k and its gradient times time the step ΔT, i.e.

$$X_{k+1} = X_k + f(X_k)\Delta t$$

Where Δt is the time step between $k+1$ and k
Then

$$\begin{aligned} X_{k+1} &= f_k(X_k) \\ &= X_k + f(X_k)\Delta t \end{aligned}$$

Here, through Euler method, the difference equation for the nonlinear system is obtained.

4.4. Measurement update

In order to better illustrate how the state of a dynamic system recursively propagates with time, we first define different state name.
$X_K{}^-$ stands for the state *apriori* to the measurement at k, while $X_K{}^+$ stands for the state *posteriori* to the measurement at k.

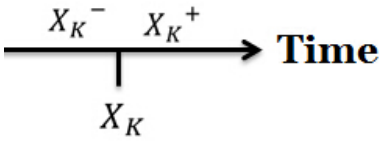

Figure 4.1: Apriori state and posteriori state

4.5. Linear Kalman Filter

In this section, the heritage of Rudolf E. Kalman - Linear Kalman Filter will be introduced, which considers discrete time dynamics and discrete time measurements. This situation is often encountered in practice. The Kalman filter operates by propagating the mean and covariance of the state through time.
Suppose we have a linear discrete-time system given as follows,

$$\begin{aligned} X_{k+1} &= F_k X_k \\ y_k &= H_k X_k + V_k \end{aligned}$$

Where H_k is the observation matrix, y_k is the measurement. Due to the fact that the measurement is not necessary to be each entries of vector X_k, but the linear combination of them, the observation matrix H_k is used to represent the combination. V_k,which has the same size of y_k, stands for the measurement white noise with zero mean value and variance for each entry,i.e.

$$V_k \sim (0, R_k)$$

where, R_k is used to describe the variance, by including the variance of each entry of V_k in the corresponding diagonal element in R_k.
The Linear Kalman Filter algorithm can be summarized into three steps. The recursive iteration of these three steps with $k = 1, 2, 3\ldots$ comprise the whole filtering process.

1. **Initiate Kalman Filter**

$$\hat{X}_0^+ = E(X_0) \tag{4.1}$$
$$P_0^+ = E[(X_0 - \hat{X}_0^+)(X_0 - \hat{X}_0^+)^T] \tag{4.2}$$

2. **State Update through dynamic property**

$$\hat{X}_k^- = F_{k-1}\hat{X}_{k-1}^+ \tag{4.3}$$
$$P_k^- = F_{K-1}P_{k-1}^+F_{K-1}^T \tag{4.4}$$

3. **State Update through measurement**

$$K_k = P_k^- H_k^T (H_k P_K^- H_k^T + R_k)^{-1} \tag{4.5}$$
$$\hat{X}_k^+ = \hat{X}_k^- + K_k(y_k - H_k\hat{X}_k^-) \tag{4.6}$$
$$P_k^+ = (I - K_k Hk)P_{k-1}^- \tag{4.7}$$

In the above notation, $\hat{X}_k$ is the estimated state vector, i.e. the filtered state, while the P matrix defines the variance of the state vector. If the diagonal element of P matrix decrease with time step, then the filtered state is more close to the true state, which means more precise and reliable estimated state vector obtained.
Both $\hat{X}_0^+$ and P_0^+ needs to be assigned of an initial value.
Equation (4.3) and (4.4) describe how the mean value $\hat{X}_{k-1}^+$ changes to $\hat{X}_k^-$, as well as the variance from P_{k-1}^+ to P_k^-.
Once the measurement is obtained, a weighted difference between measurement and priori state will be used to correct the apriori state $\hat{X}_k^-$ to posteriori state $\hat{X}_k^+$ with the help of the K matrix (Kalman gain). Meanwhile, the variance matrix will also be updated to posteriori variance matrix. The Kalman gain takes both the noise level and the variance of the apriori state into account. In the end, when the variance approaches to zero, then the state vector can be considered as the final estimated vector.
The Kalman Filter can be briefly illustrated as in Figure 4.2

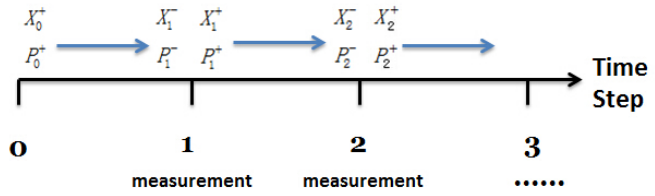

Figure 4.2: Kalman Filter

4.6. Extended Kalman Filter

The Linear Kalman Filter can only be applied to linear systems due to the intrinsic property. For non-linear systems, using equation (4.3) and (4.4) to calculate the updated mean value and variance is not applicable any more. However, this algorithm can still be expanded to the extended Kalman filter(abbreviated as EKF) to handle weak nonlinearity.
Suppose we write the dynamic system in the form of difference equation using the Euler method.

$$X_{k+1} = f_k(X_K)$$
$$y_k = h_k(X_k, V_k)$$
$$V_k \sim (0, R_k)$$

Where f_k represents the dynamic properties, y_k is the measured state at time step k, h_k is the observation matrix, V_k is the measurement noise vector with 0 mean value, and R_k variance.
The tricky part of nonlinear system is that the difference equation (observation matrix neither) cannot be written in the form of $X_{k+1} = F_k X_k$, but can only be written as $X_{k+1} = f_k(X_K)$. Due to this complexity, the variance cannot be updated using equation (4.4). In EKF, the derivative of f_k with the state vector X_k will be applied instead. This derivative is also called the **Jacobian Matrix**.
The EKF can be summarized as follows.[5]

1. **Initiate Extended Kalman Filter**

$$\hat{X}_0^+ = E(X_0) \tag{4.8}$$
$$P_0^+ = E[(X_0 - \hat{X}_0^+)(X_0 - \hat{X}_0^+)^T] \tag{4.9}$$

2. **State Update through dynamic property**

$$\hat{X}_k^- = f_{k-1}(\hat{X}_{k-1}^+) \tag{4.10}$$
$$F_{k-1} = \left.\frac{\partial f_{k-1}}{\partial X_k}\right|_{\hat{X}_{k-1}^+} \tag{4.11}$$
$$P_k^- = F_{K-1} P_{k-1}^+ F_{K-1}^T \tag{4.12}$$

3. **State Update through measurement**

$$K_k = P_k^- H_k^T (H_k P_K^- H_k^T + M R_k M^T)^{-1} \tag{4.13}$$
$$\hat{X}_k^+ = \hat{X}_k^- + K_k(y_k - h_k(\hat{X}_k^-, 0)) \tag{4.14}$$
$$P_k^+ = (I - K_k H_k) P_{k-1}^- \tag{4.15}$$

Except the state update through dynamic property, other steps in EKF is the same to Linear Kalman Filter.

4.7. Parameter Estimation for IIV

Sometimes an engineer or researcher only wants to estimate the unknown constant or slow time varying parameter(s) of a dynamic system, regardless of filtering the noise in the measurement. In this case, the EKF can also play an important role, even though the system equations are nonlinear functions of the unknown parameter(s).
Applying the EKF, a parameter estimation problem can be solved by regarding the unknown parameter(s) as state variable in the state vector, i.e. augmenting the state vector.

$$X_k' = \begin{bmatrix} X_k \\ a \end{bmatrix}$$

In the above augmented vector, $\hat{X}_k$ is the original estimated state vector, while a is the parameter that needs to be identified. Using the newly defined state vector, the parameter estimation can be solved by following the recursive update algorithm described in the previous section.
In the case of ice induced vibration, we assumed that the five coefficients ,i.e. $7.8, -18.57, 13, -2.91, 2$, respectively are unknown.
The full state vector for four parameters estimation then becomes

$$\begin{bmatrix} u \\ v \\ a \\ b \\ c \\ d \\ e \end{bmatrix}$$

Where u stands for the displacement of the structure, v represents the velocity, and a, b, c, d, e denote the coefficients to be identified, with target values of $7.8, -18.57, 13, -2.91$ and 2.

The differential equation is:

$$\dot{X} = \begin{bmatrix} \dot{u} \\ \dot{v} \\ \dot{a} \\ \dot{b} \\ \dot{c} \\ \dot{d} \\ \dot{e} \end{bmatrix} = \begin{bmatrix} v \\ F/m - ku/m - cv/m \\ 0 \\ 0 \\ 0 \\ 0 \\ 0 \end{bmatrix}$$

In the above differential equation, the first two rows comes from the equation of dynamic system. The rest four rows have been established on the assumption that the four parameters are constants.
Using Euler Method, the difference equation can be written as

$$X_{k+1} = \begin{bmatrix} u_{k+1} \\ v_{k+1} \\ a_{k+1} \\ b_{k+1} \\ c_{k+1} \\ d_{k+1} \\ e_{k+1} \end{bmatrix} = \begin{bmatrix} u_k \\ v_k \\ a_k \\ b_k \\ c_k \\ d_k \\ e_k \end{bmatrix} + \begin{bmatrix} \dot{u} \\ \dot{v} \\ \dot{a} \\ \dot{b} \\ \dot{c} \\ \dot{d} \\ \dot{e} \end{bmatrix} \times \Delta t \tag{4.16}$$

$$= \begin{bmatrix} u_k + v_k \Delta t \\ v_k + (F/m - ku_k/m - cv_k/m)\Delta t \\ a_k \\ b_k \\ c_k \\ d_k \\ e_k \end{bmatrix} \tag{4.17}$$

Where F is calculated as:

$$F = A\sigma_c \sqrt{\frac{A_0}{A}}$$

$$\dot{\sigma} = (V_{ice} - v_k)\frac{8\sigma_0}{\pi D}$$

$$\sigma_c = \begin{cases} 0 & \dot{\sigma} < 0MPa/s \\ (a\dot{\sigma} + b\dot{\sigma}^2 + c\dot{\sigma}^3 + d\dot{\sigma}^4 + e) & 0MPa/s < \dot{\sigma} \end{cases}$$

Equation (4.17) can be used to calculate the update of the mean value through the dynamic property, with its jacobian matrix to calculate the variance.
Only the displacement and velocity can be measured; The observation equation thus becomes:

$$y_k = \begin{bmatrix} 1 & 0 & 0 & 0 & 0 & 0 & 0 \\ 0 & 1 & 0 & 0 & 0 & 0 & 0 \end{bmatrix} X_k + V_k$$

$$V_k = \begin{bmatrix} v^1 \\ v^2 \end{bmatrix}$$

$$V_k \sim (0, R)$$

where the diagonal matrix R denotes the variance of noise v^1 and v^2 (with diagonal entry equalalent to the variance).
For instance, the R matrix is supposed to be $\begin{bmatrix} (20\%\sqrt{\sigma_u})^2 & 0 \\ 0 & (20\%\sqrt{\sigma_v})^2 \end{bmatrix}$ for 20% noise level both for displacement and velocity, where σ_u and σ_v is the variance of displacement and velocity respectively.
Here, apart from the noise level, let's define the concept of the R matrix level. It is said that the R matrix level is 20% for $R = \begin{bmatrix} (20\%\sqrt{\sigma_u})^2 & 0 \\ 0 & (20\%\sqrt{\sigma_v})^2 \end{bmatrix}$. During the EKF, the R matrix level is supposed to be

equal to the noise level. But sometime, this cannot be achieved due to the lack of information prior to the measurement. Thus the incorrectness of R may have influence on the result.
Similar to the LS method, the EKF will be used for all the ice velocities, in order to investigate the applicability for identifying different part of the ice crushing strength and stress rate curve.

5

EKF for low ice velocity

In this chapter, the extended Kalman filter will be implemented for parameter estimation for low ice velocity, which only unveils the polynomial range. Due to the complexity of five parameters estimation, step by step, one parameter estimation will first be carried out as a starting point.

5.1. Mathematical formulation

This section is based on the assumption that all the five coefficients are unknown. Then the augmented state vector to be:

$$X_k = \begin{bmatrix} u \\ v \\ a \\ b \\ c \\ d \\ e \end{bmatrix}$$

Where u stands for the displacement, v represent the velocity, and the rest are unknown coefficients. By means of Euler method, the difference equation can be written as:

$$X_{k+1} = \begin{bmatrix} u_{k+1} \\ v_{k+1} \\ a_{k+1} \\ b_{k+1} \\ c_{k+1} \\ d_{k+1} \\ e_{k+1} \end{bmatrix} = \begin{bmatrix} u_k + v_k \Delta t \\ v_k + (F/m - ku_k/m - cv_k/m)\Delta t \\ a_k \\ b_k \\ c_k \\ d_k \\ e_k \end{bmatrix}$$

Where F to be:

$$F = A\sigma_c \sqrt{\frac{A_0}{A}}$$

$$\dot{\sigma} = (V_{ice} - v_k)\frac{8\sigma_0}{\pi D}$$

$$\sigma_c = \begin{cases} 0 & \dot{\sigma} < 0MPa/s \\ (a\dot{\sigma} + b\dot{\sigma}^2 + c\dot{\sigma}^3 + d\dot{\sigma}^4 + e) & 0MPa/s < \dot{\sigma} \end{cases}$$

The observation is:

$$y_k = \begin{bmatrix} 1 & 0 & 0 & 0 & 0 & 0 & 0 \\ 0 & 1 & 0 & 0 & 0 & 0 & 0 \end{bmatrix} X_k + V_k$$
$$V_k = \begin{bmatrix} v^1 \\ v^2 \end{bmatrix}$$
$$V_k \sim (0, R)$$

Where diagonal matrix R denotes the variance of noise v^1 and v^2 (with diagonal entry equals to the variance).
Recall equation (2.13) and (2.14)

$$H_k = \begin{bmatrix} 1 & 0 & 0 & 0 & 0 & 0 & 0 \\ 0 & 1 & 0 & 0 & 0 & 0 & 0 \end{bmatrix}$$

Here we obtain the nonlinear difference equation which has the form of $X_{k+1} = f(X_k)$ in equation (3.1).
Summon up equation (2.10) that calculate the **Jacobian Matrix**

$$F_k = \left. \frac{\partial f_k}{\partial X_k} \right|_{\hat{X}_k^+}$$

Naturally, one can be inspired that the Jacobian Matrix is supposed to be a “piecewise matrix” due to the piecewise property of force F.
Here, we directly write out the Jacobian Matrix. Anyone who is interested can also derive it with a bit effort.
Jacobian Matrix:
For $0MPa/s < \dot{\sigma}$

$$F_k = \begin{bmatrix} 1 & \Delta t & 0 & 0 & 0 & 0 \\ \frac{-k\Delta t}{m} & \Lambda & \frac{\Delta t}{m} A\sqrt{\frac{A_0}{A}}(V_{ice}-v)\frac{8\sigma_0}{\pi D} & \frac{\Delta t}{m} A\sqrt{\frac{A_0}{A}}\left((V_{ice}-v)\frac{8\sigma_0}{\pi D}\right)^2 & \frac{\Delta t}{m} A\sqrt{\frac{A_0}{A}}\left((V_{ice}-v)\frac{8\sigma_0}{\pi D}\right)^3 & \frac{\Delta t}{m} A\sqrt{\frac{A_0}{A}}\left((V_{ice}-v)\frac{8\sigma_0}{\pi D}\right)^4 & \frac{\Delta t}{m} A\sqrt{\frac{A_0}{A}} \\ 0 & 0 & 1 & 0 & 0 & 0 & 0 \\ 0 & 0 & 0 & 1 & 0 & 0 & 0 \\ 0 & 0 & 0 & 0 & 1 & 0 & 0 \\ 0 & 0 & 0 & 0 & 0 & 1 & 0 \\ 0 & 0 & 0 & 0 & 0 & 0 & 1 \end{bmatrix} \quad (5.1)$$

Where

$$\Lambda = (1 - \frac{c\Delta t}{m}) + \frac{\Delta t A\sqrt{\frac{A_0}{A}}}{m} \times \begin{pmatrix} \frac{8\sigma_0}{\pi D} a(-1) \\ +b \times 2\left((V_{ice}-v)\frac{8\sigma_0}{\pi D}\right)\frac{8\sigma_0}{\pi D}(-1) \\ +c \times 3\left((V_{ice}-v)\frac{8\sigma_0}{\pi D}\right)^2\frac{8\sigma_0}{\pi D}(-1) \\ +d \times 4\left((V_{ice}-v)\frac{8\sigma_0}{\pi D}\right)^3\frac{8\sigma_0}{\pi D}(-1) \end{pmatrix} \quad (5.2)$$

For $\dot{\sigma} < 0MPa/s$

$$F_k = \begin{bmatrix} 1 & \Delta t & 0 & 0 & 0 & 0 & 0 \\ \frac{-k\Delta t}{m} & (1 - \frac{c\Delta t}{m}) & 0 & 0 & 0 & 0 & 0 \\ 0 & 0 & 1 & 0 & 0 & 0 & 0 \\ 0 & 0 & 0 & 1 & 0 & 0 & 0 \\ 0 & 0 & 0 & 0 & 1 & 0 & 0 \\ 0 & 0 & 0 & 0 & 0 & 1 & 0 \\ 0 & 0 & 0 & 0 & 0 & 0 & 1 \end{bmatrix} \quad (5.3)$$

Summarize equation (5.1) to (5.5), the EKF can be initiate with initial ”guessed” state (other initial state can also be used) below. It is worth to mention that the intensity of noise (i.e. R matrix) is a known parameter prior to applying the EKF.

$$X_0 = \begin{bmatrix} u \\ v \\ a \\ b \\ c \\ d \\ e \end{bmatrix} = \begin{bmatrix} 0 \\ 0 \\ 0 \\ 0 \\ 0 \\ 0 \\ 0 \end{bmatrix}$$

$$P_0 = \begin{bmatrix} 3 & 0 & 0 & 0 & 0 & 0 & 0 \\ 0 & 3 & 0 & 0 & 0 & 0 & 0 \\ 0 & 0 & 3 & 0 & 0 & 0 & 0 \\ 0 & 0 & 0 & 3 & 0 & 0 & 0 \\ 0 & 0 & 0 & 0 & 3 & 0 & 0 \\ 0 & 0 & 0 & 0 & 0 & 3 & 0 \\ 0 & 0 & 0 & 0 & 0 & 0 & 3 \end{bmatrix}$$

5.2. Result for one parameter estimation

Step by step, only one parameter a will be regarded as unknown. The target value of a is 7.8. The measurement is conducted between 0 to 60 seconds. In order to evaluate the impact to the functionality of EKF, different noise level has been used.

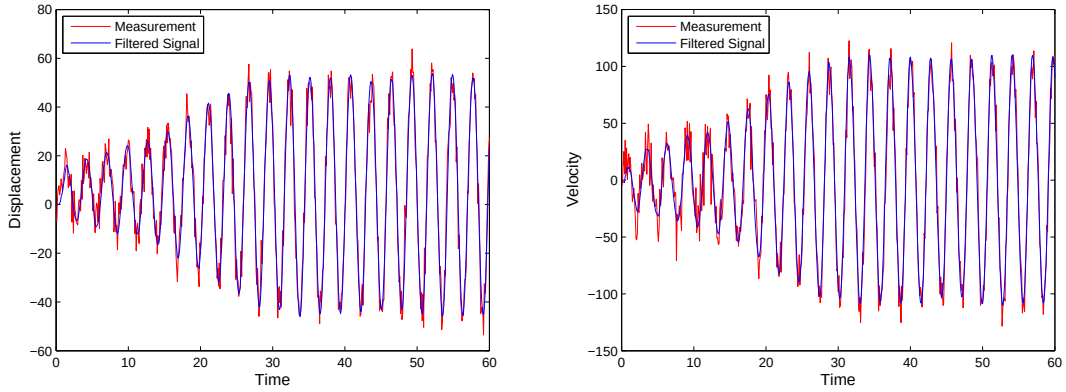

Figure 5.1: Measurement VS Filtered Signal($\Delta t = 0.1s$,Noise:20%, R matrix:20%)

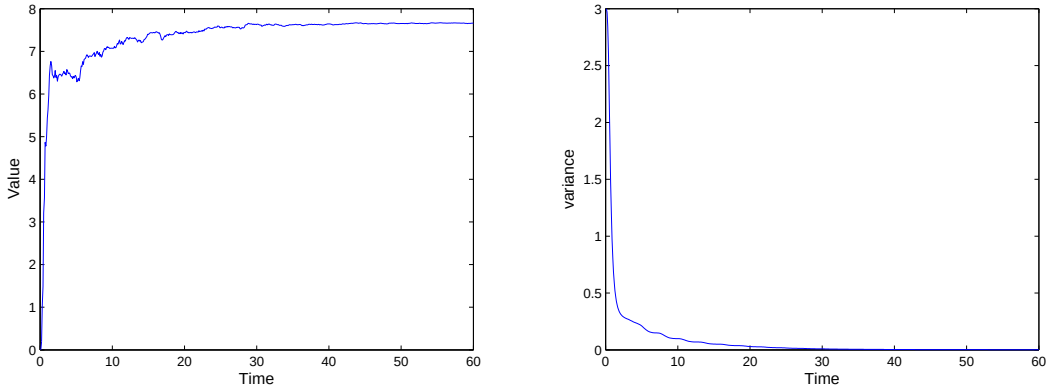

Figure 5.2: Parameter a Estimation ($a^{target} = 7.8$, $\Delta t = 0.1s$,Noise:20%, R matrix:20%)

In order to investigate the influence of noise intensity to the EKF, a 5% noise level will be applied.

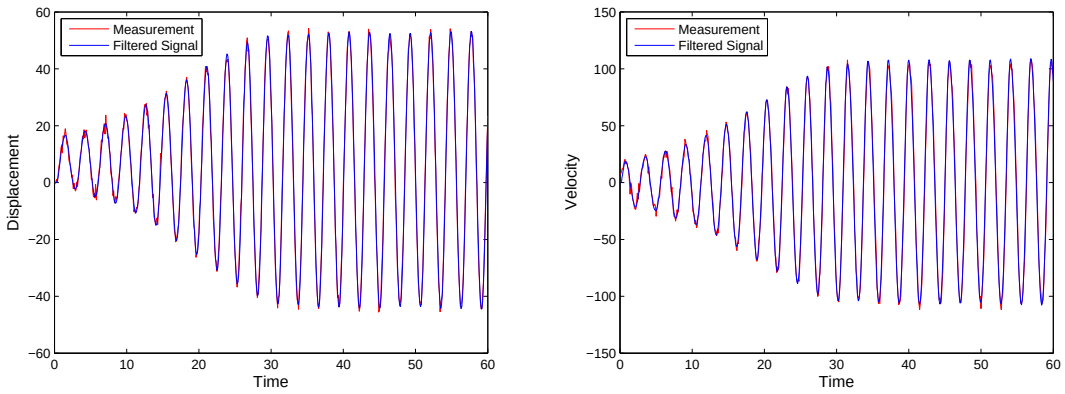

Figure 5.3: Measurement VS Filtered Signal($\Delta t = 0.1s$,Noise:5%, R matrix:5%)

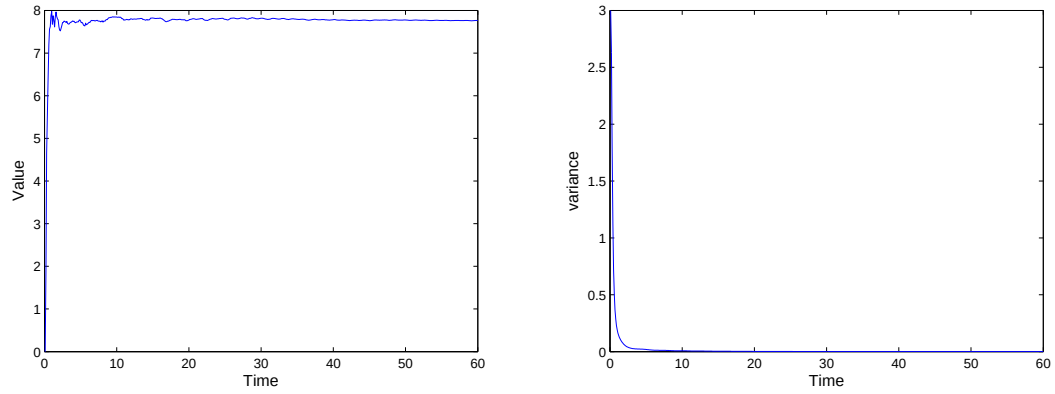

Figure 5.4: Parameter a Estimation ($a^{target} = 7.8$, $\Delta t = 0.1s$,Noise:5%, R matrix:5%)

Comparing the result from different noise level, one can conclude that the estimated parameter can approach target value much more faster when the noise level is low, with approximately 30s for 20% noise and 10s for 5% noise.
Above results are based on the assumption that the noise level is perfectly known. In another words, the R matrix level is exactly the same to the noise level. However, in reality, certain deviation of R matrix level may exist from noise level due to insufficient information of measurement instruments. In this case, it is necessary to simulate the EKF using incorrect R matrix.

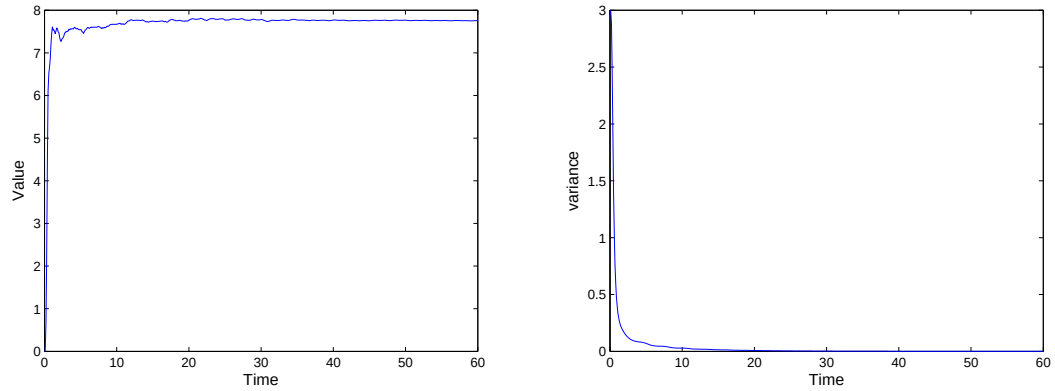

Figure 5.5: Parameter a Estimation ($a^{target} = 7.8$, $\Delta t = 0.1s$,Noise:5%, R matrix:10%)

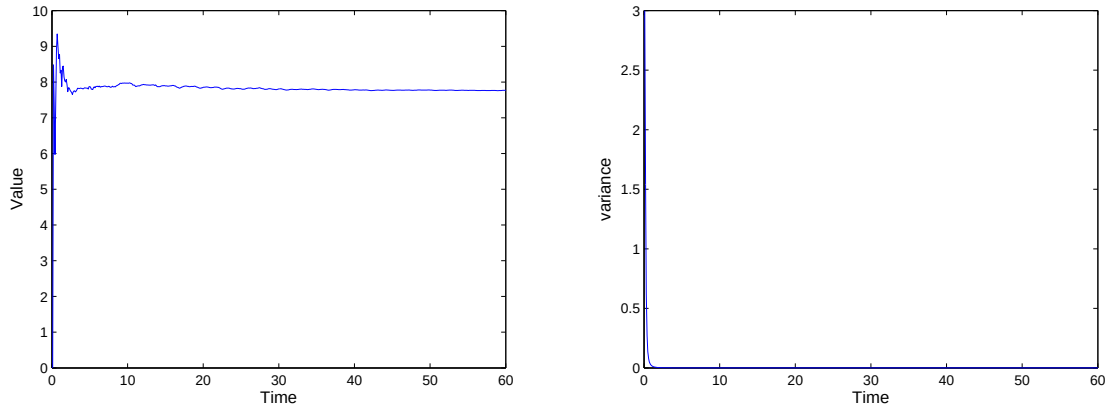

Figure 5.6: Parameter a Estimation ($a^{target} = 7.8$, $\Delta t = 0.1s$,Noise:5%, R matrix:1%)

In figure 5.6, the value of estimated parameter changes drastically over 0 to 5s. This is the result of choosing small R matrix, which tells the EKF to trust the measurement and rapidly change the parameter a to adapt to the noisy measurement. However, after certain time period of collecting enough information to calculation the best solution, the EKF successfully find the target value.

5.2.1. Conclusion for one parameter estimation

The unknown parameter can be well estimated both in 20% noise level and 5% noise level. However, in the case of less noise, the target value can be reached more faster. Moreover, the incorrectness of R matrix cannot have substantial influence on the result of one parameter estimation.

5.3. Result for two parameters estimation

In this section, coefficient a and b are regarded as unknown. The target value of a and b are 7.8 and -18.57 respectively.

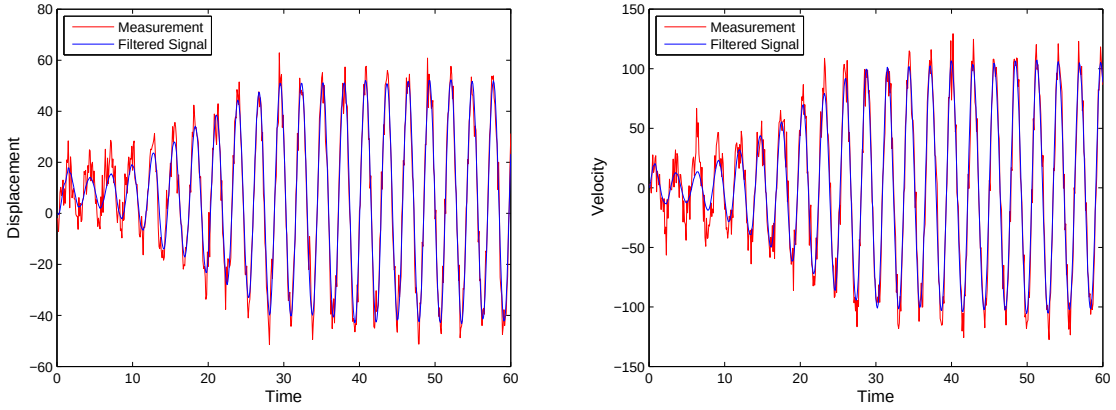

Figure 5.7: Measurement VS Filtered Signal($\Delta t = 0.1s$,Noise:20%, R matrix:20%)

From figure 5.8 and figure 5.9, it is obvious that the estimated parameters still have some deviation from the target value. This may due to the reason of relatively large measurement time step Δt. Using Euler Method to discretize the differential equation is an approximation method. the Jacobian Matrix in equation (5.1) cannot fully represent the original dynamic properties. Thus, decreasing the measurement time step Δt may increase the accuracy of result.

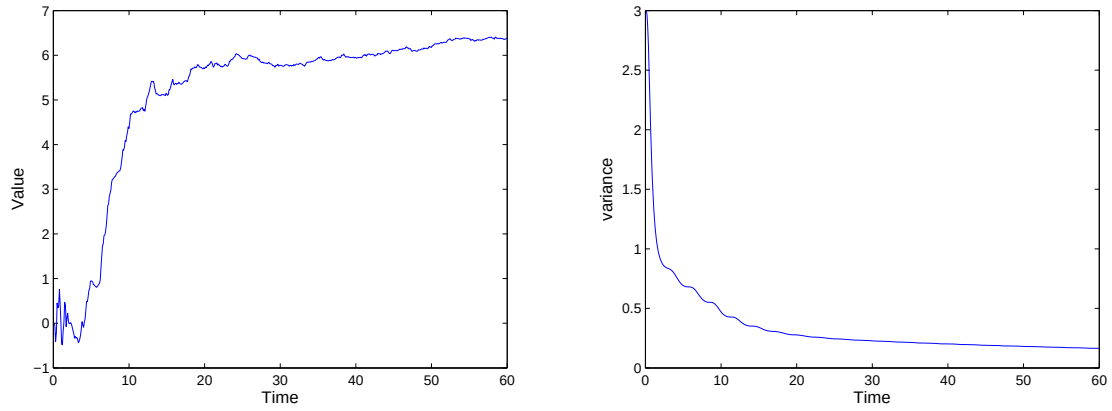

Figure 5.8: Parameter Estimation for a($a^{target} = 7.8$, $\Delta t = 0.1s$,Noise:20%, R matrix:20%)

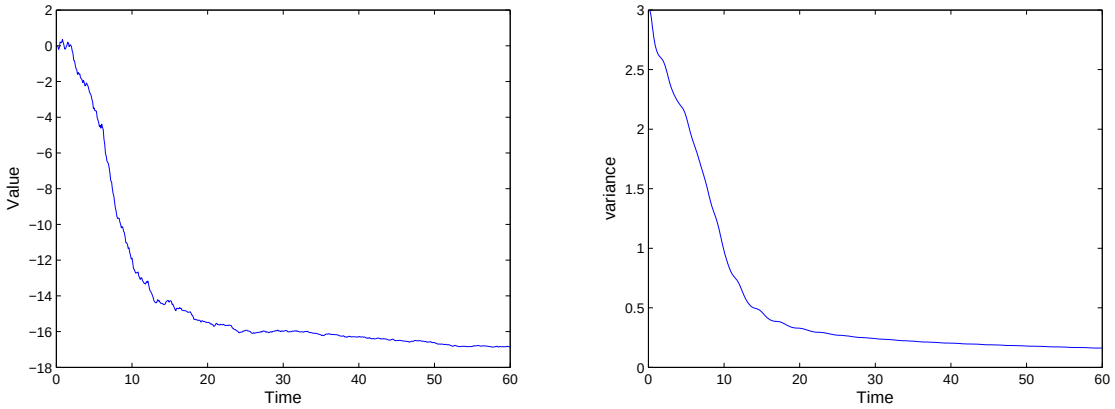

Figure 5.9: Parameter Estimation for a($b^{target} = -18.57$, $\Delta t = 0.1s$,Noise:20%, R matrix:20%)

Below is the result of applying $\Delta t = 0.01s$.

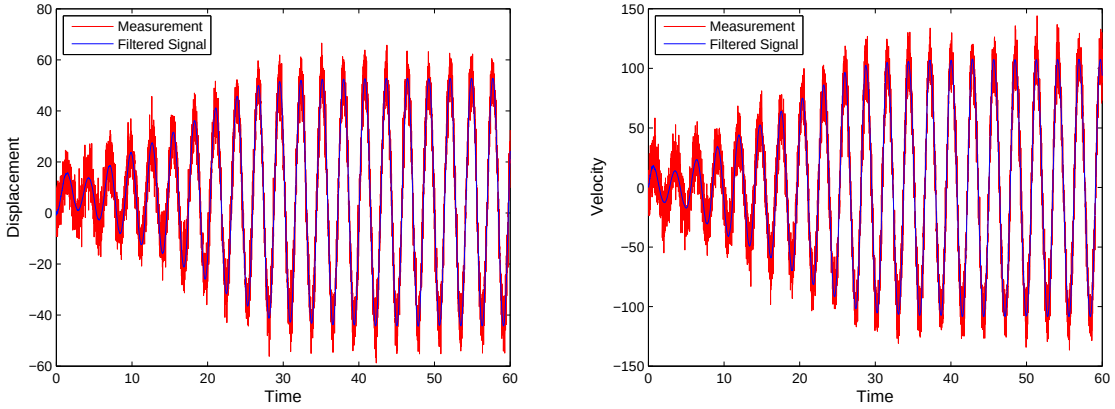

Figure 5.10: Measurement VS Filtered Signal($\Delta t = 0.01s$,Noise:20%, R matrix:20%)

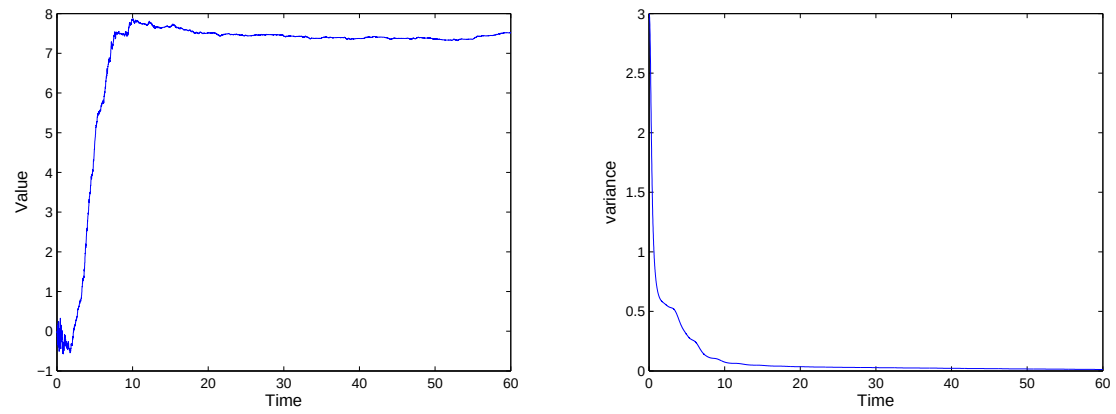

Figure 5.11: Parameter Estimation for a($a^{target} = 7.8$, $\Delta t = 0.01s$,Noise:20%, R matrix:20%)

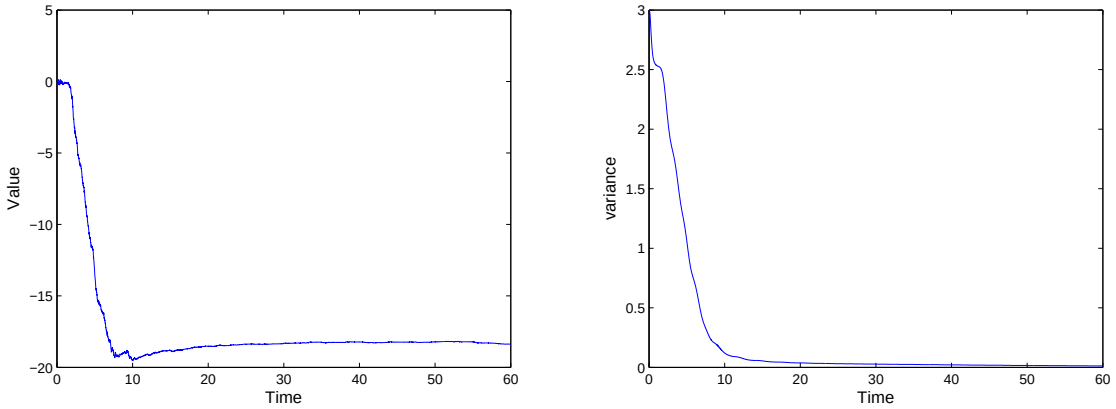

Figure 5.12: Parameter Estimation for b($b^{target} = -18.57$, $\Delta t = 0.01s$,Noise:20%, R matrix:20%)

Comparing figure 5.8 and figure 5.11, decreasing the measurement time step Δt indeed can effectively boost the estimation accuracy from 6.5 to 7.8 for coefficient a. Same effect to the coefficient b. Again, the influence of noise level will be assessed. Below is the result for noise level of 5%.

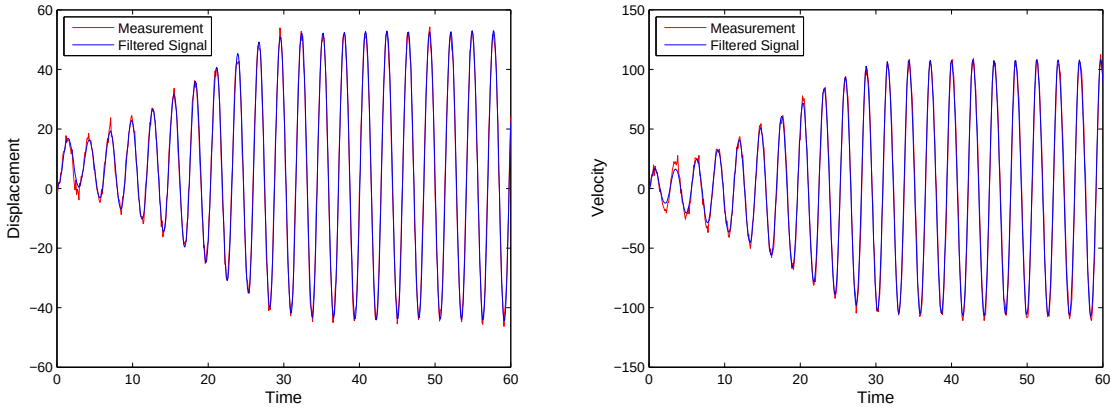

Figure 5.13: Measurement VS Filtered Signal($\Delta t = 0.1s$,Noise:5%, R matrix:5%)

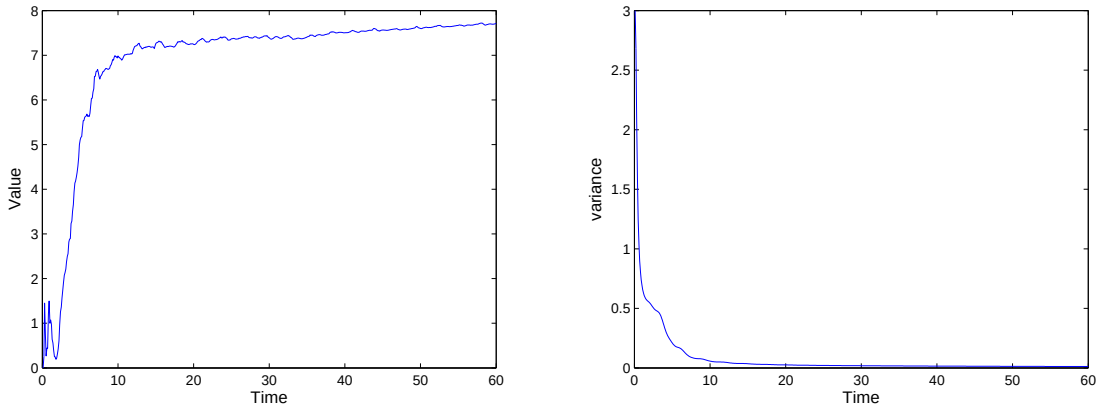

Figure 5.14: Parameter Estimation for a($a^{target} = 7.8$, $\Delta t = 0.1s$,Noise:5%, R matrix:5%)

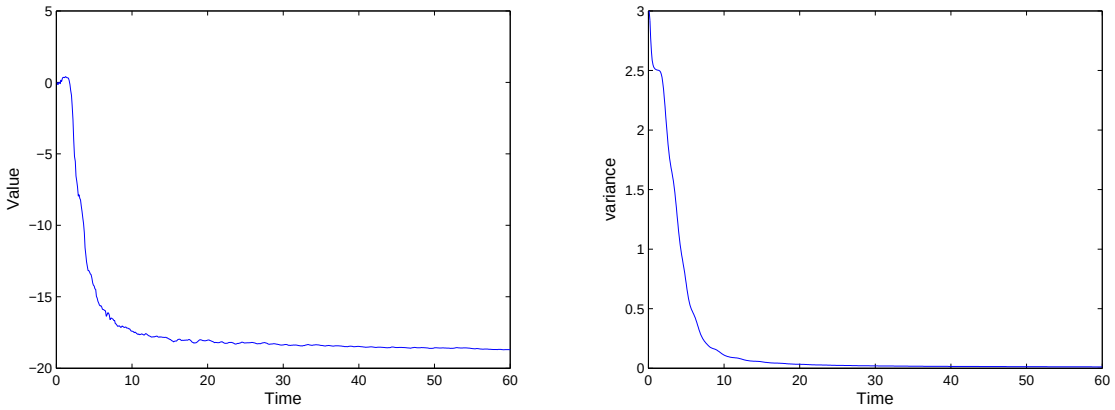

Figure 5.15: Parameter Estimation for b($b^{target} = -18.57$, $\Delta t = 0.1s$,Noise:5%, R matrix:5%)

The EKF can work quite well for two parameters (a and b) estimation in case of 5% noise level. The influence to the quality of result due to the incorrectness of R matrix has been evaluated as below.

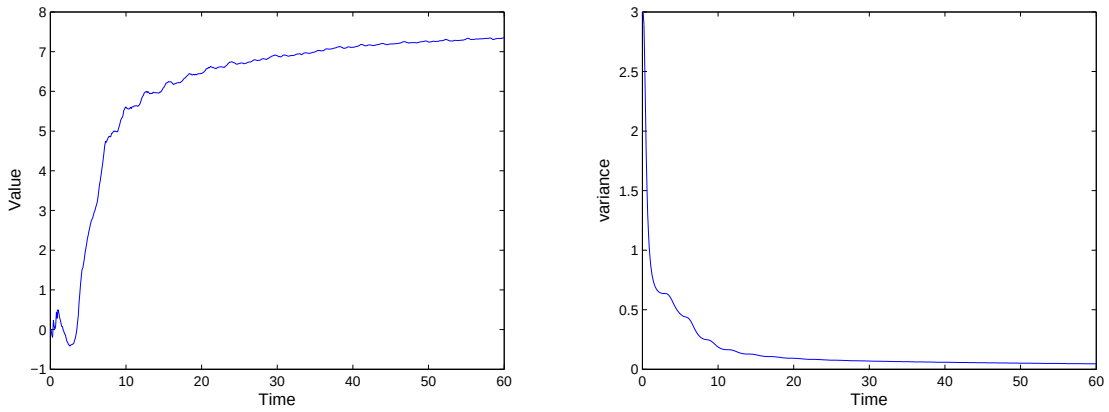

Figure 5.16: Parameter Estimation for a($a^{target} = 7.8$, $\Delta t = 0.1s$,Noise:5%, R matrix:10%)

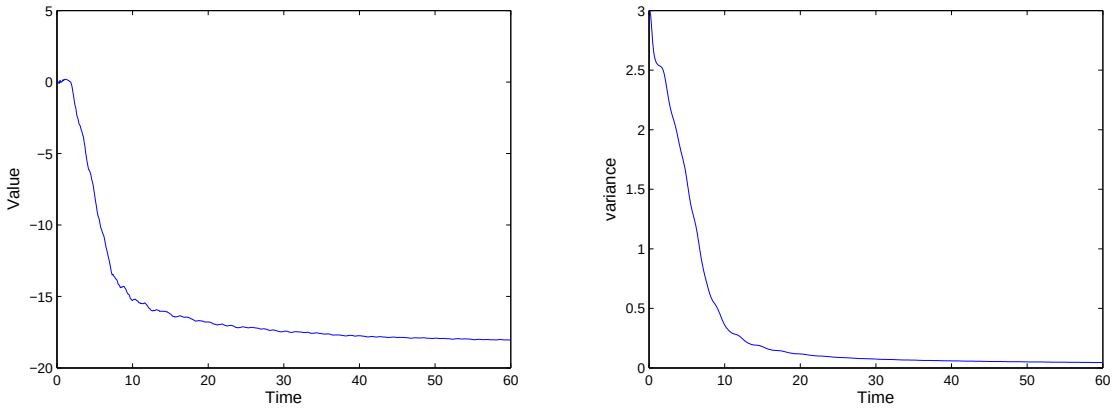

Figure 5.17: Parameter Estimation for b($b^{target} = -18.57$, $\Delta t = 0.1s$,Noise:5%, R matrix:10%)

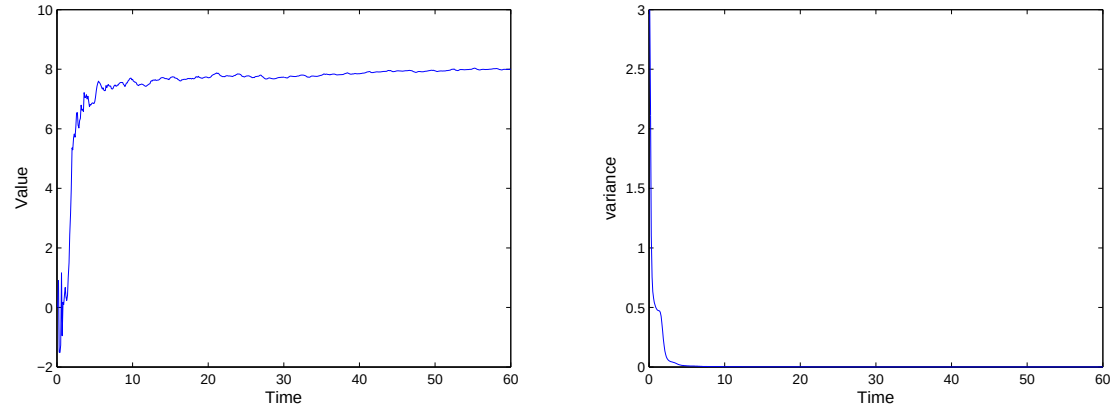

Figure 5.18: Parameter Estimation for a($a^{target} = 7.8$, $\Delta t = 0.1s$,Noise:5%, R matrix:1%)

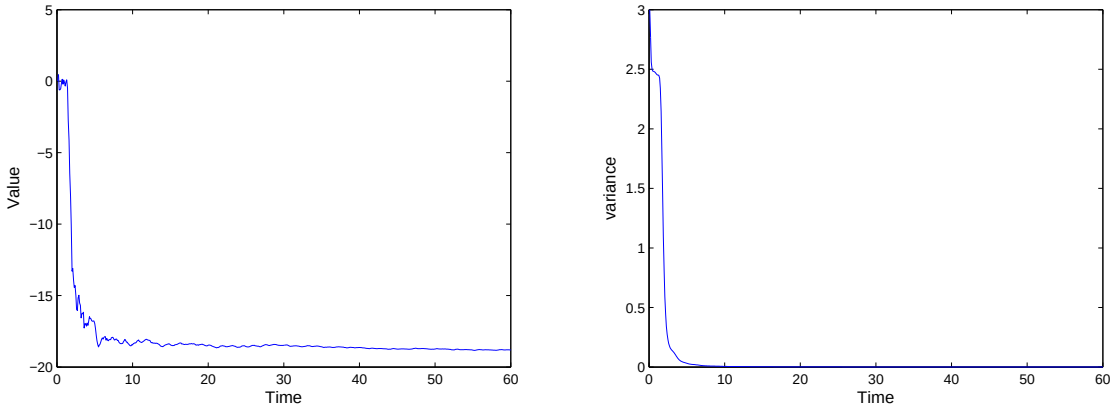

Figure 5.19: Parameter Estimation for b($b^{target} = -18.57$, $\Delta t = 0.1s$,Noise:5%, R matrix:1%)

In the above figures, the estimated parameters more or less deviated from the target value a bit, both for the larger R matrix and smaller R matrix level. The result is not as good as the perfect R matrix in figure 5.14 and figure 5.15. Moreover, the variance with bigger R matrix is obviously larger than that with smaller R matrix, which means the result may not converge in the case of bigger R matrix. This can also be deduced from left side plot in figure 5.16 and 5.17, that parameters still have a tendency to increase. In the case of smaller R matrix, the estimated value of a is 8,instead of 7.8.

5.3.1. Conclusion for two parameters estimation

The two unknown parameters can be well estimated in the case of 5% noise level at $\Delta t = 0.1s$ using EKF. However, higher noise level (20%) can deteriorate the quality of result at time step $\Delta t = 0.1s$. The reason is that the Euler Method is an first order approximation algorithm. Larger inaccuracy can be introduced into EKF in every system update through Jacobian Matrix at larger measurement time step Δt. Meanwhile, the conjecture that decreasing measurement time step can increase accuracy of result has been proven in figure 5.11 and 5.12. At last, unlike the conclusion of one parameter estimation, the inaccuracy in R matrix can induce deviation of estimation from target value. More specifically, larger entries of R matrix may induce misconvergence, smaller entries of R matrix can result in unreliable estimation, though it converges.

5.4. Result for three parameters estimation

In this section, the coefficient of a,b and c are unknow. Similar to the previous sections, different noise level will be applied. Below is the result for 20% noise level.

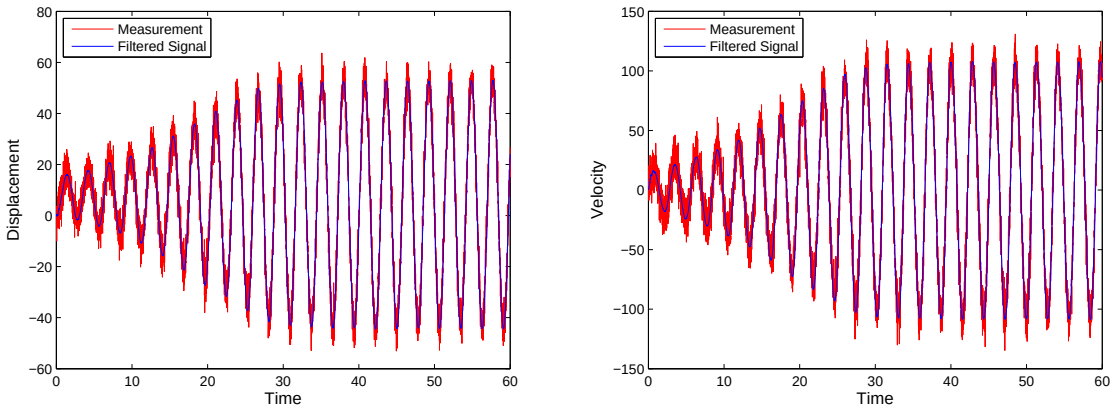

Figure 5.20: Measurement VS Filtered Signal($\Delta t = 0.01s$,Noise:20%, R matrix:20%)

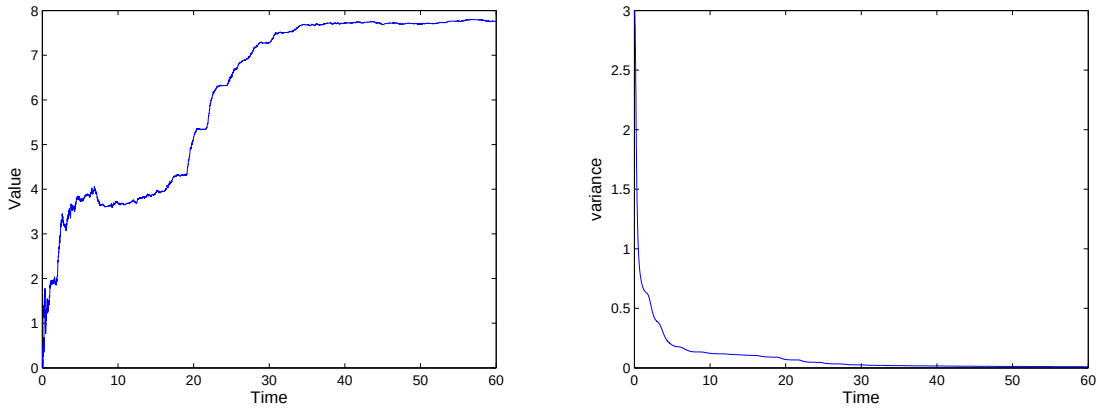

Figure 5.21: Parameter Estimation for a($a^{target} = 7.8$, $\Delta t = 0.01s$,Noise:20%, R matrix:20%)

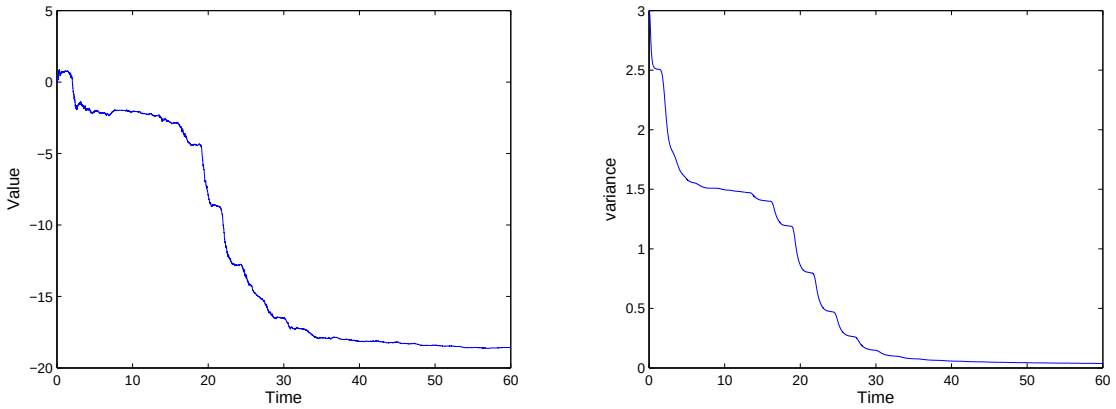

Figure 5.22: Parameter Estimation for b($b^{target} = -18.57$, $\Delta t = 0.01s$,Noise:20%, R matrix:20%)

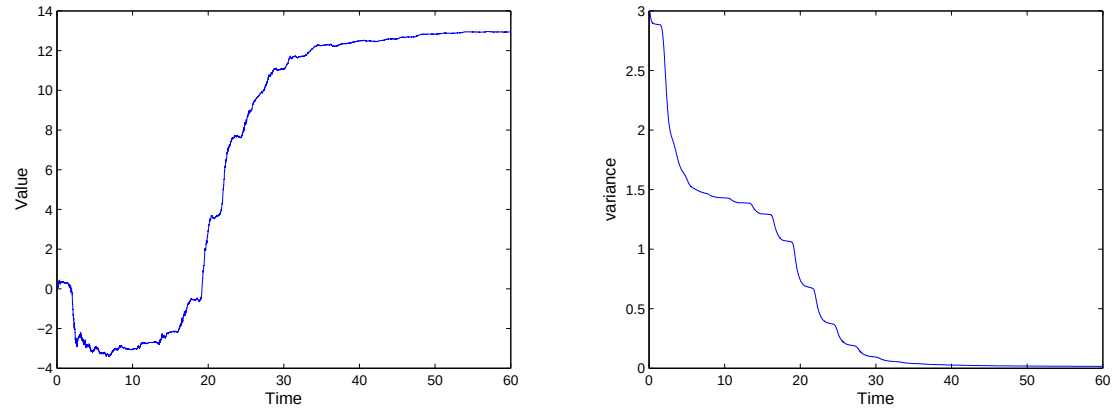

Figure 5.23: Parameter Estimation for c($c^{target} = 13$, $\Delta t = 0.01s$,Noise:20%, R matrix:20%)

From the figures above, all the three coefficients can be well identified. Meanwhile, the parameters can quickly converge to the target value. In order to verified the conclusion that target value can be reached faster under less noise scenario, a case of 5% noise level will be implemented below.

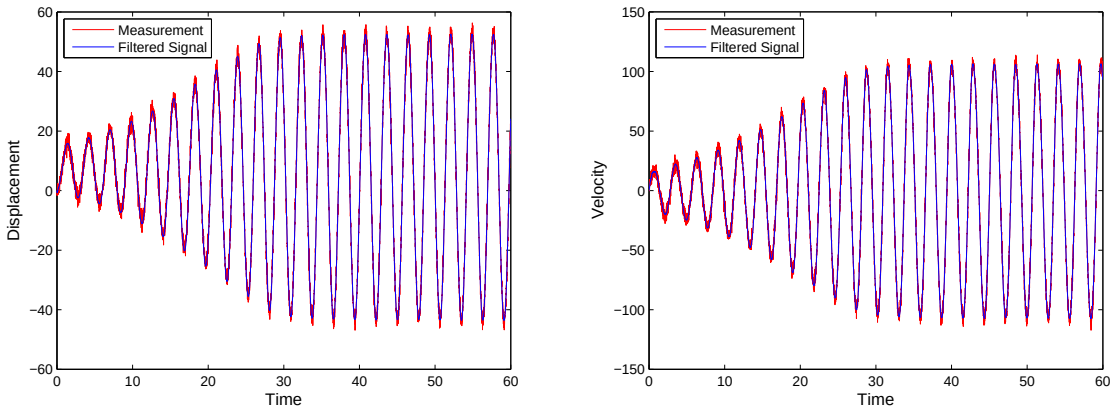

Figure 5.24: Measurement VS Filtered Signal($\Delta t = 0.01s$,Noise:5%, R matrix:5%)

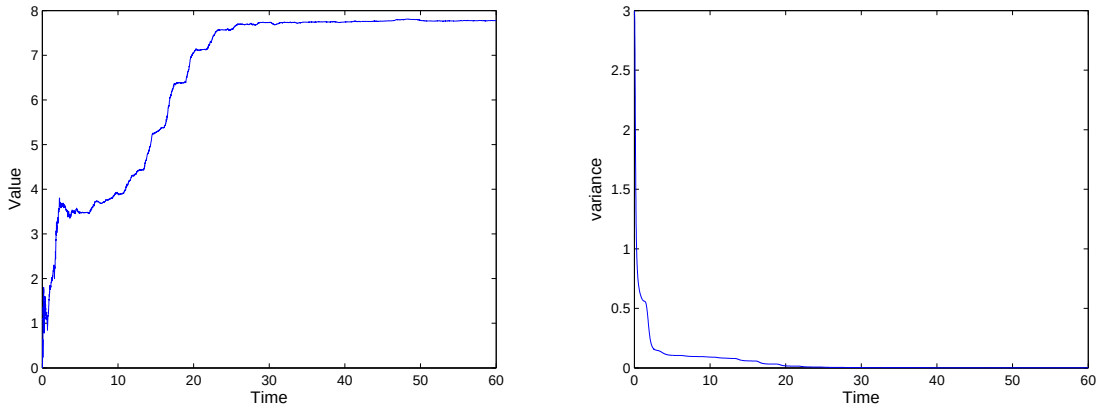

Figure 5.25: Parameter Estimation for a($a^{target} = 7.8$, $\Delta t = 0.01s$,Noise:5%, R matrix:5%)

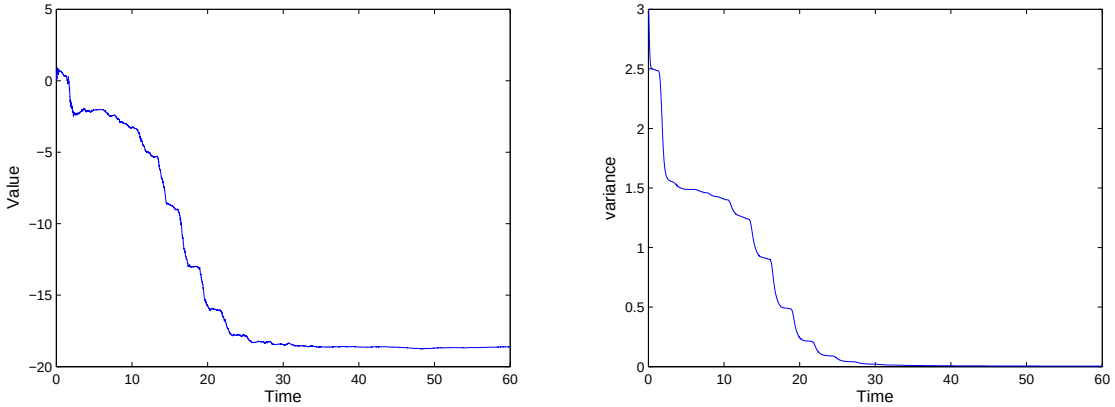

Figure 5.26: Parameter Estimation for b($b^{target} = -18.57$, $\Delta t = 0.01s$,Noise:5%, R matrix:5%)

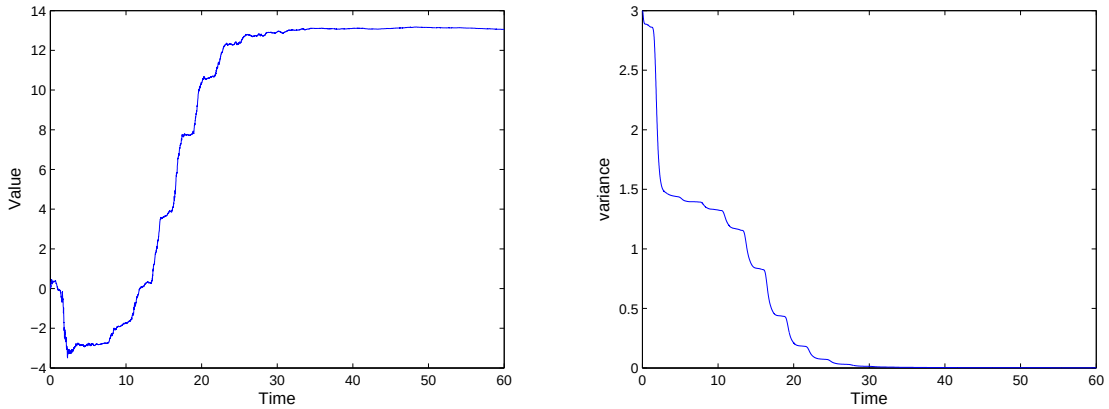

Figure 5.27: Parameter Estimation for c($c^{target} = 13$, $\Delta t = 0.01s$,Noise:5%, R matrix:5%)

From the figures above, it is clear that all three unknown parameters can be well estimated at 5% noise level. Moreover, estimation under higher noise level indeed requires more time to reach target value.
Below shows the impact of incorrectness in R matrix.

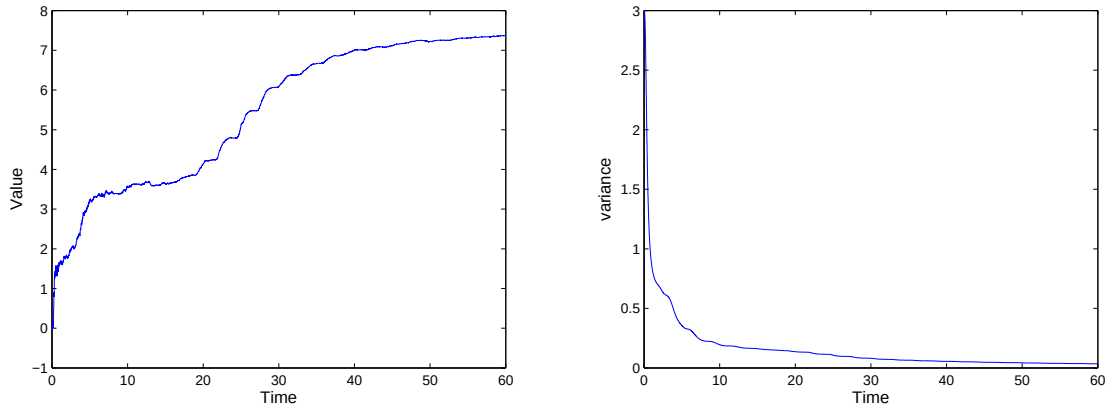

Figure 5.28: Parameter Estimation for a($a^{target} = 7.8$, $\Delta t = 0.01s$,Noise:5%, R matrix:10%)

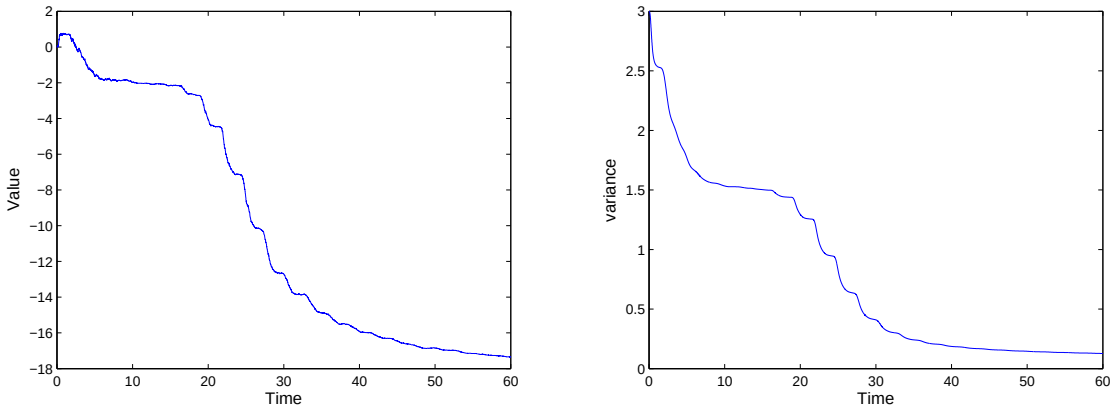

Figure 5.29: Parameter Estimation for b($b^{target} = -18.57$, $\Delta t = 0.01s$,Noise:5%, R matrix:10%)

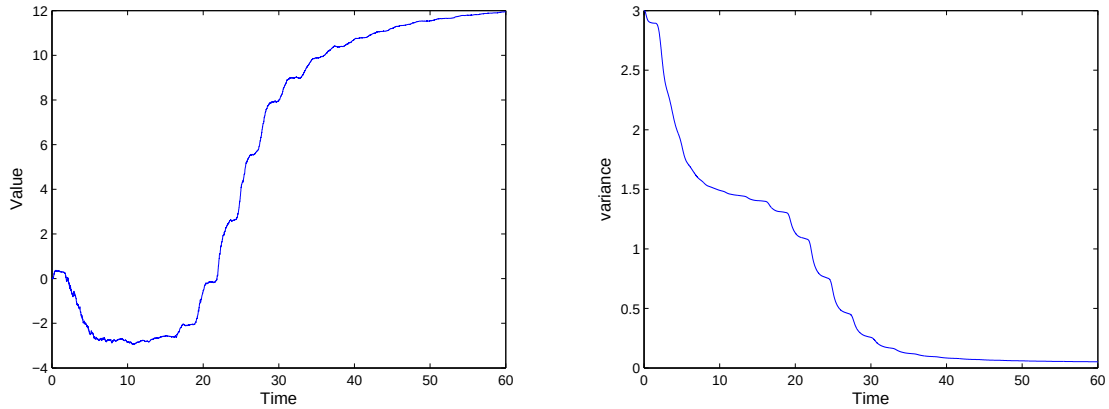

Figure 5.30: Parameter Estimation for c($c^{target} = 13$, $\Delta t = 0.01s$,Noise:5%, R matrix:10%)

After artificially increasing the R matrix to 10%, all the three parameters are not accurate as when R is correct. Moreover, the estimated parameters haven't converged to a stable value when R matrix chosen 10%.
For smaller R matrix level of 1%, the result has been shown below.

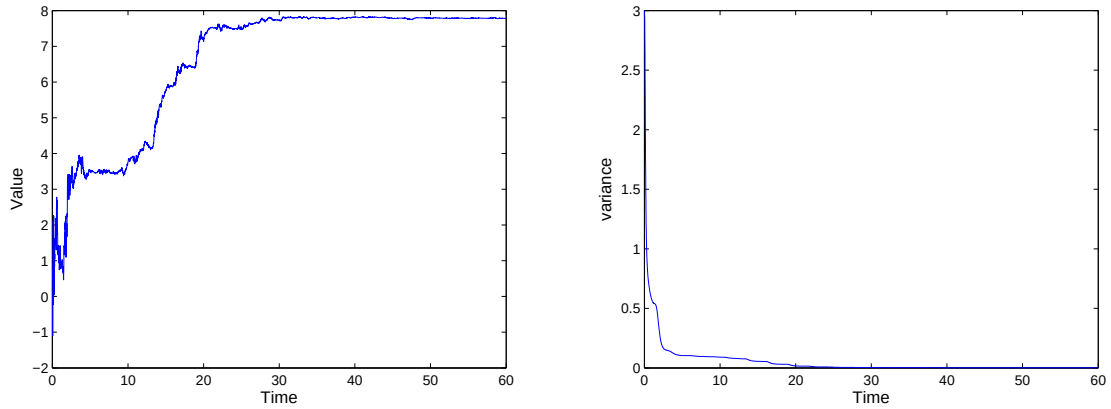

Figure 5.31: Parameter Estimation for a($a^{target} = 7.8$, $\Delta t = 0.01s$,Noise:5%, R matrix:1%)

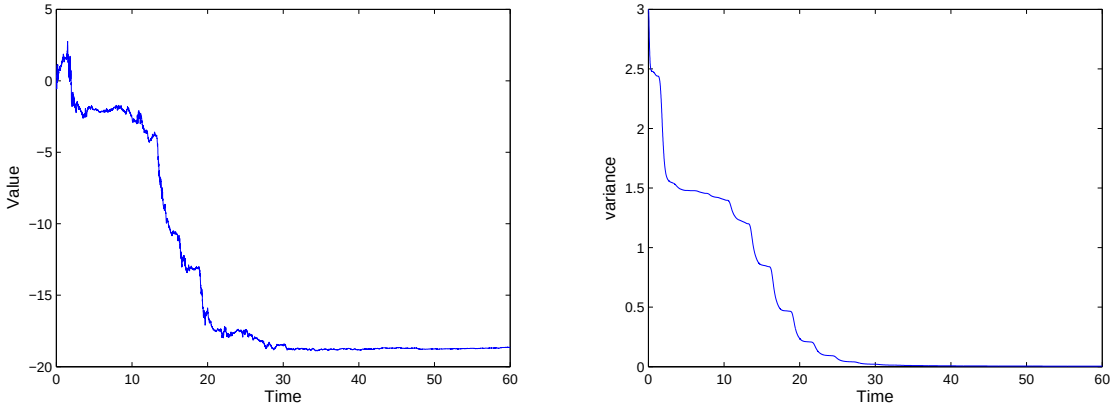

Figure 5.32: Parameter Estimation for b($b^{target} = -18.57$, $\Delta t = 0.01s$,Noise:5%, R matrix:1%)

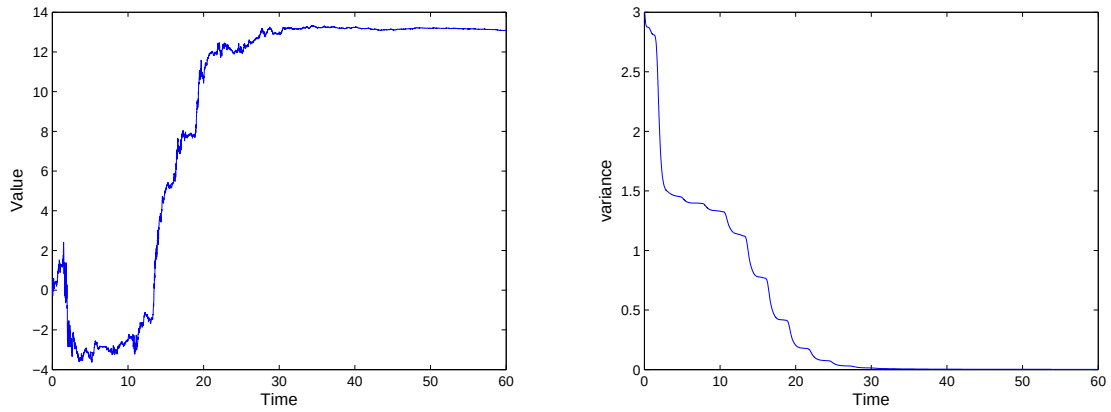

Figure 5.33: Parameter Estimation for c($c^{target} = 13$, $\Delta t = 0.01s$,Noise:5%, R matrix:1%)

Unlike the result of two parameters estimation, the result of choosing smaller R matrix is still fairly good for three parameters estimation. Meanwhile, the target values have been reached more earlier than using correct R matrix.

5.4.1. Conclusion for three parameters estimation

In the case of three parameters estimation, all the three parameters can be well estimated. The conclusion that larger noise level requires more time to achieve stable estimation has been again verified. In addition, incorrect R matrix with larger entries may result in misconvergence of estimation.

5.5. Result for four parameters estimation

This section concerns one more step further, i.e. four parameters need to be identified, with $a = 7.8, b = -18.57, c = 13, d = -2.91$. Below is the result under 20% noise level with $\Delta t = 0.001s$.

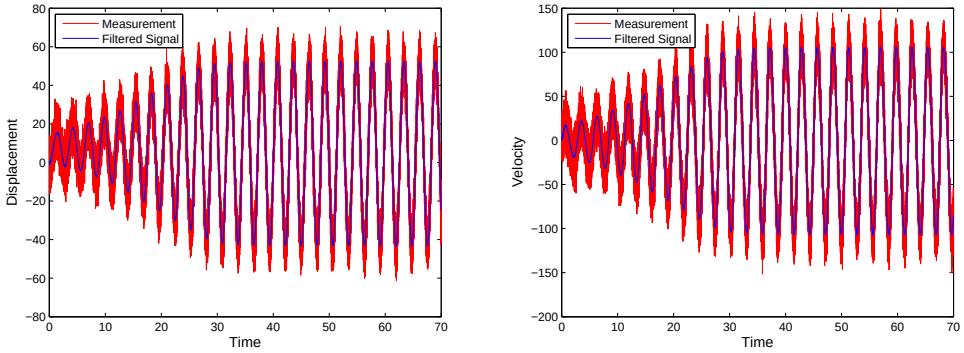

Figure 5.34: Measurement VS Filtered Signal($\Delta t = 0.001s$,Noise:20%, R matrix:20%)

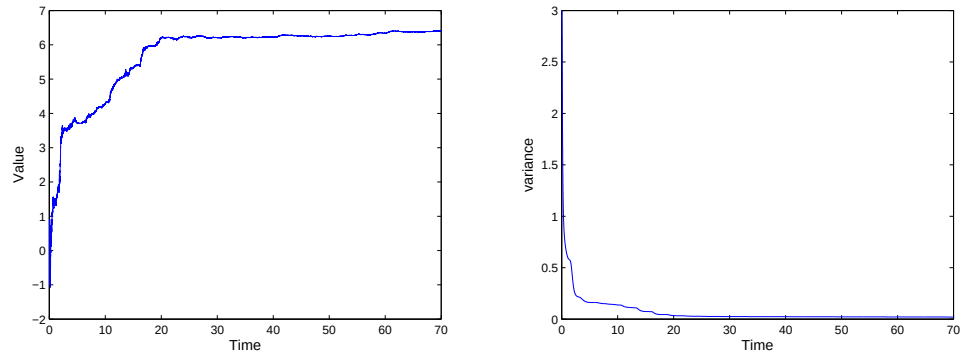

Figure 5.35: Parameter Estimation for a($a^{target} = 7.8$, $\Delta t = 0.001s$,Noise:20%, R matrix:20%)

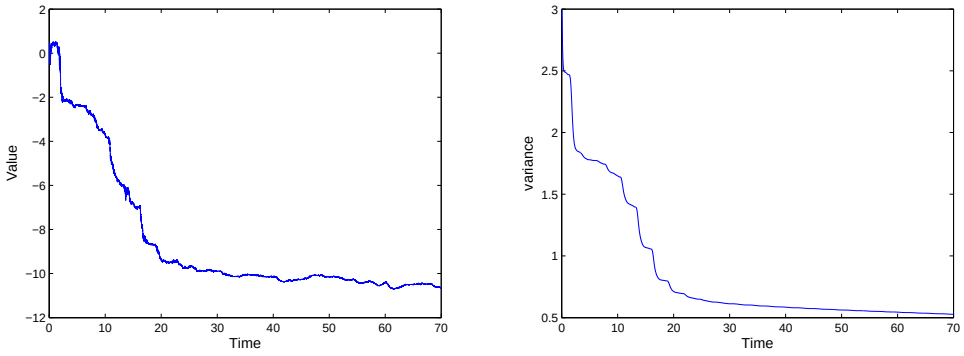

Figure 5.36: Parameter Estimation for b($b^{target} = -18.57$, $\Delta t = 0.001s$,Noise:20%, R matrix:20%)

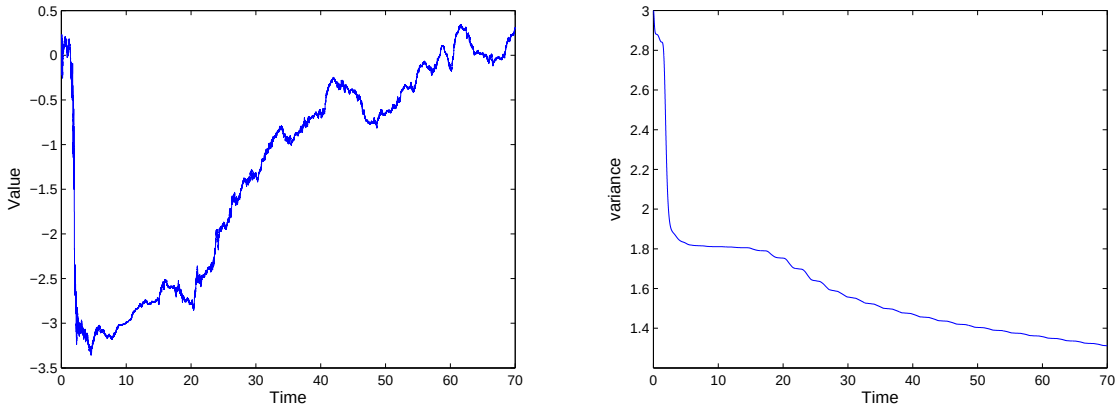

Figure 5.37: Parameter Estimation for c($c^{target} = 13$, $\Delta t = 0.001s$,Noise:20%, R matrix:20%)

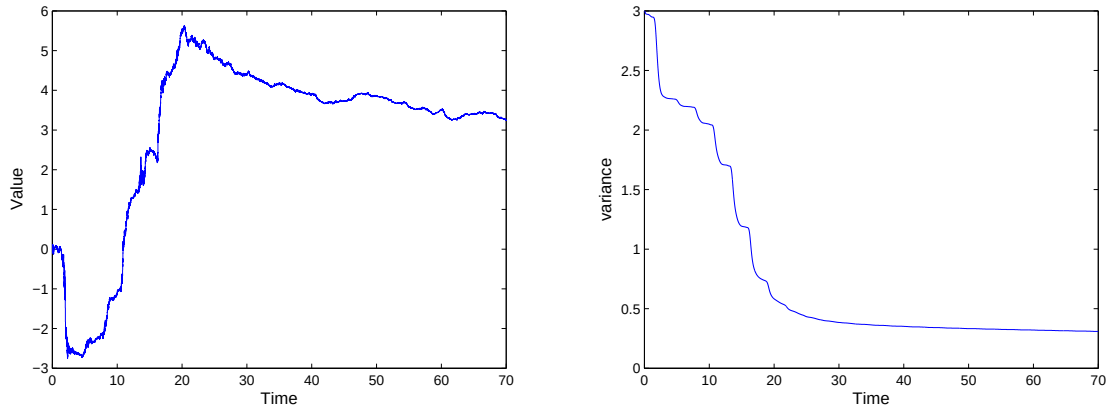

Figure 5.38: Parameter Estimation for d($d^{target} = -2.91$, $\Delta t = 0.001s$,Noise:20%, R matrix:20%)

The result is very poor, which can also be deduced from the variance plot. This may due to relatively large measurement time step in the case of four parameters estimation. Let's decrease the time step to $\Delta t = 0.0001s$.

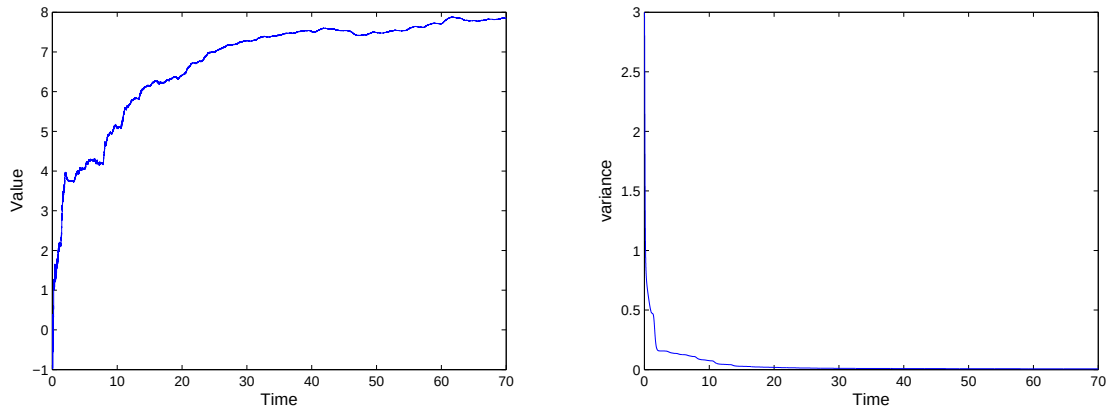

Figure 5.39: Parameter Estimation for a($a^{target} = 7.8$, $\Delta t = 0.0001s$,Noise:20%, R matrix:20%)

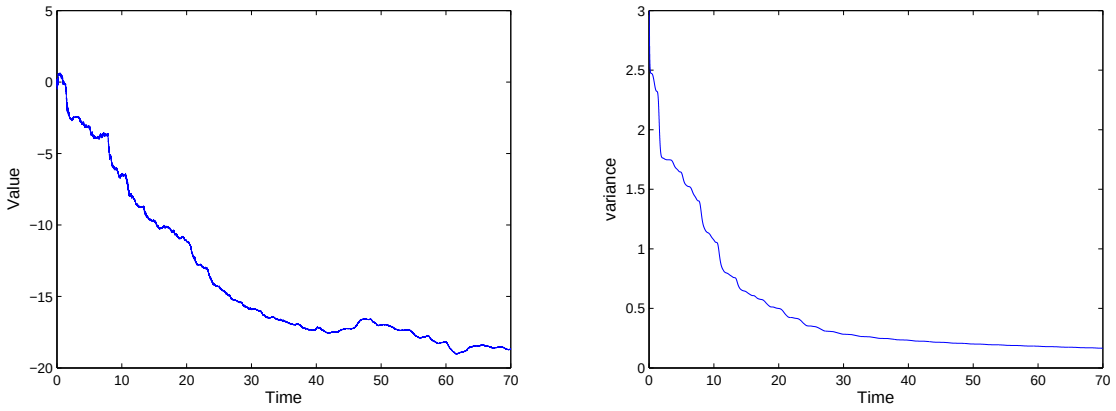

Figure 5.40: Parameter Estimation for b($b^{target} = -18.57$, $\Delta t = 0.0001s$,Noise:20%, R matrix:20%)

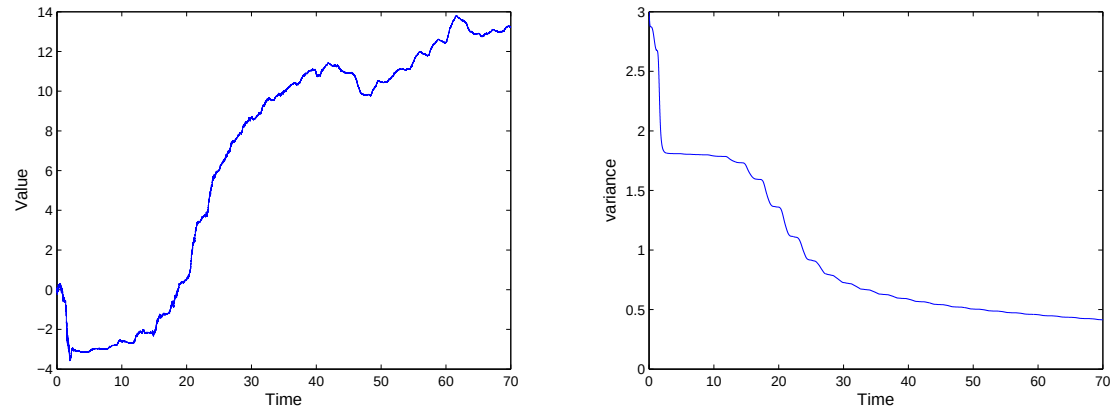

Figure 5.41: Parameter Estimation for c($c^{target} = 13$, $\Delta t = 0.0001s$,Noise:20%, R matrix:20%)

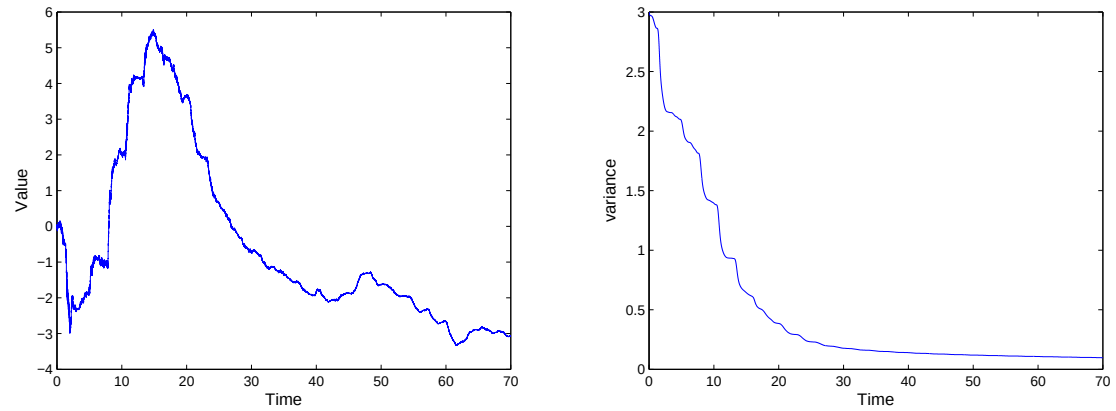

Figure 5.42: Parameter Estimation for d($c^{target} = 13$, $\Delta t = 0.0001s$,Noise:20%, R matrix:20%)

The result is much better at $\Delta t = 0.0001s$. Decreasing measurement time step can increase accuracy of estimation has been verified again. However, at the end of the estimation, the parameters still have a tendency to vary instead of converging to target values. As in the previous section, less noise level is supposed to help the estimation reach stable values faster than large noise level. Below the case of 5% noise level will be implemented.

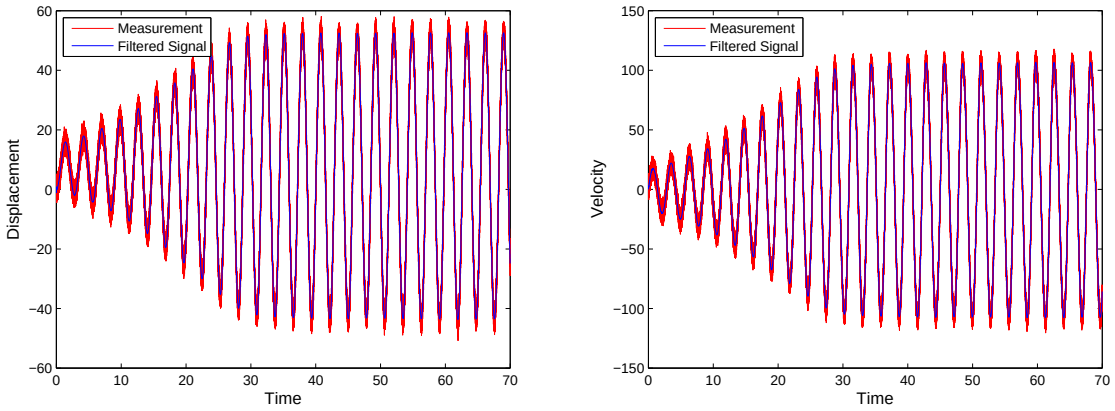

Figure 5.43: Measurement VS Filtered Signal($\Delta t = 0.0001s$,Noise:5%, R matrix:5%)

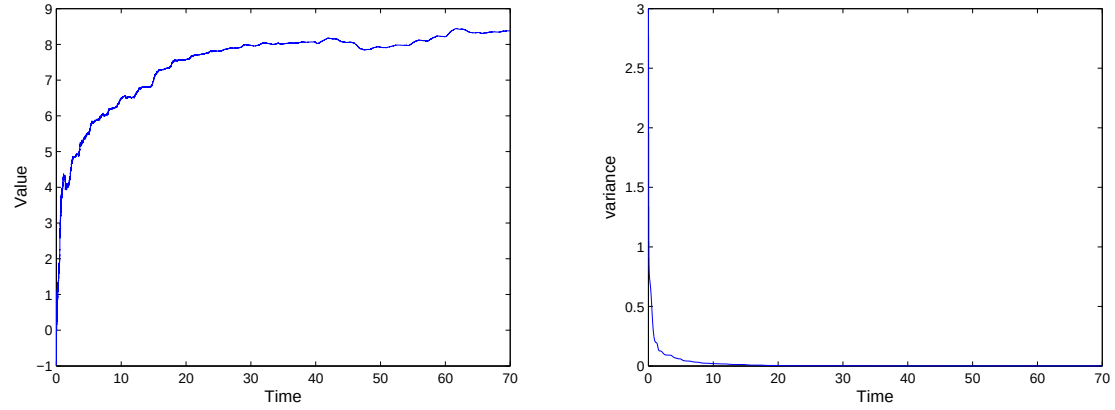

Figure 5.44: Parameter Estimation for a($a^{target} = 7.8$, $\Delta t = 0.0001s$,Noise:5%, R matrix:5%)

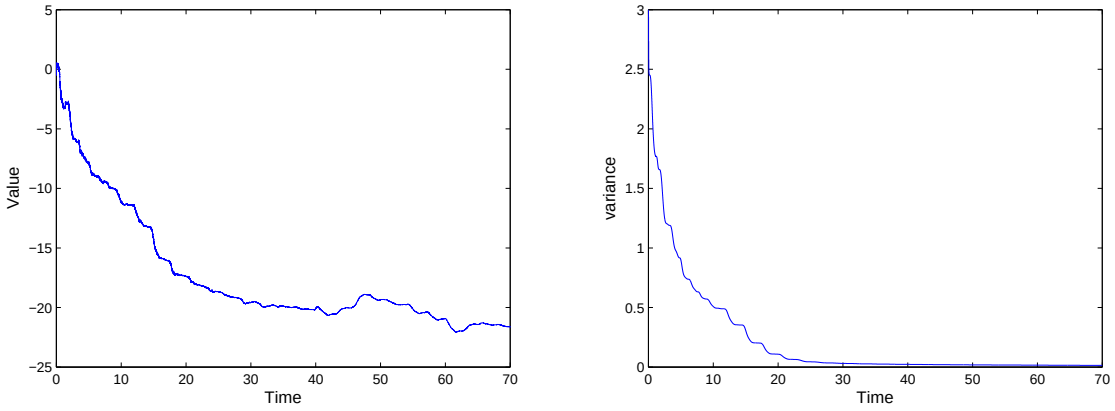

Figure 5.45: Parameter Estimation for b($b^{target} = -18.57$, $\Delta t = 0.0001s$,Noise:5%, R matrix:5%)

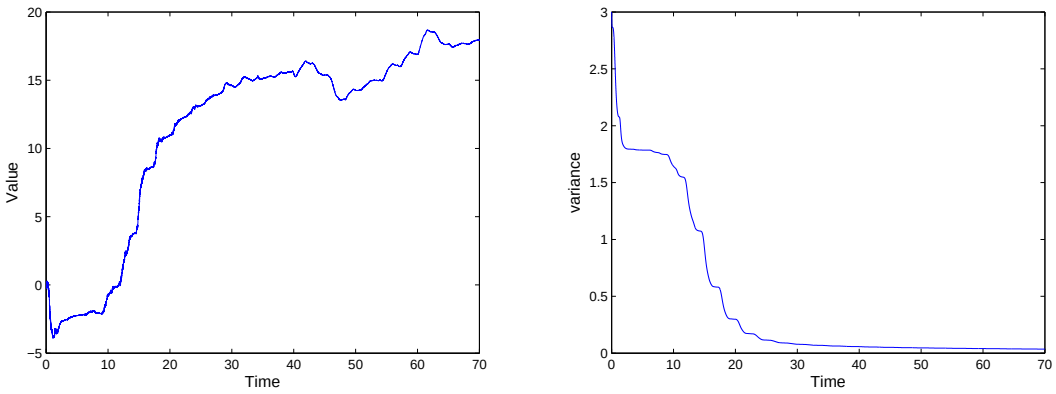

Figure 5.46: Parameter Estimation for c($c^{target} = 13$, $\Delta t = 0.0001s$,Noise:5%, R matrix:5%)

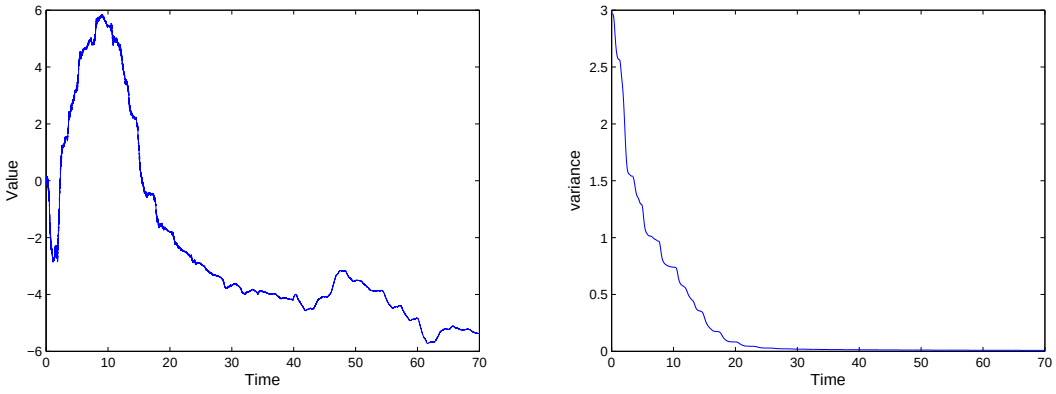

Figure 5.47: Parameter Estimation for d($d^{target} = -2.91$, $\Delta t = 0.0001s$,Noise:5%, R matrix:5%)

From the figures above, it is very clear that the result is again deteriorated under less noise. All the four coefficients haven't converged the corresponding target value.
However, when looking back the result under 20% noise level, even though the four parameters reach target values, however, havn't fully converge to the target values. So extending the measurement time to $100s$ may help us understand whether it's out of luck that we obtain good result.

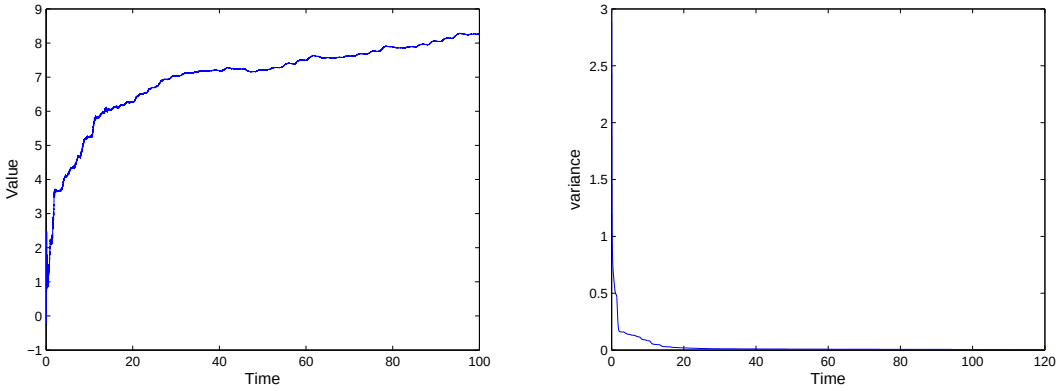

Figure 5.48: Parameter Estimation for a($a^{target} = 7.8$, $\Delta t = 0.0001s$,Noise:5%, R matrix:5%)

After extending the measurement time to $100s$, instead of reaching a stable value, the parameters still

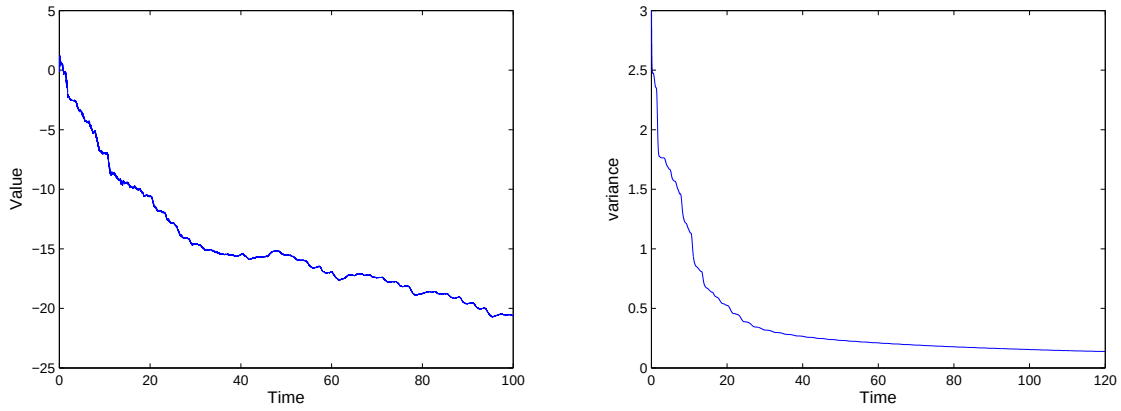

Figure 5.49: Parameter Estimation for b($b^{target} = -18.57$, $\Delta t = 0.0001s$,Noise:5%, R matrix:5%)

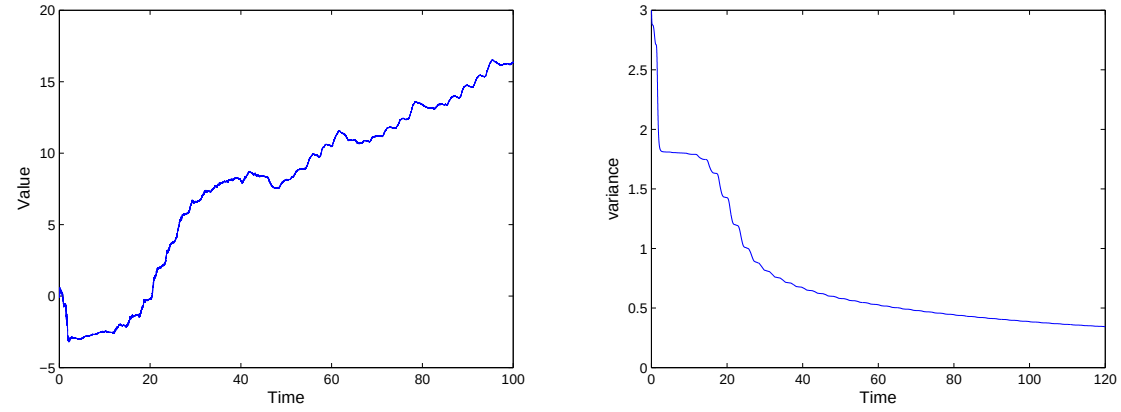

Figure 5.50: Parameter Estimation for c($c^{target} = 13$, $\Delta t = 0.0001s$,Noise:5%, R matrix:5%)

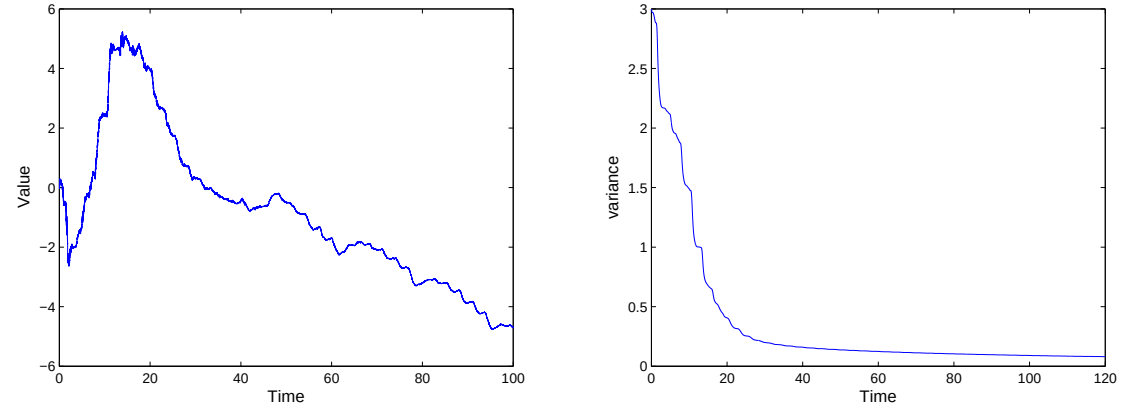

Figure 5.51: Parameter Estimation for d($d^{target} = -2.91$, $\Delta t = 0.0001s$,Noise:5%, R matrix:5%)

vary and become deviated from the target value that have reached.

5.5.1. Conclusion for four parameters estimation

In the case of four parameters estimation, all the parameters don't converge to the corresponding target value. This may due to the reason that there exist multiple combination of the four parameters to

minimize the cost function in EKF at each time step. This nonuniqueness issue makes the estimation vary instead of converge. This explanation can be verified in the case of five parameters estimation.

5.6. Result for five parameters estimation

For simplicity, the EKF of five parameters estimation will only be implemented for 5% noise level at $\Delta t = 0.0001s$. Below is the result.

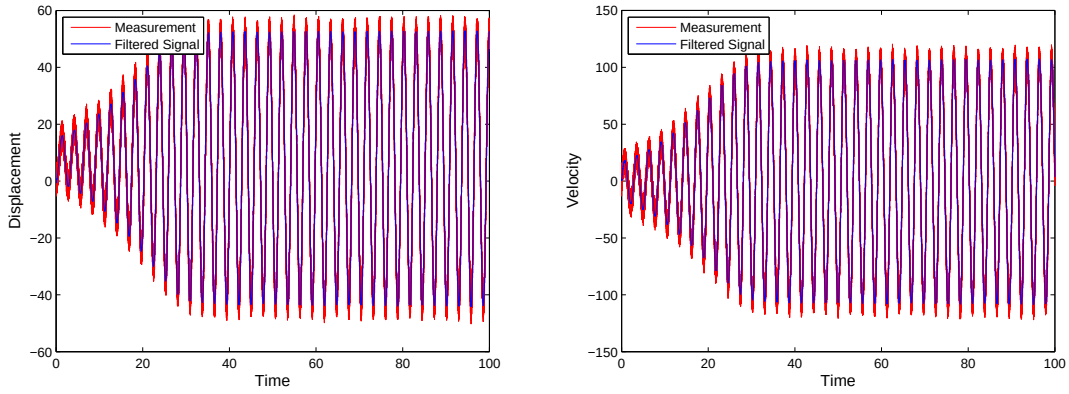

Figure 5.52: Measurement VS Filtered Signal($\Delta t = 0.0001s$,Noise:5%, R matrix:5%)

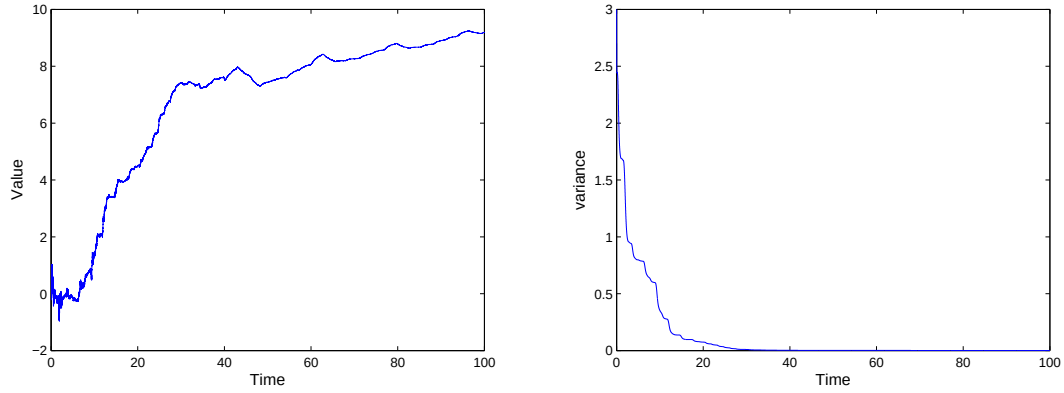

Figure 5.53: Parameter Estimation for a($a^{target} = 7.8$, $\Delta t = 0.0001s$,Noise:5%, R matrix:5%)

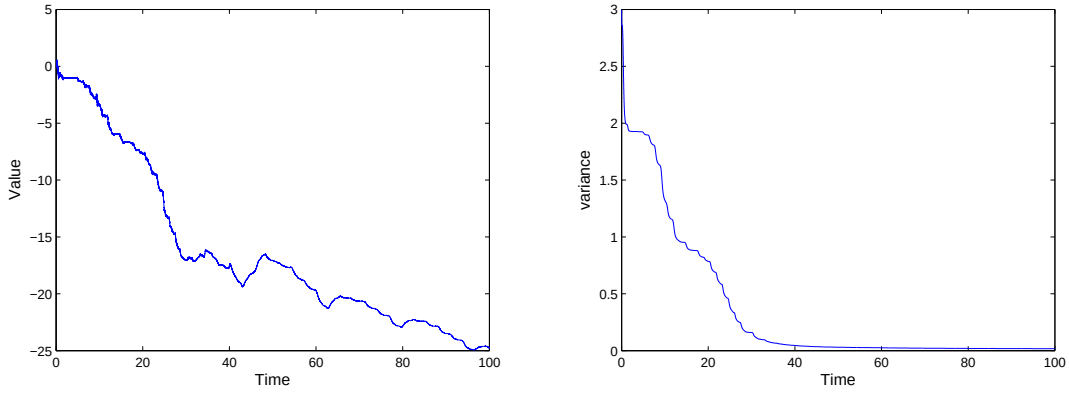

Figure 5.54: Parameter Estimation for b($b^{target} = -18.57$, $\Delta t = 0.0001s$,Noise:5%, R matrix:5%)

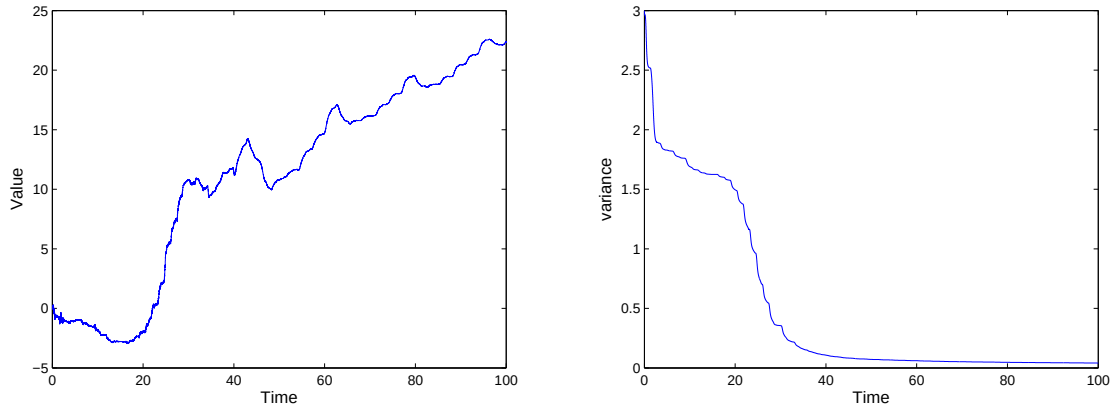

Figure 5.55: Parameter Estimation for c($c^{target} = 13$, $\Delta t = 0.0001s$,Noise:5%, R matrix:5%)

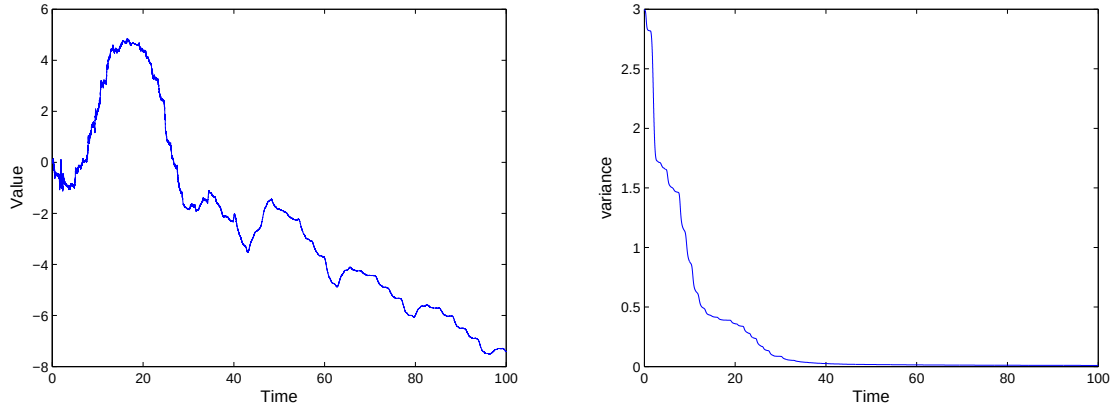

Figure 5.56: Parameter Estimation for d($d^{target} = -2.91$, $\Delta t = 0.0001s$,Noise:5%, R matrix:5%)

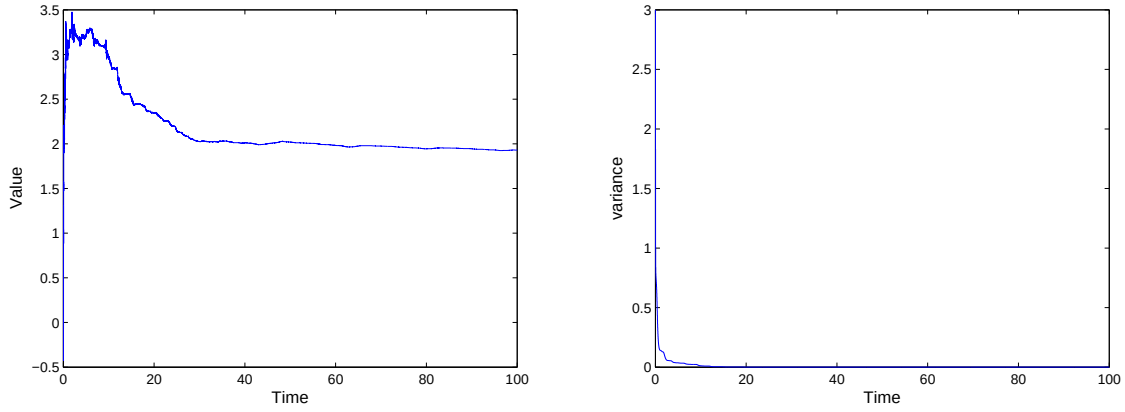

Figure 5.57: Parameter Estimation for e($e^{target} = 2$, $\Delta t = 0.0001s$,Noise:5%, R matrix:5%)

From the above figures, it is clear that all the parameters havn't converged to the corresponding

target values. At the end of the time, the estimation of parameters is :

$$a = 9.22$$
$$b = -24.79$$
$$c = 22.32$$
$$d = -7.38$$
$$e = 1.92$$

A comparison can be made between the original ice crushing strength and stress rate curve and the estimated one.

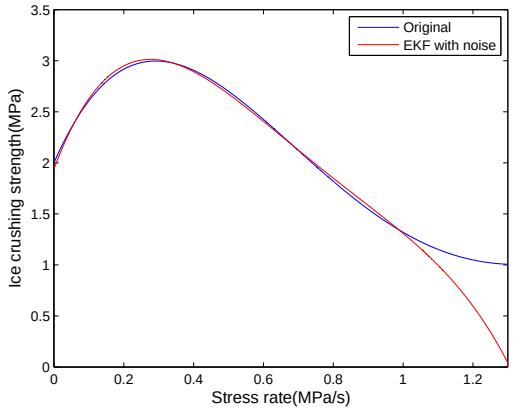

Figure 5.58: Comparison between the original ice crushing strength and stress rate curve and the estimation from EKF

Figure 5.58 only uses the estimated coefficients at the end of the EKF. However, at each time step between $t = 0s$ and $t = 100s$, there still exist information in the combination of each coefficient, even though each of them are varying. At each time step, the estimated parameters can be used to rebuild the ice crushing strength on the base of $\dot{\sigma}$, which can be obtained from the measured velocity. In this case, a point, whose X axis is the corresponding $\dot{\sigma}$ and Y axis represents the ice crushing strength calculated by the estimated coefficients, can be obtained at each time step.

$$\sigma_n = a_n\dot{\sigma}_n + b_n\dot{\sigma}_n^2 + c_n\dot{\sigma}_n^3 + d_n\dot{\sigma}_n^4 + e_n \tag{5.4}$$

Below are the points(marked with red color). After obtaining the ice crushing strength points, a curve

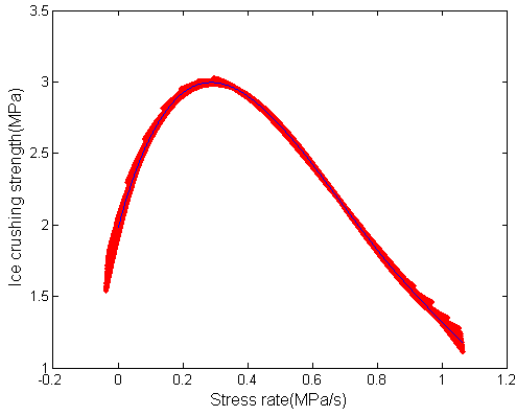

Figure 5.59: Ice crushing strength points and original curve

can be used to fit the points. A six order polynomial has been used.

$$\sigma_c = 8.39\dot{\sigma} - 23.08\dot{\sigma}^2 + 27.77\dot{\sigma}^3 - 27.4\dot{\sigma}^4 + 20.15\dot{\sigma}^5 - 6.50\dot{\sigma}^6 + 1.98 \tag{5.5}$$

Below is the comparison between the original curve and the one obtained from curve fitting, it is obvious that the difference is very small.

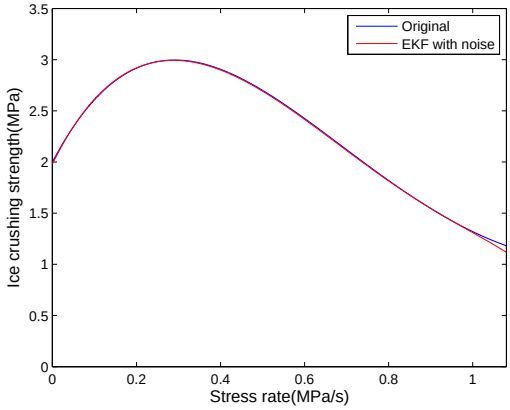

Figure 5.60: Comparison between the original ice crushing strength curve and the estimation from curve fitting

5.6.1. Conclusion for five parameters estimation

Instead of converging to the target value, the five parameters still varying with time during EKF. The reason is that similar to the case of four parameters estimation, there exist multiple combination of the five parameters to minimize the cost function in EKF.
In order to make use of the combination of the parameters at each time step, the ice crushing strength points at each time step have been obtained. A polynomial with 6 order is used to fit the points. The shape of the polynomial is very similar to the original ice crushing strength and stress rate curve within the evoked $\dot{\sigma}$.

5.7. conclusion of EKF for low ice velocity

In the case of low ice velocity, only the polynomial range in the ice crushing strength and stress rate curve has been evoked. The five unknown model parameters don't converge to the corresponding target value. However, the estimated curve obtained from fiting the ice crushing strength poins is very similar to the original one.

6

EKF for high ice velocity

Under the ice velocity of $0.3m/s$, the ice crushing strength is constant($1MPa$). All the formulation of EKF for high ice velocity is exactly the same to the formulation in section 5.5 of chapter 5.

6.1. Result for high ice velocity

The estimated parameters are shown below:

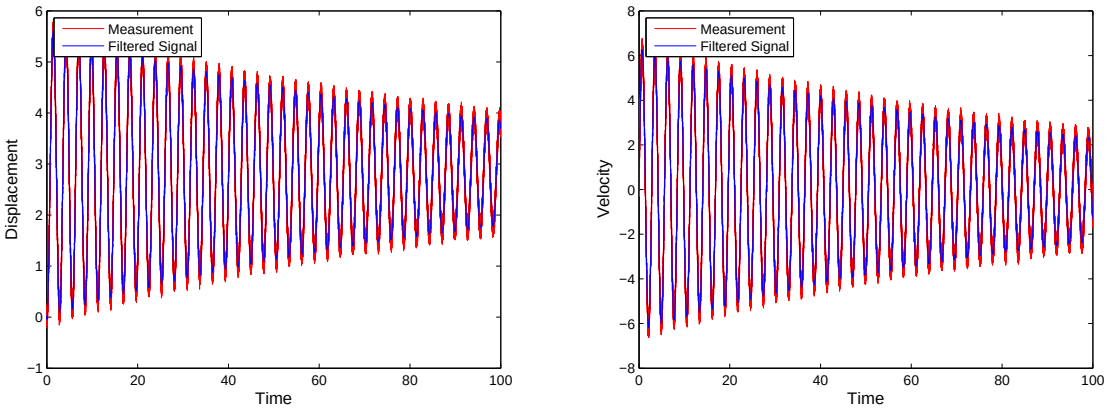

Figure 6.1: Measurement VS Filtered Signal($\Delta t = 0.0001s$,Noise:5%, R matrix:5%)

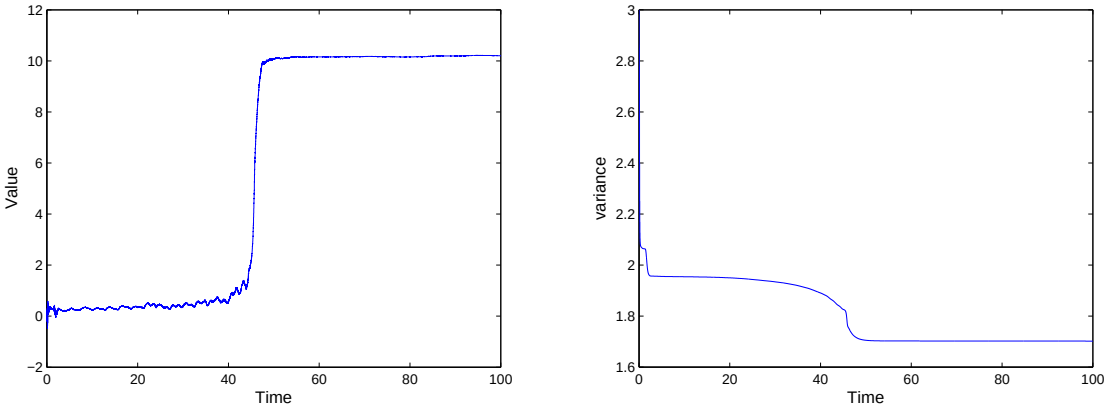

Figure 6.2: Parameter Estimation for a($a^{target} = 0$, $\Delta t = 0.0001s$,Noise:5%, R matrix:5%)

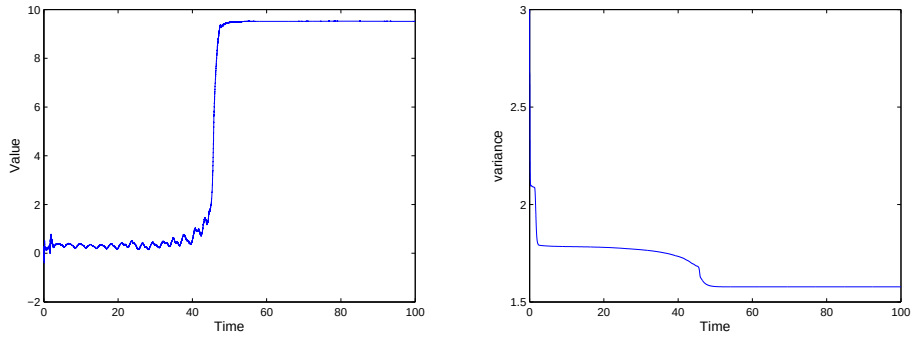

Figure 6.3: Parameter Estimation for b($b^{target} = 0$, $\Delta t = 0.0001s$,Noise:5%, R matrix:5%)

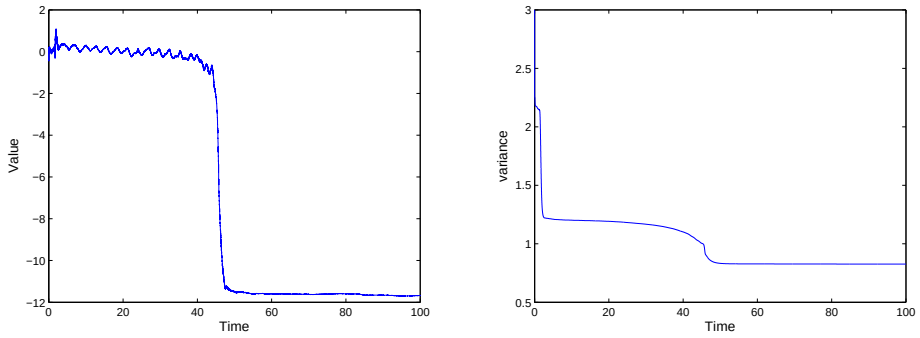

Figure 6.4: Parameter Estimation for c($c^{target} = 0$, $\Delta t = 0.0001s$,Noise:5%, R matrix:5%)

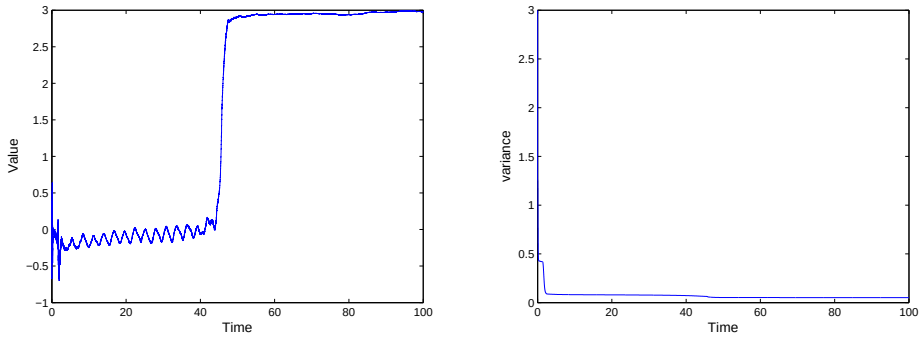

Figure 6.5: Parameter Estimation for d($d^{target} = 0$, $\Delta t = 0.0001s$,Noise:5%, R matrix:5%)

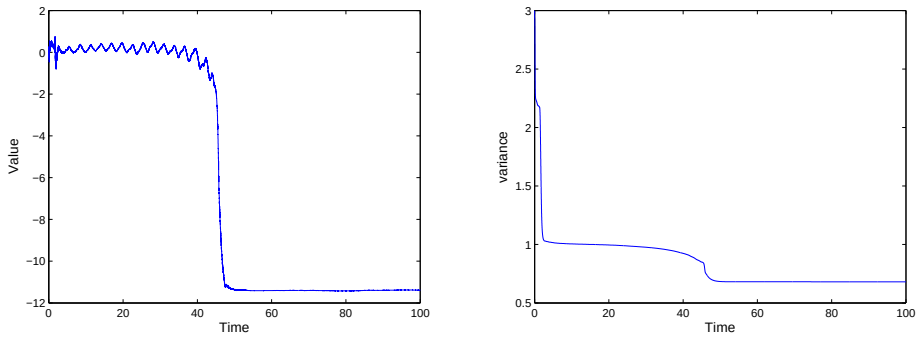

Figure 6.6: Parameter Estimation for e($e^{target} = 1$, $\Delta t = 0.0001s$,Noise:5%, R matrix:5%)

At the end of the time, the estimation is :

$$a = 10.20$$
$$b = 9.52$$
$$c = -11.67$$
$$d = 2.97$$
$$e = -11.39$$

The comparison between the original curve and the estimated one is as below. Moreover, under high ice velocity, only part of the curve ($1.4MPa/s < \dot{\sigma} < 1.6MPa/s$) is evoked, as shown in Figure 3.7.

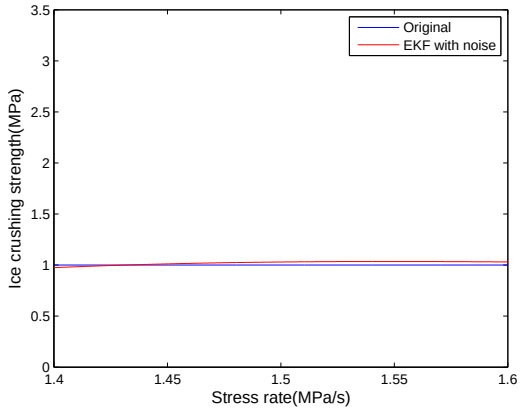

Figure 6.7: Comparison between the original ice crushing strength and stress rate curve and the estimation

Again, similar to the EKF for low ice velocity, the ice crushing strength points at each time step can be obtained as below:
It is clear that the ice crushing strength is almost equivalent to $1MPa$, which is the target value.

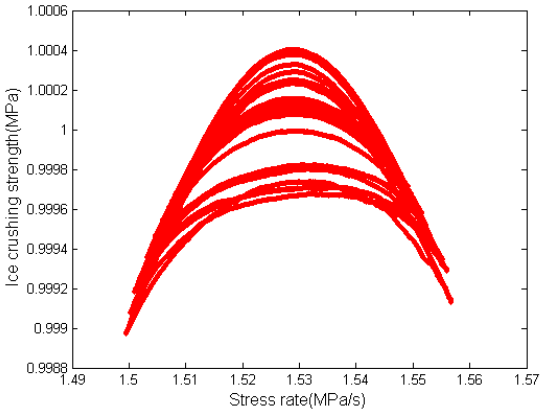

Figure 6.8: Ice crushing strength points

6.2. conclusion of EKF for high ice velocity

From Figure 6.8, it is obvious that the estimated ice crushing strength is very close to the target value. Thus, the EKF is applicable of identifying the ice crushing strength at high ice velocity by obtaining the ice crushing strength points.

7

EKF for medium ice velocity

Under ice velocity of $0.18m/s$, both the polynomial range and the constant range of the ice crushing strength and stress rate curve are evoked. Again, all the formulation of EKF for high ice velocity is exactly the same to the formulation in section 5.5 of chapter 5.

7.1. Result for medium ice velocity

The estimated parameters are shown below:

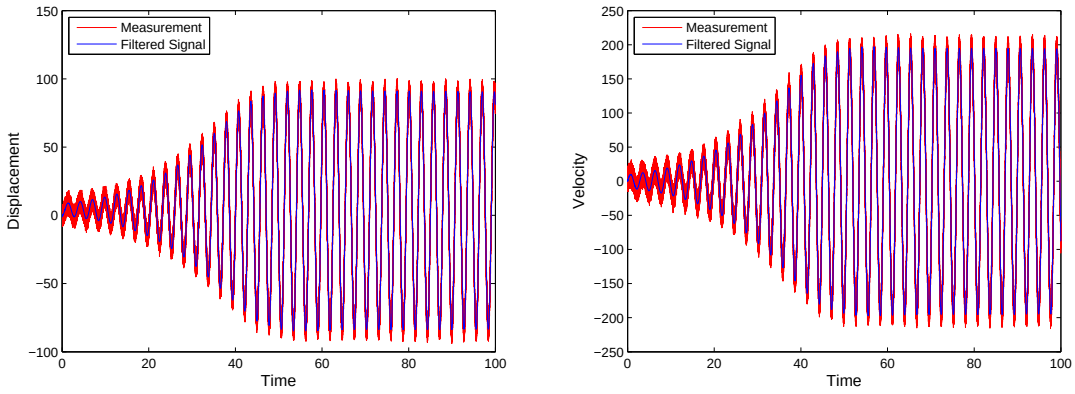

Figure 7.1: Measurement VS Filtered Signal($\Delta t = 0.0001s$,Noise:5%, R matrix:5%)

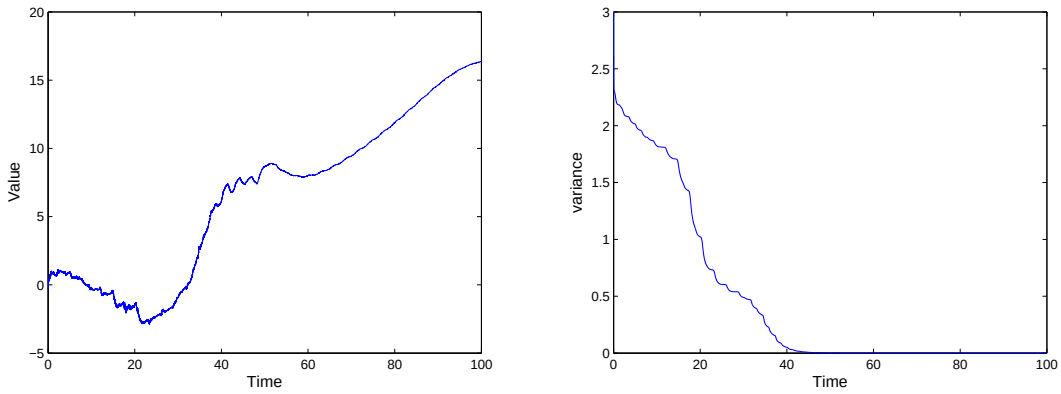

Figure 7.2: Parameter Estimation for a($\Delta t = 0.0001s$,Noise:5%, R matrix:5%)

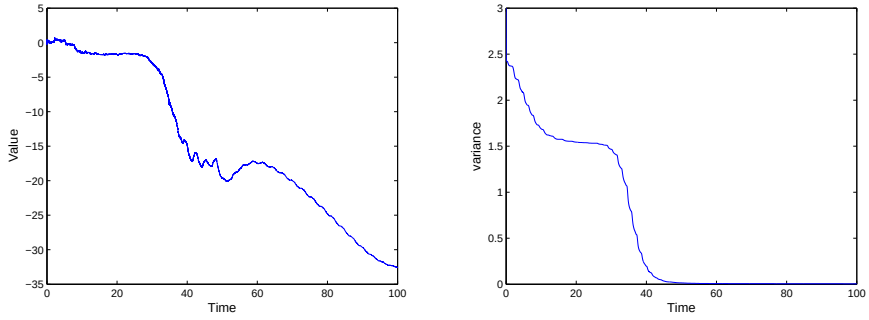

Figure 7.3: Parameter Estimation for b($\Delta t = 0.0001s$,Noise:5%, R matrix:5%)

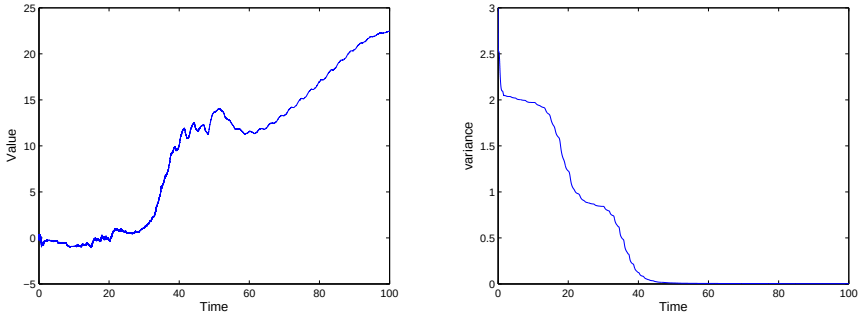

Figure 7.4: Parameter Estimation for c($\Delta t = 0.0001s$,Noise:5%, R matrix:5%)

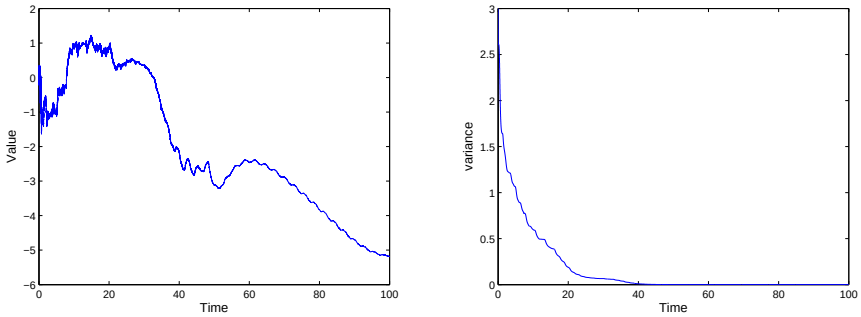

Figure 7.5: Parameter Estimation for d($\Delta t = 0.0001s$,Noise:5%, R matrix:5%)

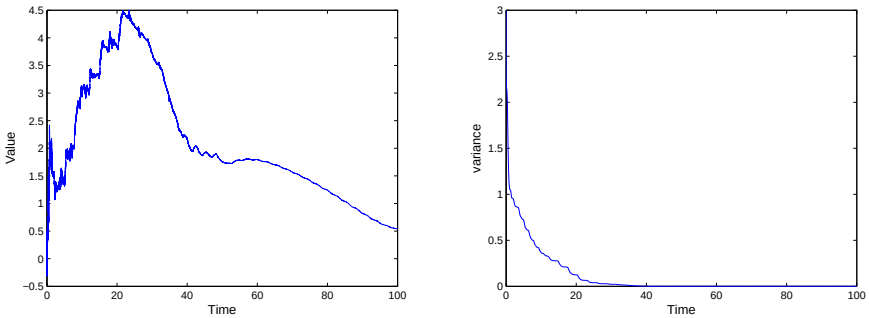

Figure 7.6: Parameter Estimation for e($\Delta t = 0.0001s$,Noise:5%, R matrix:5%)

At the end of the time, the estimation is :

$$a = 16.25$$
$$b = -32.10$$
$$c = 22.06$$
$$d = -5.09$$
$$e = 0.51$$

Due to the fact the range of stress rate between $0MPa/s$ and $1.9MPa/s$ has been evoked in Figure, then the comparison between the estimation and origin will be made within $0MPa/s < \dot{\sigma} < 1.9MPa/s$.

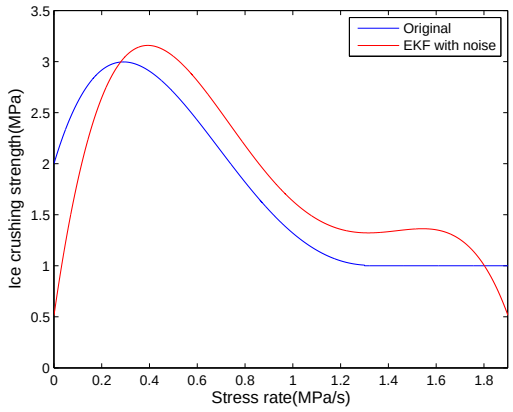

Figure 7.7: Comparison between the original ice crushing strength and stress rate curve and the estimated one

From Figure 7.7, it is obvious that the difference between the estimated curve and the original one is very large. What's more, all the estimated parameters still have large tendency to change based on the Figure 7.2 to Figure 7.6. The estimated curve in Figure 7.7 only represents the result at $t = 100s$. However, there exist enormous combination of the parameters between $t = 0s$ and $t = 100s$. At each time step, the combination of each parameter can be used to reconstruct the ice crushing strength based on corresponding stress rate $\dot{\sigma}$. In addition, the corresponding $\dot{\sigma}$ can be obtained by measurement. In this case, at each time step a point whose x axis is $\dot{\sigma}$ and y axis is ice crushing strength can be obtained. The information between $t = 0s$ and $t = 100s$ thus can be represented by all the points. Below is the result.

After obtaining the ice crushing strength points(marked with red color in Figure 7.8), a polynomial can

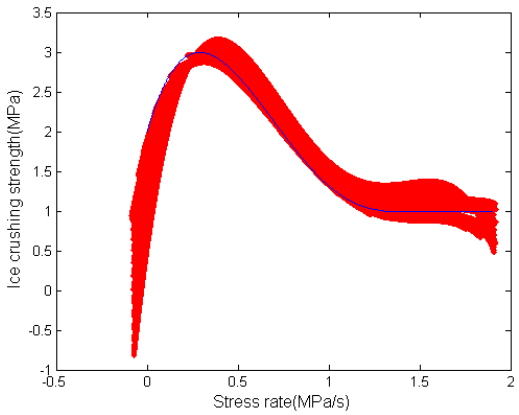

Figure 7.8: Ice crushing strength point and original curve

be used to fit the points. In this case, a polynomial has to both fit the polynomial range($0MPa/s < \dot{\sigma} <$

$1.3MPa/s$) and the constant range($1.3MPa/s < \dot{\sigma}$). In order to increase the accuracy, the polynomial is chosen as six order. The result is shown in blue color in Figure 7.8, with the expression as:

$$\sigma_c = 11.26\dot{\sigma} - 24.46\dot{\sigma}^2 + 17.02\dot{\sigma}^3 - 3.3\dot{\sigma}^4 - 0.69\dot{\sigma}^5 + 0.2\dot{\sigma}^6 + 1.32 \tag{7.1}$$

The comparison between the original ice crushing strength and stress rate curve and the estimated one is: From Figure 7.9, the estimation is very close to the original curve within $0.4MPa/s < \dot{\sigma} < 1.6MPa/s$.

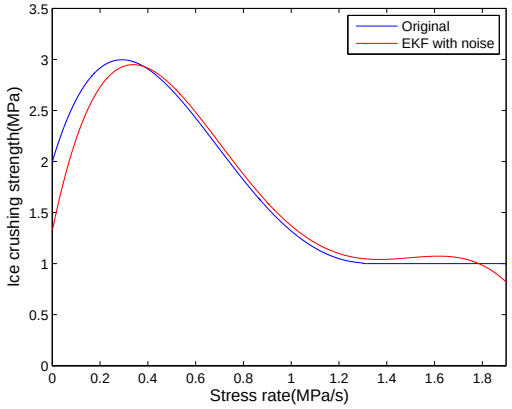

Figure 7.9: Comparison bewteen original ice crushing strength and stress rate and the estimation

7.2. Conclusion of EKF for medium ice velocity

Compared with Figure 7.7, the result from curve fitting of the ice crushing strength points at each time step is much better than directly taking the result at the end of EKF. Moreover, the estimation is close to the target curve within $0.4MPa/s < \dot{\sigma} < 1.8MPa/s$.

8

Conclusion

This thesis applies LS method and EKF respectively to identify the ice crushing strength and stress rate curve, in Maattanan's numerical model used for describing frequency lock-in of ice structure interaction, under low, medium and high ice velocity based on measurement. Under different ice velocities, different parts of the ice crushing strength and stress rate curve have been evoked. The measurement data has been generated by the model with addition of white noise.

For the least squares method, all the unknown parameters perfectly reach the target value under zero noise level in the case of low ice velocity. However, the result of estimation under the existence of noise is not good any more. The reason is the discontinuity at $\dot{\sigma} = 0MPa/s$ in the ice crushing strength and stress rate curve. In terms of medium ice velocity, the estimation differs a lot from the original curve. While for the case of high ice velocity, the estimation fails due to the lack of information.

In terms of EKF, good estimation has been obtained. Due to the fact that the parameters still vary instead of converging at the end of the analyzed time period, the ice crushing strength points at each time step are obtained for curve fitting. Under low ice velocity, the estimated curve from fitting the ice crushing points is very similar to the original one. For high ice velocity, the ice crushing strength points are almost allocated at target strength of $1MPa$. While for the medium ice velocity, the estimated curve is close to the original curve within mixed range.

Comparing the result from LS method and EKF, the EKF works better for identifying different part of the ice crushing strength and stress rate curve under different ice velocities. Moreover, the EKF can be expanded to multi-degree of freedom system, which is more realistic for real structures.

9

Further Research

1. The extended Kalman filter can be applied to real measurement data when it's available. Except using the 4th order polynomial in relationship between force and velocity, trying polynomial with less order may also help us understand the frequency lock-in if the estimation converges.

2. Instead of extended Kalman filter, unscented Kalman filter, which has huge advantage for non-linear system, is another option for estimation.

3. The author only applies the estimation algorithm to single degree of freedom system. However, in reality offshore platforms, light houses as well as piers can be all regarded as slender structures with multiple degree of freedom systems. Thus, extending the object of research to multiple degree of freedom system would be a huge step forward.

4. This thesis holds the assumption that the dynamic properties of the structure are known. Unfortunately, achieving this is not easy in reality. Another technique, system identification, uses statistical methods to build mathematical models of dynamical systems based on input (force) and output (response), regardless of the details inside the system. More information can be found in Lennart Ljung's work [19].

A

Numerical method for solving differential equation

> Finally, we make some remarks on why **linear systems** are so important. The answer is simple: because we can solve them!.
> –*Richard Feynman*

Linear system can be perfectly solved without any approximation. However, in order to artificially generate the displacement and velocity signals of the response, several numerical methods, as well as the ODE45 command in MATLAB will be introduced here, due to the nonlinearity in the ice crushing strength and stress rate curve.
Without loss of generality, consider the simples form of dynamic equation:

$$m\ddot{u} + c\dot{u} + ku = F(t) \tag{A.1}$$

Where, external force $F(t)$ can be anything.
Define the following variables:

$$x_1 = u$$
$$x_2 = \dot{u}$$

Then the dyanmic equation can be rewrited as:

$$\dot{x}_2 = -\frac{c}{m}x_2 - \frac{k}{m}x_1 + F(t) \tag{A.2}$$

which can be written into a state-space form:

$$\begin{bmatrix} \dot{x}_1 \\ \dot{x}_2 \end{bmatrix} = \begin{bmatrix} 0 & 1 \\ -\frac{k}{m} & -\frac{c}{m} \end{bmatrix} \begin{bmatrix} x_1 \\ x_2 \end{bmatrix} + \begin{bmatrix} 0 \\ \frac{1}{m} \end{bmatrix} F(t) \tag{A.3}$$

So if some kind of function which performs integration of time is given, new displacement x_1 and velocity x_2 can be obtained.

A.1. Euler Method

Euler method is the most basic explicit method for numerical integration of ordinary differential equations and is the simplest Runge–Kutta method. It is named after Leonhard Euler, who treated it in his book ≪ Institutionum calculi integralis ≫.
The principle idea behind Euler method is that the new state can be obtained by adding the product of state gradient at this moment and time step to the previous state.

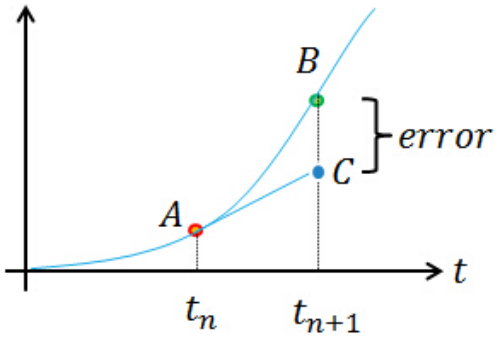

Figure A.1: Euler method

A.2. 4th order Runge-Kutta

From figure A.1, it is very clear that the error, which is proportional to the square of the time step size by the help of Taylor Series Expansion, using Euler method is enormous. In order to reduce the error and improve the performance of integration, some other algorithm has been developed, for instance 4th order Runge-Kutta method.
Let an ordinary differential equation be specified as follows:

$$\dot{y} = f(t, y) \tag{A.4}$$

The state of $n + 1$ is:

$$y_{n+1} = y_n + \frac{\Delta t}{6}(k_1 + 2k_2 + 2k_3 + k_4) \tag{A.5}$$

where

$$\begin{aligned} k_1 &= f(t_n, y_n) \\ k_2 &= f(t_n + \frac{\Delta t}{2}, y_n + \frac{\Delta t}{2}k_1) \\ k_3 &= f(t_n + \frac{\Delta t}{2}, y_n + \frac{\Delta t}{2}k_2) \\ k_4 &= f(t_n + \Delta t, y_n + \Delta t k_3) \end{aligned}$$

k_1 is the increment based on the slope at the beginning of the interval (Euler method).
k_2 is the increment based on the slope at the midpoint of the interval, using $y + \frac{\Delta t}{2}k_1$.
k_3 is again the increment based on the slope at the midpoint of the interval, but using $y + \frac{\Delta t}{2}k_2$.
k_4 is the increment based on the slope at the end of the interval, using $y + \Delta t k_3$.
The 4th order Runge-Kutta method reduce the error by means of the slope at midpoint. A general calculation procedure can be presented below in Figure A.2.

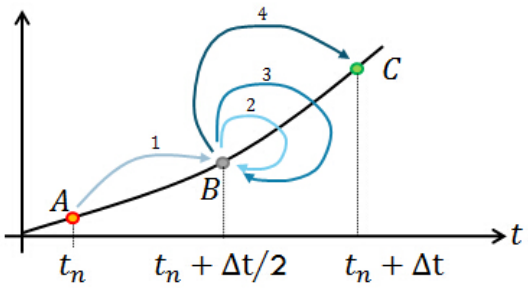

Figure A.2: 4th order Runge-Kutta method

A.3. ODE45

The ODE45 command used for solving differential equation in MATLAB is based on the 4th order Runge-Kutta method. The only difference is that ODE45 will automatic change the time step based on comparing the error with other numerical method (Adpative time stepping).

B

Singular value decomposition

In terms of the inverse problem, least square method is not the only approach. Singular value decomposition can be used to calculate the pseudoinverse to solve linear square problems.
Suppose vector x with size of n in the below equation needs to be solved.

$$\mathbf{Ax=b} \tag{B.1}$$

The least square solution is:

$$S = ||Ax - b||_2 \tag{B.2}$$
$$x_{LS} = argmin_x(S) = (A^T A)^{-1} A^T b \tag{B.3}$$
(B.4)

The singular value decomposition solution is:

$$x_{SVD} = A^{\dagger} b = \sum_{i=1}^{r} \frac{\mathbf{u}_i^T \mathbf{b}}{\sigma_i} \mathbf{v}_i \tag{B.5}$$

Where $\mathbf{u}_i$,σ_i and $\mathbf{v}_i$ come from the sigular value decomposition of A matrix:

$$\mathbf{A} = \sum_{i=1}^{r} \mathbf{u}_i \sigma_i \mathbf{v}_i^T \tag{B.6}$$

When matrix A, which has size of $m \times n$, has $rank(A) = n$, the least square solution and singular value decomposition solution would be the same.
In equation (B.5), if singular value σ_i is very small, then minimal error in vector **b** would largely change the estimated value x_{SVD}. In another words, the sensitivity to error of the least square method can be evaluated by means of the singular value decompostion of matrix A. Below is the five singular values of **A** for low ice velocity case in chapter 3.

$$\sigma_1 = 33.7768$$
$$\sigma_2 = 13.5697$$
$$\sigma_3 = 3.3783$$
$$\sigma_4 = 0.5632$$
$$\sigma_5 = 0.0602$$

From the above five singular values, it is clear that the case of low ice velocity is a well-conditioned problem. The five singular values of **A** for high ice velocity case are shown below.

$$\sigma_1 = 78.41$$
$$\sigma_2 = 0.87$$
$$\sigma_3 = 0.01$$
$$\sigma_4 = 0.00$$
$$\sigma_5 = 0.00$$

There are two singular values are zero in the case of high ice velocity. Hence, it's a ill-conditioned problem.
The five singular values of **A** for medium ice velocity case are shown below.

$$\sigma_1 = 39.40$$
$$\sigma_2 = 11.39$$
$$\sigma_3 = 2.90$$
$$\sigma_4 = 0.74$$
$$\sigma_5 = 0.11$$

Similar to the case of low ice velocity, the case of medium ice velocity is also a well-conditioned problem.

Bibliography

[1] B.D.O. Anderson and J.B. Moore. Optimal filtering. 1979.

[2] K.A. Blenkarn. Measurement and analysis of ice forces on cook inlet structures. *Offshore Technology Conference*, VOLUME2:365–378, 1970.

[3] A. Corigliano and S. Mariani. Parameter identification in explicit structural dynamics: performance of the extended kalman filter. *Comput. Methods Appl. Mech. Engrg*, pages 3807–3835, 2004.

[4] E. Croot. Maximum likelihood estimators and least squares. *nothing*, 2010.

[5] S. Dan. Optimal state estimation. 2006.

[6] A. Dempster, N. Laird, and D. Rubin. Maximum likelihood from incomplete data via the em algorithm. *Journal of the Royal Statistical Society*, pages 39(1):1–38, 1977.

[7] Van der Pol. A theory of the amplitude of free and forces triode vibrations. *Radio Review*, VOLUME1:701–754, 1920.

[8] R. A. Fisher. On an absolute criterion for fitting frequency curves. *Messenger of Mathematics*, pages 41:155–160, 1912.

[9] R. A. Fisher. On the mathematical foundations of theoretical statistics. *Philosophical Transactions of the Royal Society Series A*, pages 222:309–368, 1922.

[10] R. Frederking, D. Masterson, B. Wright, and P. Spence. Ice load measuring panels the next generation. *Ice in the Environment: Proceedings of the 16th IAHR International Symposium on Ice*, 2002.

[11] J.E. Gibson. Nonlinear automatic control. 1963.

[12] H. Hendrikse, G.L. Kuiper, and A.V. Metrikine. Ice induced vibrations of flexible offshore structures: the effect of load randomness, high ice velocities and higher structural modes. *Proceedings of the 21st International Conference on Port and Ocean Engineering under Arctic Conditions*, 2011.

[13] P.E. Hollandsworth and H.R. Busby. Impact force identification using the general inverse technique. *International Journal of Impact Engineering*, VOLUME8:315–322, 1989.

[14] G. Huang and P. Liu. A dynamic model for ice-induced vibration of structures. *Journal of Offshore Mechanics and Arctic Engineering*, page 131, 2009.

[15] M. Jefferies, B. Rogers, M. Hardy, and B. Wright. Ice load measurement on molikpaq: Methodology and accuracy. *Proceeding of the 21st International Conference on Port and Ocean Engineering under Arctic Conditions*, 2011.

[16] R. E. Kalman. A new approach to linear filtering and prediction problems. *Journal of Basic Engineering*, pages 35–45, 1960.

[17] T. Karna and R. Turunen. Dynamic response of narrow structures to ice crushing. *Cold Region and Technology*, pages 173–1870, 1989.

[18] R.I. Leine and H. Nijmeijer. Dynamics and bifurcations of non-smooth mechanical systems. 2013.

[19] Lennart Ljung. System identification — theory for the user. 1999.

[20] M.P. Maattanen. On conditions for the rise of self-excited ice induced autonomous oscillations in slender marine pile structures. *Phd Thesis*, 1978.

[21] M.P. Maattanen. Numerical model for ice-induced vibration load lock-in and synchronization. *Ice in Surface Waters*, VOLUME2:923–931, 1999.

[22] W. Mader, Y. Linke, and M. Mader. A numerically efficient implementation of the expectation maximization algorithm for state space models. *Applied Mathematics and Computation*, pages 222–232, 2014.

[23] H. Matlock, W.P. Dawkins, and J.J. Panak. A model for the prediction of ice-structure interaction. *Proceedings of the first Offshore Technology Conference*, VOLUME1:687–694, 1969.

[24] G. McLachlan and T. Krishnan. The em algorithm and extensions. *Wiley series in probability and statistics*, 1997.

[25] A.V. Metrikine. The synchronization phenomenon in modern structural dynamics: vortex-, ice-, and pedestrain-induced vibrations of engineering structures. *Proceedings of the 8th International Conference on Structural Dynamics*, 2011.

[26] A. Romanenko and J.A.A.M. Castro. The unscented filter as an alternative to the ekf for nonlinear state estimation: a simulation case study. *Computer and Chemical Engineering 28*, pages 347–355, 2004.

[27] D.S. Sodhi. A theoretical model for ice-structure interaction. *Proceeding of the OMAE-94 Conference*, 1994.

[28] P. Spencer. A review of the medof panels installed on the molikpaq structure in the canadian beaufort sea. *International Conference on Port and Ocean Engineering under Arctic Conditions*, 2013.

[29] J. W. Strutt. On maintained vibrations. *Philosophical Magazine*, VOLUME15:229, 1883.

[30] B. S. Thomas. Estimation of nonlinear dynamic systems theory and applications. *Phd thesis*, 2006.

[31] G.W. Timco, B. Wright, M. Johnston, and R. Frederking. First-year ice ridge loads on the molikpaq. *Proceedings 4th International Conference on Development of the Russian Arctic Offshore*, pages Part2:172–179, 1999.

[32] S. Nord Torodd and E. Lourens. Model-based force and state estimation in experimental ice-induced vibrations by means of kalman filtering. *Cold Regions Science and Technology*, VOLUME1:13–26, 2015.

[33] S. Nord Torodd, M. Määttänen, and O. Øiseth. Frequency domain force identification in ice-structure interaction. *Proceedings of the 22nd International Conference on Port and Ocean Engineering under Arctic Conditions*, 2013.

[34] T.S.J. van Dijk. Drifting-ice structure interaction, a dynamical systems approach. *Master Thesis*, 2015.

[35] B. Wright. Ice pressure distributions from first-year sea ice features interacting with the molikpaq in the beaufort sea. *Proceedings of the Ninth (1999) International Offshore and Polar Engineering Conference*, VOLUME2:541–541, 1999.